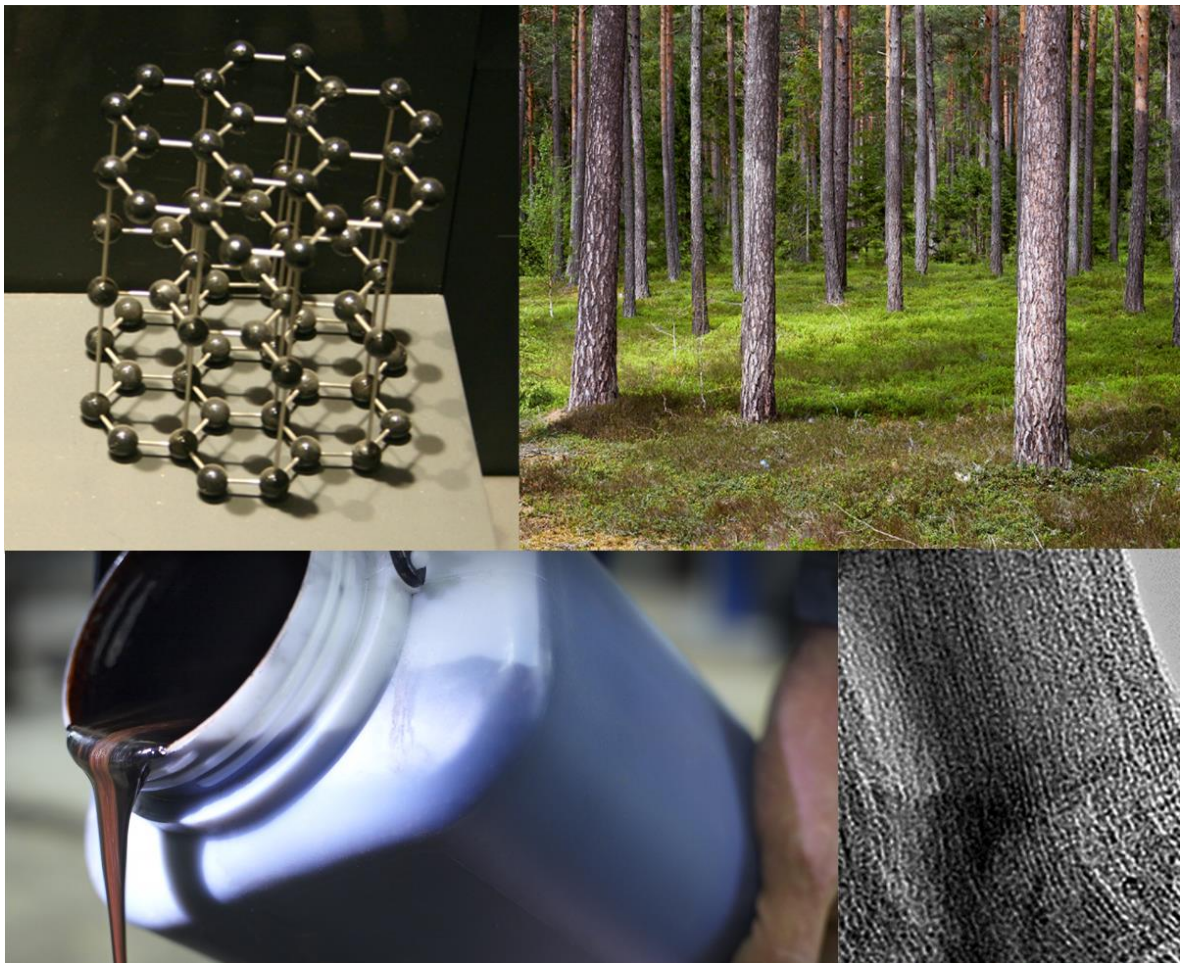

# Graphite materials –Production from biomass?


## *Magnus Gimåker* and Hjalmar Granberg**

*RISE – Research Institutes of Sweden, Bioeconomy and Health

*Digital Cellulose Center (digitalcellulosecenter.se)


Project 1 – "Cyclability of DCC materials and case study on carbonized wood" within the Digital Cellulose Center


**ISBN** 978-91-89561-87-8

# Summary

## Graphitic carbon –Production from biomass?

Graphite materials show high electrical and thermal conductivity making them useful in electronics both as electrical conductor, but as of today primarily used as a thermal conductor for thermal management and as the dominating anode material in lithium ion batteries. The conductivities depend on for example the degree of graphitisation, that is how close the material is to perfect graphite. Graphite materials can occur naturally in the earth's bedrock and can thus be extracted by mining and is then called natural graphite. Graphitic carbon materials can also be synthesised and are then usually referred to a synthetic or artificial graphite, even though they should be referred to as graphite materials if being strict, as they never reach the structure of perfect graphite and always contain some defects and irregularities.

This report starts with a short description of all carbon allotropes, i.e. structurally different forms of the same element due to how the atoms are chemically bonded to each other. It then continues with an overview of how graphitic carbon materials can and should be characterised, as well as analytical methods for making this characterisation. After this a section on production methods for graphite materials follows, that dependent on the principles they operate by are divided into:

- Mining for graphite that occurs naturally in the earth's bedrock.
- High temperature heat-treatment, so called carbonisation, hydrothermal carbonisation if done in water, and graphitisation.
- Chemical vapour deposition, i.e. depositing molecules or atoms in gas phase on a solid surface, that is used to synthesise pyrolytic carbon and graphite.
- Extraction from a steelmaking by-product called Kish to obtain so called Kish graphite.
- Thermal decomposition of carbides.

This is followed by a section on the today most common and important graphite materials, which are: natural graphite (mined), anisotropic synthetic graphite, isotropic synthetic graphite, pyrolytic carbon and graphite. This section also includes specific production process details for the above listed graphite materials, their main properties, advantages, and common uses. Two of the most common and important uses of graphite materials, i.e. as anode in lithium ion batteries and for thermal management in electronics, are described somewhat more in depth.

The focus of this report is biomass derived graphitic materials and this focus start fully first in section number four, which compares published values on electrical and thermal conductivity of different fossil and bio-based graphitic carbon materials. This comparison clearly shows that it is very challenging to derive graphitic carbon materials with high conductivities from biomass. This is because essentially all biomass is so-called non-graphitising or hard carbon precursor meaning that it is not transformed into highly graphitic carbon no matter how high temperature it is heated to. Catalytic graphitisation using metals salts or oxides can increase the degree of graphitisation that can be achieved, but all substances used for catalysing graphitisation forms solid nanoparticles which leaves

voids when removed by for example acid dissolution, making the resulting graphitic material porous which in turn limits its electrical and thermal conductivity.

Of all production processes reviewed here to create highly electrically and thermally conductive graphitic carbon materials from biomass, requiring a high degree of graphitisation and dense material, two methods stand out as especially interesting:

- Chemical vapour deposition on suitable substrate (carbon materials, metals or ceramics) using biomass as carbon source.
- Resistive heating of biomass derived films/objects.

Bio-based free-standing graphene film with very high electrical and thermal conductivity have been produced using chemical vapour deposition technique. From a practical handling perspective, it would be beneficial to create thicker highly graphitic carbon films to make them stronger, although it may reduce the conductivities of the material. Methods based on chemical vapour deposition may be improved to be able to produce thicker graphitic films. Resistive heating of a film made of e.g. biobased lignin, mixed with mined graphene to 2192 °C have been shown to create a highly graphitic carbon film with the excellent electrical conductivity of 4480 S/cm. By substituting the mined graphene to bio-based ditto may open up for the production of a fully biobased, highly graphitic film with excellent conductive properties. It is suggested that the way to achieve fully biobased highly graphitic and dense films is to further refine the chemical vapour deposition and the resistive heating method.

Keywords: Graphitic carbon, graphite, graphite material, carbon, biomass, bio-based, graphene, pyrolysis, carbonisation, graphitisation, electrical conductivity, thermal conductivity, electronics, electrical energy storage, lithium ion battery, anode material, heat spreading, heat spreader, heat sink, thermal management.

Stockholm, December 2021

# Preface

Carbon is a complex element by itself, even when it is not covalently bound to other elements forming a myriad of chemical substances (i.e. the chemistry of life), since it can form many allotropes (structurally different forms of the same element) due to its valence electron configuration. In addition most carbon materials have a complex ultrastructure and very seldomly consist of only one pure carbon allotrope.

Many carbon allotropes show high electrical conductivity and/or high thermal conductivity, making them interesting to use in e.g. electronics and electrical applications both as electrical conductor and as heat sinks and spreaders. It is primarily graphitic, $sp^2$-bonded carbons (including graphene and fullerenes) that show the combination of high electrical and thermal conductivity. These materials are today mined as in natural graphite or synthesised from petroleum coke and coal tar pitch. The petroleum coke precursor can be produced by a coking process in which remaining volatile compounds are removed from crude oil refining. The coal tar pitch precursor is a by-product from the refining of coal into coke and coal gas. During the synthesisation process, the precursor mixture is graphitized at an elevated temperature, typically 2000-3000 °C. This turns them into graphitic carbon which is different from graphite. The degree of graphitisation, i.e. how close to actual graphite the material becomes, depends on the precursor material as well as the details of the conversion process. Today most graphitic materials are produced using fossil raw material.

If graphitic carbon including graphenes, could be produced from biomass instead of fossil raw material, this may result in sustainability gains as long as the production processes using biomass are energy efficient and do not use toxic or otherwise problematic chemicals. No biobased raw material (biomass) show high electrical and/or thermal conductivity but can be converted into materials with high carbon content, that to some extent show these properties, by thermal processes, e.g. pyrolysis (i.e. high-temperature treatment in inert atmosphere, a process which at lower temperature (200-320 °C) is usually referred to as torrefaction and at higher temperatures (>320 °C) as carbonisation) and hydrothermal carbonisation (heating in water to typically around 200 °C at an elevated pressure), without or in combination with chemical treatment.

The focus of this report is on if and how highly graphitic carbon materials can be derived from biomass and starts with a general overview of carbon and graphitic carbon materials. First an overview of the element carbon and the different allotropes it forms is given. This is followed by a section on how graphitic carbon materials can and should be characterised, as well as analytical methods for making this characterisation. Then follows a section on the four main principle processes for synthesizing graphitic carbon. These are high temperature treatment, chemical vapour deposition, i.e. depositing molecules or atoms in gas phase on a solid surface, extraction from a steelmaking by-product called Kish, and by thermal decomposition of carbides. This is followed by a section on the most common and important graphite materials today. These are: natural graphite, anisotropic synthetic graphite, isotropic synthetic graphite, pyrolytic carbon and graphite. This section includes production process details, essential properties, advantages, and common uses. Two of the most common and important uses of graphite materials are as anode in lithium ion batteries and heat conducting material for thermal management, especially in electronics. These are described somewhat more in depth.

A comparison of the electrical and thermal conductivity of a variety of biomass-derived graphitic carbon materials to their fossil-based dittos is made. Finally, the results of the comparison are used to draw conclusions about the most promising methods for producing bio-based graphitic carbon with high electrical and thermal conductivity.

# Content

# 1 Introduction to carbon material fundamentals and characterisation

Carbon is the sixth element of the periodic table with the electron configuration $1s^2 2s^2 2p^2$, and can form carbon-carbon bonds of the hybrid orbitals of $sp^3$, planar $sp^2 + \pi$, curved $sp^2 + \pi$ and $sp + 2\pi$. Carbon materials can be classified depending on how carbon atoms bond to each other as shown in Figure 1. The meaning and importance of stacking regularity will be described further in section 1.2.1. The structurally different forms of the same element, as in the case of carbon, are usually referred to as allotropes. It is somewhat difficult to establish the general allotropes of carbon, but a common definition of the main carbon allotropes is: diamond, amorphous carbon, graphite (including graphene), fullerenes (including different nanocarbons such as carbon nanotubes), glass-like carbon, atomic and diatomic carbon, carbon nanofoam, carbide-derived carbon, lonsdaleite (hexagonal diamond), carbyne (or linear acetylenic carbon) and cyclocarbons, with diamond and graphite probably being the two most well-known allotropes. Due to the variety of bonding, structures and textures, there is a myriad of carbon materials, and they all have very different physical properties. Figure 2 gives an over-view of some important physical properties of a few different carbon materials.

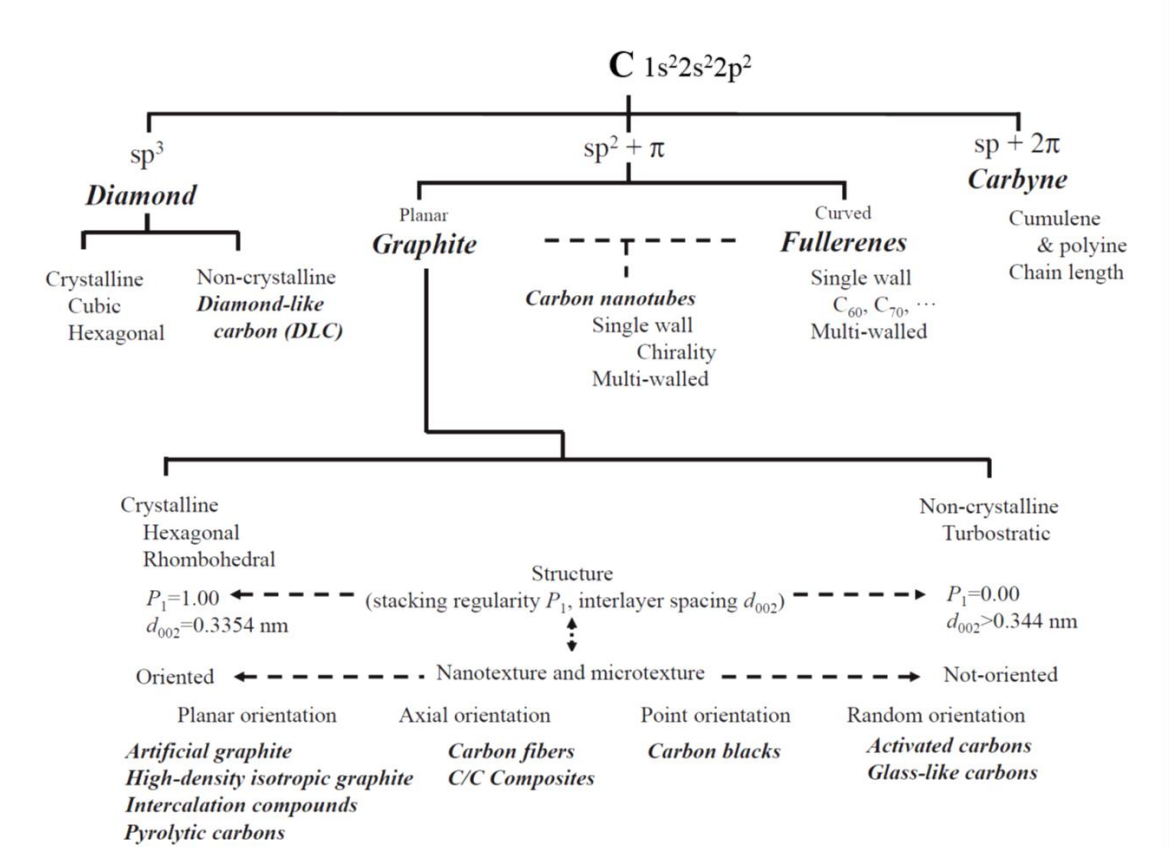


Figure 1. Classification of carbon materials based on carbon-carbon bond nature and varieties in structures and textures (Inagaki and Kang 2016).

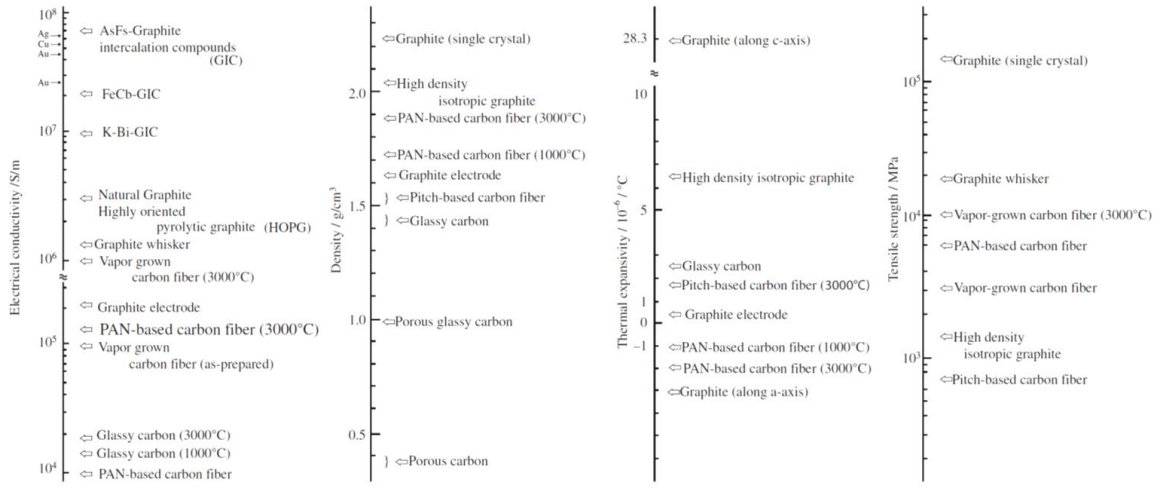


Figure 2. Some important physical properties, i.e. electrical conductivity, density, thermal expansivity and tensile strength of a few different carbon materials including graphite intercalation compounds (Inagaki and Kang 2014).

This report focuses on graphitic carbons derived from biomass, but a basic knowledge of the other carbon allotropes is still good to have, and therefore the above listed carbon allotropes are somewhat more detailed described below. However, there is a lot more to know about these allotropes than can be included in this report due to the focus on graphitic carbons, and the interested reader is advised to read e.g. the book “Handbook of carbon, graphite, diamonds and fullerenes: processing, properties and applications” by Pierson (2012). Other unusual forms of carbon exist at very high temperatures or extreme pressures, and 522 hypothetical 3-periodic allotropes of carbon are presently known, according to the Samara Carbon Allotrope Database (Proserpio, Golov et al. 2019). These hypothetical carbon allotropes are not considered in this report.

Carbon and graphene quantum dots are very interesting new nanomaterials due to the potential to use these in optoelectronics (i.e. the study and application of electronic devices and systems that source, detect and control light, and usually considered a sub-field of photonics). Example of optoelectronic devices are photovoltaic cells (solar cells), photodiodes (a semiconductor device that converts light into an electrical current) and opto-isolators (an electronic component that transfers electrical signals between two isolated circuits by using light and thus preventing high voltages from affecting the circuit receiving the signal). These components are all likely to be very important in the development of the electronics of tomorrow. However, there is still a debate whether these quantum dots should be considered true carbon allotropes, (Yang, Ren et al. 2018). No more information about carbon and graphene quantum dots are given in this report.

A short section on the complexity of carbon materials is also included since most carbon materials normally are mixtures of different carbon allotropes. Finally, a rather comprehensive section on how graphitic carbon materials are and can be characterised.

# 1.1 Allotropes of carbon

## 1.1.1 Diamond

Diamond is probably the most well-know and famous allotrope of carbon. The hardness of diamonds and their light dispersion properties make them useful in jewellery and industrial applications. Diamond is the hardest known natural mineral, though lonsdaleite (hexagonal diamond) has a hardness that is theoretically superior to that of diamond (up to 58% more), according to computational simulations, but natural specimens exhibited somewhat lower hardness than diamond. The cause is speculated as being due to the samples having been riddled with lattice defects and impurities (Carlomagno 2011).

Howard Tracy Hall was an American physical chemist and the first person who grew a synthetic diamond by a reproducible, verifiable, and witnessed process, using a press of his own design that could reach pressures and temperatures not previously achievable (Bundy, Hall et al. 1955, Hall 1960). At the pressure (10 GPa) and temperature (~3150 K) that was simultaneously achievable in Hall's new press, diamond is the thermodynamically stable carbon allotrope and forms spontaneously. Due to the High Pressure and Temperature requirement, this process of synthezising diamond is referred to as the HPHT process and diamonds made using the process as HPHT diamonds. Today there are four established methods for producing synthetic diamond: the HPHT process, chemical vapour deposition (CVD), detonation of explosives and ultrasound cavitation. The HPHT and CVD process are the two most important.

Naturally occurring diamonds usually have high thermal conductivity, and a value of 2000 W/(m·K) at 320 K have been reported by e.g. Burgemeister (1978). Also, synthetic diamonds have equally high thermal conductivity 2003 W/(m·K) at 323.15 K as reported by (Wort and Balmer 2008) making them interesting to use as a heat sinks in electronic devices. Normally diamonds are electric insulators, but if they are doped with impurities like boron and phosphor they become semiconducting (Denisenko and Kohn 2005, Wort and Balmer 2008). Boron contain one more valence electron than carbon and turn synthetic diamond into p-type semiconductor. Phosphor contains one less valence electron than carbon and turns synthetic diamond into an n-type semiconductor.

CVD diamond is made by chemical vapor deposition (CVD) using a gas mix of hydrogen and hydrocarbons. Usually a mixture of hydrogen (> 90%) and methane is used and combined with a high-temperature gas activator, like an intense plasma or a hot filament, to break up the hydrogen molecules into atomic hydrogen and to create carbon containing neutral and ionic radicals. The exact mechanisms behind the formation of CVD diamond is not fully understood, but it is generally agreed that the carbon containing neutral and ionic radicals reform into diamond at the growth substrate surface. Atomic hydrogen probably has several important roles, but one specific is that it selectively etch graphite that is also created during CVD diamond growth and thus contribute to the purity of the produced diamond.

Another useful property of synthetic CVD diamond for electronics is high carrier mobility, which reaches 4500 $cm^2/(V·s)$ for electrons in single-crystal CVD diamond (Isberg, Hammersberg et al. 2002). High mobility is favourable for high-frequency operation and

field-effect transistors made from diamond have already demonstrated promising high-frequency performance above 50 GHz (Ueda, Kasu et al. 2006, Russell, Sharabi et al. 2012).

The wide band gap of diamond (5.5 eV) gives it excellent dielectric properties. Combined with the high mechanical stability of diamond, those properties are being used in prototype high-power switches for power stations (Isberg, Gabrysch et al. 2006).

There are no commonly known methods to create diamond from bio-based raw material. Therefore diamond synthesis using bio-based raw material will not be reviewed in depth in this report, but here follows a few sentences how bio-based raw material could be used: The HPHT process uses graphite as a starting material, and hence bio-based graphite could be an interesting raw material for this process. The diamond CVD process normally uses hydrocarbons as carbon source. However, since e.g. graphene have been synthesised using CVD technology using bio-based and renewable raw materials (Ruan, Sun et al. 2011, Seo, Pineda et al. 2017), it could indicate that CVD diamond can perhaps be produced from bio-based raw material?

### 1.1.2 Amorphous carbon

Amorphous carbon is according to IUPAC (International union of pure and applied chemistry) defined as *"A carbon material without long-range crystalline order. Short-range order exists, but with deviations of the interatomic distances and/or interbonding angles with respect to the graphite lattice as well as to the diamond lattice. The term amorphous carbon is restricted to the description of carbon materials with localized π-electrons as described by P. W. Anderson (Phys. Rev., 1958, 109, 1492). Deviations in the C–C distances greater than 5% (i.e.* $\frac{\Delta x}{x_0} > 0.05$*, where* $x_0$ *is the inter-atomic distance in the crystal lattice for the* $sp^2$ *as well as for the* $sp^3$ *configuration) occur in such materials, as well as deviations in the bond angles because of the presence of 'dangling bonds'. The above description of amorphous carbon is not applicable to carbon materials with two-dimensional structural elements present in all pyrolysis residues of carbon compounds as polyaromatic layers with a nearly ideal interatomic distance of a=142 pm and an extension greater than 1000 pm."* (Amorphous carbon - Chalk 2019).

True amorphous carbon, due to its lack of crystallinity and presence of dangling bonds makes it chemically reactive. Dangling bond means that there is an unsatisfied valence on an immobilized atom, also referred to as an immobilized free radical or an immobilized radical, a reference to its structural and chemical similarity to a free radical. Amorphous carbon materials may be stabilized by terminating dangling-π bonds with hydrogen. As with other amorphous solids, some short-range order can be observed. Amorphous carbon is often abbreviated to aC for general amorphous carbon, aC:H or HAC for hydrogenated amorphous carbon, or to ta-C for tetrahedral amorphous carbon (also called diamond-like carbon) (Robertson 1986, Robertson 1991, Robertson 2002).

With the development of modern thin film deposition and growth techniques in the latter half of the 20th century, such as chemical vapour deposition, sputter deposition, and cathodic arc deposition, it became possible to fabricate truly amorphous carbon materials

(Gibson, Holohan et al. 1946, Blue and Danielson 1957, McLintock and Orr 1973, Robertson 1986, Comelli, Stöhr et al. 1988, Mounier, Bertin et al. 1996).

However, most amorphous carbon, such as coal (sedimentary rock), charcoal, and soot actually contains microscopic crystals of graphite-like (Vander Wal 1996, Gupta 2007) or even diamond-like carbon (Robertson 1991, Robertson 2002) within an amorphous carbon matrix, as well as often containing large amounts of hydrogenated amorphous carbon.

The properties of amorphous carbon films vary depending on the parameters used during deposition. The primary method for characterizing amorphous carbon is through the ratio of $sp^2$ to $sp^3$ hybridized bonds present in the material. Graphite consists purely of $sp^2$ hybridized bonds, whereas diamond consists purely of $sp^3$ hybridized bonds. Materials that are high in $sp^3$ hybridized bonds are referred to as tetrahedral amorphous carbon, owing to the tetrahedral shape formed by $sp^3$ hybridized bonds, or as diamond-like carbon (owing to the similarity of many physical properties to those of diamond).

Although the characterization of amorphous carbon materials by the $sp^2$-$sp^3$ ratio may seem to indicate a one-dimensional range of properties between graphite and diamond, this is most definitely not the case. Research is currently ongoing to find better and new methods to characterize and expand the property range offered by amorphous carbon materials.

### 1.1.3 Graphite and graphene

IUPAC defines *graphite* as: *"An allotropic form of the element carbon consisting of layers of hexagonally arranged carbon atoms in a planar condensed ring system graphene layers. The layers are stacked parallel to each other in a three-dimensional crystalline long-range order. There are two allotropic forms with different stacking arrangements, hexagonal and rhombohedral. The chemical bonds within the layers are covalent with sp2 hybridization and with a C–C distance of 141.7 pm. The weak bonds between the layers are metallic with a strength comparable to van der Waals bonding only."* (Graphite - Chalk 2019). The term *graphite* is commonly, but erroneously, used to refer to graphitic materials. These graphitic materials are either *graphitic carbons*, i.e. materials consisting of carbon with the graphite structure but with several structural defects, or *non-graphitic carbons*, i.e. materials consisting of carbon atoms with the planar hexagonal networks of the graphite structure, but lacking the crystallographic order in the *c* direction. This is the direction perpendicular to the layers of hexagonally arranged carbon atoms in the planar condensed ring systems. An exception might be defect free graphene that some scientist claim to have manufactured, see for example the reviews on graphene synthesis by Choi, Lahiri et al. (2010) and Avouris and Dimitrakopoulos (2012).

Hexagonal graphite is the thermodynamically stable form of graphite with an ABAB stacking sequence of the graphene layers. Hexagonal graphite is thermodynamically stable below approximately 2600 K and 6 GPa. The exact crystallographic description of this allotropic form is given by the space group $D6h^4$ – $PG_3/mmc$ (unit cell constants – a = 0.2456 nm, c = 0.6708 nm), see left part of Figure 3. The interlayer spacing ($d_{(002)}$ – distance between graphene sheets in a graphite crystal) is fundamentally important, since it is closely linked to the degree of graphitisation and hence also e.g. conductivities, and this distance is also shown in the left part of Figure 3. The importance of the interlayer

spacing will be further discussed and methods for determining it will be described in section 1.2.1. The average size (height $L_{c(002)}$and width $L_{a(110)}$) of graphite crystals also have a large impact on the physical properties of graphitic carbon materials and are often used for characterisation as well. There is a covariation between $L_{c(002)}$, $L_{a(110)}$ and $d_{(002)}$, and the crystallite dimensions increase with decreasing interlayer spacing. A general "true" correlation has never been established, although correlations based on empirical data exist, they most likely do not hold for all different types of graphitic materials.

Rhombohedral graphite is a thermodynamically unstable allotropic form of graphite. The structure of rhombohedral graphite can as best be considered an extended stacking fault in hexagonal graphite. Rhombohedral graphite cannot be isolated in pure form (natural graphite and laboratory preparations contain <40% of rhombohedral graphite in combination with hexagonal graphite). The distinction between rhombohedral graphite and hexagonal graphite is not further addressed in this report.

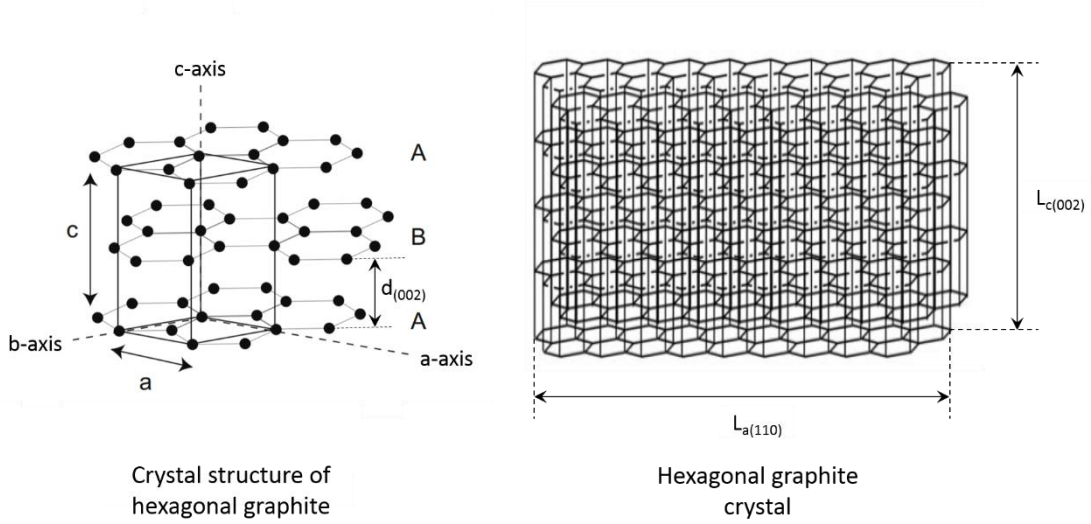


Figure 3. (Left) Crystal structure of hexagonal graphite with the unit cell constants a = 0.2462 nm and c = 0.6708 nm (since it is a hexagonal lattice a = b), as well as the inter-layer distance $d_{(002)}$. (Right) Hexagonal graphite crystal with the crystal width along the a-axis $L_{a(110)}$ and the crystal height $L_{c(002)}$ marked.

IUPAC defines *graphene* as: *"A single carbon layer of the graphite structure, describing its nature by analogy to a polycyclic aromatic hydrocarbon of quasi infinite size.",* with the note: *"Previously, descriptions such as graphite layers, carbon layers or carbon sheets have been used for the term graphene. Because graphite designates that modification of the chemical element carbon, in which planar sheets of carbon atoms, each atom bound to three neighbours in a honeycomb-like structure, are stacked in a three-dimensional regular order, it is not correct to use for a single layer a term which includes the term graphite, which would imply a three-dimensional structure. The term graphene should be used only when the reactions, structural relations or other properties of individual layers are discussed."* (Graphene - Chalk 2019). This, in another wording, means that graphene is a single graphite layer, consisting of a hexagonally arranged, two-dimensionally $sp^2$ bonded carbons. Single-layer graphene was explored theoretically already in 1947 (Wallace 1947), but it was first unambiguously produced and identified in 2004 by Novoselov, Geim et al. However, Andre Geim and Konstantin Novoselov credit

Hanns-Peter Boehm and his co-workers for the experimental discovery of graphene in 1962 (Boehm, Clauss et al. 1962). Boehm together with Setton and Stumpp also later suggested that *"A single carbon layer of the graphitic structure would be the final member of infinite size of this series. The term graphene layer should be used for such a single carbon layer."* (Boehm, Setton et al. 1986). This suggestion became generally accepted and was also officially adopted by IUPAC.

Even if, IUPAC defines graphene as *"*A *single carbon layer of the graphite structure"* the terms two-, three and few-layer graphene are commonly used in the scientific literature. This is because most graphene synthesis methods do not give perfect single layer graphene and in addition many methods give films or dispersions with varying number of graphene layers.

Graphene has a special set of properties which set it apart from other allotropes of carbon even graphite (although it is still here described in the graphite section since it is the basic building-block of graphite). Monolayer graphene shows a strength of 130 GPa (by assuming 0.335 nm thickness) (Lee, Wei et al. 2008), which is about 87 times stronger than the strongest (martensitic) steels, providing ultimate strength in final products of up to 1.5 GPa. Still, graphene's mass density of 2267 kg/m$^3$ is dramatically lower than any steel since low density steels being developed for the automotive sector typically do not reach below 6600 kg/m$^3$ (Zuazo, Hallstedt et al. 2014). In addition, graphene conducts heat and electricity very efficiently and is nearly transparent. Graphene also shows a large and nonlinear diamagnetism, even greater than that of graphite, and can be levitated by Nd-Fe-B magnets (Li, Chen et al. 2015).

### 1.1.4 Fullerenes (including other nanocarbons)

IUPAC defines fullerenes as *"Compounds composed solely of an even number of carbon atoms, which form a cage-like fused-ring polycyclic system with twelve five-membered rings and the rest six-membered rings. The archetypal example is [60]fullerene, where the atoms and bonds delineate a truncated icosahedron. The term has been broadened to include any closed cage structure consisting entirely of three-coordinate carbon atoms."* (Fullerenes - Chalk 2019). This with the broadened term means that fullerenes are molecules consisting of carbon atoms connected by single and double bonds to form a closed (according to IUPAC) or partially closed mesh (as it is used in the scientific litterature), with fused rings of five to seven atoms. Forming hollow spheres, ellipsoids, tubes, or many other shapes and sizes. Graphene (isolated atomic layers of graphite), which is a flat mesh of regular hexagonal rings, is an extreme member of the family, although it is here described as a member of the graphite allotrope since it is the basic building-block of graphite.

The 1996 Chemistry Nobel Prize was awarded to Harold W. Kroto, Robert F. Curl and Richard E. Smalley for their discovery of the new carbon allotrope fullerene in 1985. The new form was found to have the structure of truncated icosahedrons and was named Buckminsterfullerene, after the architect Buckminster Fuller who designed geodesic domes in the 1960's. The buckminsterfullerene then also gave name to the entire allotrope family, that is fullerenes.

Fullerenes with a closed mesh topology are informally denoted by their empirical formula $C_n$, often written Cn, where n is the number of carbon atoms. However, for some values of n there maybe more than one isomer. The closed fullerenes, especially $C_{60}$, are also informally called buckyballs for their geometrical resemblance of the standard football ("soccer-ball" in US English). Nested closed fullerenes have been named buckyonions. Cylindrical fullerenes are called carbon nanotubes or buckytubes. The bulk solid form of pure or mixed fullerenes is called fullerite.

Fullerenes have been extensively researched for several biomedical applications including the design of high-performance magnetic resonance imaging (MRI) contrast agents, X-ray imaging contrast agents, photodynamic therapy and drug and gene delivery, summarized in several comprehensive reviews, e.g. (Lalwani and Sitharaman 2013).

The cylindrical fullerenes, that is carbon nanotubes, can exhibit very high electrical and thermal conductivity, as well as high tensile strength due to their nanostructure and strength of the bonds between carbon atoms. These outstanding properties have resulted in already existing commercial uses especially within composites and adhesives. Current use of nanotubes has mostly been limited by the fact that current nanotubes available in bulk quantities contain rather unorganised fragments of nanotubes. Bulk nanotube materials may never achieve a tensile strength like that of individual tubes, but such composites may, nevertheless, yield strengths enough for many applications. Examples of use in composites and adhesives are Zyvex Technologies (2020), that produces carbon fiber prepegs and epoxy adhesives reinforced with carbon nanotubes, and Amroy Europe Oy (Pagni 2010) that for example produces a carbon nanotube reinforced epoxy resin HYBTONITE® that have used by Peltonen Ski Oy in their high-end cross-country skis (Peltonen Ski Oy 2018).

The high electrical and thermal conductivity as well as strength of carbon nanotubes have also led to a belief of more and refined commercial applications, in areas such as electronics, optics and composites. These areas are heavily researched and several reviews covering these future possibilities are available, for example (Sinnott and Andrews 2001, Li, Thostenson et al. 2008, Ma, Siddiqui et al. 2010, Cao, Cong et al. 2017).

### 1.1.5 Glass-like carbon

IUPAC defines glass-like carbon as *"An agranular non-graphitizable carbon with a very high isotropy of its structural and physical properties and with a very low permeability for liquids and gases. The original surfaces and the fracture surfaces have a pseudo-glassy appearance."* (Glass-like carbon - Chalk 2019). IUPAC further notes that "*The often used synonyms 'glassy carbon' and 'vitreous carbon' have been introduced as trademarks and should not be used as terms. From a scientific viewpoint, all synonymous terms suggest a similarity with the structure of silicate glasses which does not exist in glass-like carbon, except for the pseudo-glassy appearance of the surface. Glass-like carbon cannot be described as amorphous carbon because it consists of two-dimensional structural elements and does not exhibit 'dangling' bonds.".*

Due to its bonding and mesoscale structure, as described above, glass-like carbon gets properties that are a combination of glassy and ceramic properties and of graphite properties. As a consequence, glass-like carbons have high temperature resistance, high

hardness (7 Mohs), low density, low electrical resistance, low friction, low thermal resistance, extreme resistance to chemical attack and good barrier to gases and liquids. Due to its physical properties, glass-like carbon is widely used as an electrode material in electrochemistry, as well as for high temperature crucibles and as a component of some prosthetic devices, especially artificial heart valves (Sarna, Kozakiewicz et al. 2016). Glass-like carbon is normally manufactured by controlled pyrolysis of an organic polymer (Sarna, Kozakiewicz et al. 2016). The processing must be precisely controlled and the thickness in at least one dimension small to ensure elimination of the volatile products generated by the pyrolysis.

The structure of glassy carbon has long been a subject of debate. Early structural models assumed that both $sp^2$- and $sp^3$-bonded atoms were present, but it is now known that glassy carbon is very close to 100% $sp^2$ (Terranova, Polini et al. 1992, O'Malley, Snook et al. 1998). More recent research has suggested that glassy carbon has a fullerene-related structure (Harris 2004).

Glass-like carbon, often also referred to as vitreous carbon, can be produced as a foam. It is then called reticulated vitreous carbon (RVC). This foam was first developed in the mid to late 1960s as a thermally insulating, microporous glassy carbon electrode material. RVC foam is a strong, inert, electrically and thermally conductive, and corrosion resistant porous form of carbon with a low resistance to gas and fluid flow. Due to these characteristics, the most widespread scientific and commercial use of RVC is as a three-dimensional electrode in electrochemistry (Walsh, Arenas et al. 2016). Additionally, RVC foams are characterized by an exceptionally high void volume, high surface area, and very high thermal resistance in non-oxidising environments, which allows for heat sterilization and therefore the material have gained research interest in the medical field and some limited clinical use (Pec, Reyes et al. 2010, Czarnecki, Blackmore et al. 2014).

The typical production process of reticulated vitreous carbon starts with reticulation of a polyurethane foam, that is making the foam even more porous and light by mechanical, thermal or chemical means. The reticulated polyurethane foam is then impregnated with a thermosetting resin such as furfuryl alcohol or phenyl-formaldehyde resin or a thermally stable polymer that is easy to carbonise such as polyimides. Thereafter, the polymer composite is carbonised at high temperature, and the polyurethane is then decomposed whereas the resin or thermally stable polymer, e.g. polyimide, is turned into $sp^2$-bonded glass-like carbon (Sarna, Kozakiewicz et al. 2016).

One particularly interesting thing with glass-like carbon and reticulated vitreous carbon are that they have been successfully produced from biomass. Törmälä and Romppanen (1981) successfully produced glass-like carbon from different lignin's and lignin condensates, although this has not been done on a commercial scale. Yuan, Ding et al. (2016) produced carbon foam, similar to reticulated vitreous carbon, from ordinary baking flour. The carbon foam was obtained by mixing the flour with water and fermenting with conventional yeast, followed by baking at 180 °C for 40 min and drying the bread at 80 °C for 18 hours, before finally carbonizing the bread in an inert atmosphere at temperatures ranging from 500 to 2000 °C. The carbon foam obtained by carbonisation at 2000 °C was both stiff with a compressive modulus of 60 MPa, had a rather low density with a value of 273 kg/m$^3$, and was somewhat electrically conductive with an electrical conductivity of 0.38 S/cm. The elastic modulus of 60 MPa obtained at 2000 °C is lower to a commercial reticulated vitreous carbon foam Duocel® from ERG Aerospace Corporation which shows

an elastic modulus of 100 MPa. However, Yuan, Ding et al. (2016) obtained the highest elastic modulus of 120 MPa after carbonisation at 1000 °C, which is rather similar as the commercial vitreous carbon foam. The commercial foam still, showed a much lower density of 45 kg/m$^3$ and higher electrical conductivity of 3 S/cm compared to best values obtained by Yuan, Ding et al. (2016), that were 80 kg/m$^3$ (HTT 500 °C) respectively 0.38 S/cm (HTT 2000 °C). Despite the inferior density and electrical conductivity, the ability to make rather well performing carbon foam from bread, is inspiring and show potential for biomass derived reticulated vitreous carbon.

### 1.1.6 Atomic and diatomic carbon

Free atomic and diatomic carbon are extremely unstable at ambient conditions and will immediately auto-polymerise. Though, atomic carbon can be formed and studied by passing large electric currents through carbon under very low pressures (Shevlin 1972). Atomic carbon is also an intermittent product used in the creation of carbenes. Diatomic carbon can be found under certain conditions and can be detected spectroscopically in extra-terrestrial bodies, including comets and certain stars (Chaffee Jr and Lutz 1978, Federman and Huntress Jr 1989).

### 1.1.7 Carbon nanofoam

Carbon nanofoam is a three-dimensional structure that consists of several carbon tendrils (slender threadlike structures) loosely bound together to form a mist-like arrangement similar to that observed in the case of an silica based aerogels (Dorcheh and Abbasi 2008, Katagiri, Ishikawa et al. 2015). Carbon nanofoam was discovered in 1997 by Andrei V. Rode and co-workers at the Australian National University in Canberra whom by ultrafast laser ablation of a carbon target in Argon gas at low pressure (1-100 torr) was able to produce the material (Rode, Hyde et al. 1999). The tendrils are made of randomly interconnected nano-sized clusters of sp$^2$-bonded carbon with a regular hexagonal pattern, just like in a graphite sheet, but given a negative curvature owing to the inclusion of heptagons (this is the opposite of what happens in the case of buckminsterfullerene's in which carbon sheets are given positive curvature by the inclusion of pentagons), with the clusters being bonded together by sp$^3$-bonds (and the ratio of sp$^3$ bonds usually being 15-45%) (Rode, Gamaly et al. 2000).

The material is very light, with a density of 2 kg/m$^3$, which is not far from standard air density at mean-sea-level of 1.225 kg/m$^3$ (ISO 2533:1975). The density of carbon nanofoam is also much lower than that of carbon aerogels based on polymerization of resorcinol (1,3-dihydroxybenzene) with formaldehyde followed by carbonisation which do not reach below 30 kg/m$^3$ (Pekala and Schaefer 1993), but superseded by the extremely low density of graphene cellular elastomers that reaches densities as low as 0.16 kg/m$^3$, by excluding the weight of the air within the material (Qiu, Huang et al. 2017).

### 1.1.8 Carbide-derived carbon

Carbide-derived carbon (CDC), also known as tuneable nanoporous carbon, is the common term for carbon materials derived from carbide precursors, such as binary (e.g. SiC, TiC), or ternary carbides e.g. $Ti_2AlC$, $Ti_3SiC_2$, using chlorine treatment, hydrothermal synthesis, or high-temperature selective metal desorption under vacuum (Presser, Heon et al. 2011). Depending on chosen synthesis method, carbide precursor and specific conditions, different carbon allotropes can be generated ranging from particles composed of predominantly amorphous carbon, carbon nanotubes, epitaxial graphene, nanocrystalline diamond, onion-like carbon, to graphitic ribbons, barrels, and horns. Thus, carbide-derived carbon can be seen as a methodology to achieve other carbon allotropes, but the ability to control the pore size at sub-Ångström accuracy (Gogotsi, Nikitin et al. 2003), make carbide-derived carbons extremely interesting for many different applications.

### 1.1.9 Lonsdaleite - hexagonal diamond

Lonsdaleite, also called hexagonal diamond in reference to the crystal structure, is an allotrope of carbon with a hexagonal lattice. In nature, it forms when meteorites containing graphite strike the Earth. It is believed that the great heat and stress of the impact transforms the graphite into diamond, but retains graphite's hexagonal crystal lattice (Frondel and Marvin 1967).

Hexagonal diamond was first synthesised in the laboratory by Bundy and Kasper (1967) by applying a static pressure exceeding 13 GPa and a temperature greater than 1000 °C to a well-crystallised graphite sample. It has also later been produced by chemical vapor deposition (Bhargava, Bist et al. 1995), as well as by the thermal decomposition of poly(hydridocarbyne) under argon atmosphere at 1000 °C and atmospheric pressure (Nur, Pitcher et al. 2008).

The hardness of lonsdaleite is theoretically superior to that of the common cubic diamond (Xiao-Ju, Bo et al. 2008, Pan, Sun et al. 2009, Fan, Chai et al. 2018), but measurements on natural specimens have not strengthened this theory and it has been speculated that the cause was that the natural samples contained excessive lattice defects and impurities (Carlomagno 2011).

### 1.1.10 Carbyne - linear acetylenic carbon

Carbyne, also called linear acetylenic carbon, is a carbon allotrope of linear repeating alkyne units, i.e. $(-C\equiv C-)_n$, which gives alternating single and triple bonds. A. M. Sladkov and Y.P. Kudryavtsev claimed to have synthesised carbyne in the 1960s (Sladkov and Kudryavtsev 1969). However, Smith and Buseck re-examined these results in 1982 and claimed that the carbynes which had generally been recognized by their characteristic hexagonal electron diffraction pattern, in reality came from silicate minerals giving rise to hexagonal diffraction patterns with a similar range of interplanar spacings as carbyne was said to have (Smith and Buseck 1982). They recommended *"that in future searches for carbyne, energy-dispersive X-ray analyses should be conducted to verify the chemistry of individual, carbyne-candidate grains"*.

Since then the existence or non-existence of carbyne has been heavily researched and debated. Many studies suggesting successful synthesis of carbyne have been published, but most have been criticised by other scientists who argued and made publications suggesting that it was not true. As an example, Lagow, Kampa et al. (1995) claimed that they had successfully synthesised carbynes although containing some fullerenes, but later Kroto (2010) simply stated that "*The existence of carbyne is myth based on bad science and perhaps even wishful thinking*" using arguments such that the synthesis conditions used to synthesise carbynes (in publications claiming their existence) had previously resulted in fullerenes and not carbynes. Shi, Rohringer et al. (2016) synthesised linear chains of up to 6,000 sp-hybridised carbon atoms inside double-walled carbon nanotubes, giving rather convincing arguments for the existence of carbynes.

Theoretical simulations have predicted that carbyne will have an elastic modulus of 43.5 TPa, which is approximately forty times more than for cubic diamond which has an elastic modulus of 1050 GPa (Itzhaki, Altus et al. 2005). Later theoretical simulations have predicted a somewhat lower, but still very high, elastic modulus of 32.7 TPa (Liu, Artyukhov et al. 2013). These later simulations also addressed the tensile strength and predicted it to be impressively 2.2 TPa. In 2012 S. A. Kotrechko et al. published the first experimental measurements on the tensile strength of carbyne to be 181 GPa at 77 K, a value obtained by high-field mechanical loading in a field-ion microscope (Kotrechko, Mazilov et al. 2012). It should be noted that this is significantly higher than the record high tensile strength of 130 GPa reported for graphene (Lee, Wei et al. 2008). In a later publication Kotrechko, Mikhailovskij et al. (2015) also considered the elastic modulus, which was obtained to be 4631 GPa after calculations based on experimental. In this publication they also "up-graded" the strength of carbyne to 251 GPa at T = 77 K. These extreme mechanical properties (real or not), naturally make carbyne an interesting material in the nanotechnology field.

### 1.1.11 Cyclocarbons

A cyclo[n]carbon is a chemical compound consisting solely of an n number of carbon atoms covalently linked in a ring. Since the compound is composed only of carbon atoms, it is considered an allotrope of carbon. Possible bonding patterns include all double bonds (a cyclic cumulene) or alternating single bonds and triple bonds (a cyclic polyyne). The smallest cyclo[n]carbon, predicted to be thermodynamically stable, is C18, with a computed strain energy of 72 kilocalories per mole (Diederich, Rubin et al. 1989, Adamson and Rees 1996). In 2019 an IBM/Oxford based team claimed to have synthesized this molecule in solid state (Kaiser, Scriven et al. 2019), and according to them the molecule has alternating triple and single bonds, rather than being made of entirely of double bonds.

### 1.1.12 Complexity of carbon materials

Despite the already complex classification of carbons into different allotropes, the picture of carbon materials is even more complex since most/all carbon materials at the ultrastructure level consist of different allotropes. One example is natural and synthetic graphite that always contain some turbostratic (a crystal structure in which basal planes

have slipped out of alignment) carbon, and thus cannot be said to be graphitic. The amount of turbostratic carbon (inverse to degree of graphitisation) depend on raw material and processing conditions (Franklin 1951, Akamatu, Inokuchi et al. 1956, Ōya and Marsh 1982, Oberlin 1984, González, Montes-Morán et al. 2002, Kwiecińska and Petersen 2004)

## 1.2 Characterisation of graphitic carbon materials

To understand and develop carbon materials, one need to know the fundamentals of what gives them their properties, and ways of measuring them. Depending on the intended use of a carbon material, different physical properties become relevant. Since the present review report focuses on graphitic carbon materials, this entire section is attributed to characterisation of graphitic carbons.

In Figure 4 below an overview of the six steps that are needed for a complete characterisation of a carbon material and thirteen different methods that are relevant for characterisation. The crystal structure and degree of graphitisation are detrimental for itselectrical and thermal conductivity, which are the two most important properties for applications within electronics and electrical energy storage. This further highlights the importance of being able to correctly analyse the structure of graphitic carbons. Because of this, the focus will here be mostly on the “structure” part, i.e. crystalline vs amorphous, graphitic vs turbostratic, and size of crystallites. Orientation of the crystallites is also important for the electrical and thermal conductivity, especially for the anisotropy of these two properties.

Common methods to study and determine the degree of graphitisation and other important properties, such as crystallite size and orientation, are X-ray powder diffraction (XRD), sometimes also referred to as X-ray crystallography (XRC), Raman spectroscopy, measurement of magnetoresistance (i.e. change of resistance with applied magnetic field) and transmission electron microscopy (TEM). XRD is usually the preferred method, and the below descriptions on how to determine the important parameters show how this is done. While good and most often preferred, XRD give average values, while TEM on the other hand is the only technique able to bring out the heterogeneity of phases which are different in morphology and in micro-texture. In addition to what is written below about determining important parameters for graphitic carbon materials using XRD, it may be difficult to operate the equipment. Iwashita (2016) advices on what an operator needs to consider.

Also, a section on Raman microscopy is included, since some reviewed articles included this technique, which can be compared to publications where XRD was used. Then it is good to have knowledge about how Raman spectroscopy data can be converted into XRD measured parameters, while being aware that this conversion will never be perfect. To get the very best characterisation of graphitic carbon materials, especially for understanding the development from less-ordered carbon towards graphite structure, it is recommended to combine XRD, Raman spectroscopy and TEM. This is exemplified in the article by Vázquez-Santos, Geissler et al. (2011), whom studied the graphitization of poly(p-

phenylene benzobisoxazole) (PBO) fibres by increased heat-treatment and clearly saw that the three different methods gave complementary information.

For the reader interested in deeper knowledge of carbon materials characterisation in general, the book "Materials science and engineering of carbon: characterization" by Inagaki and Kang (2016) is highly recommended.

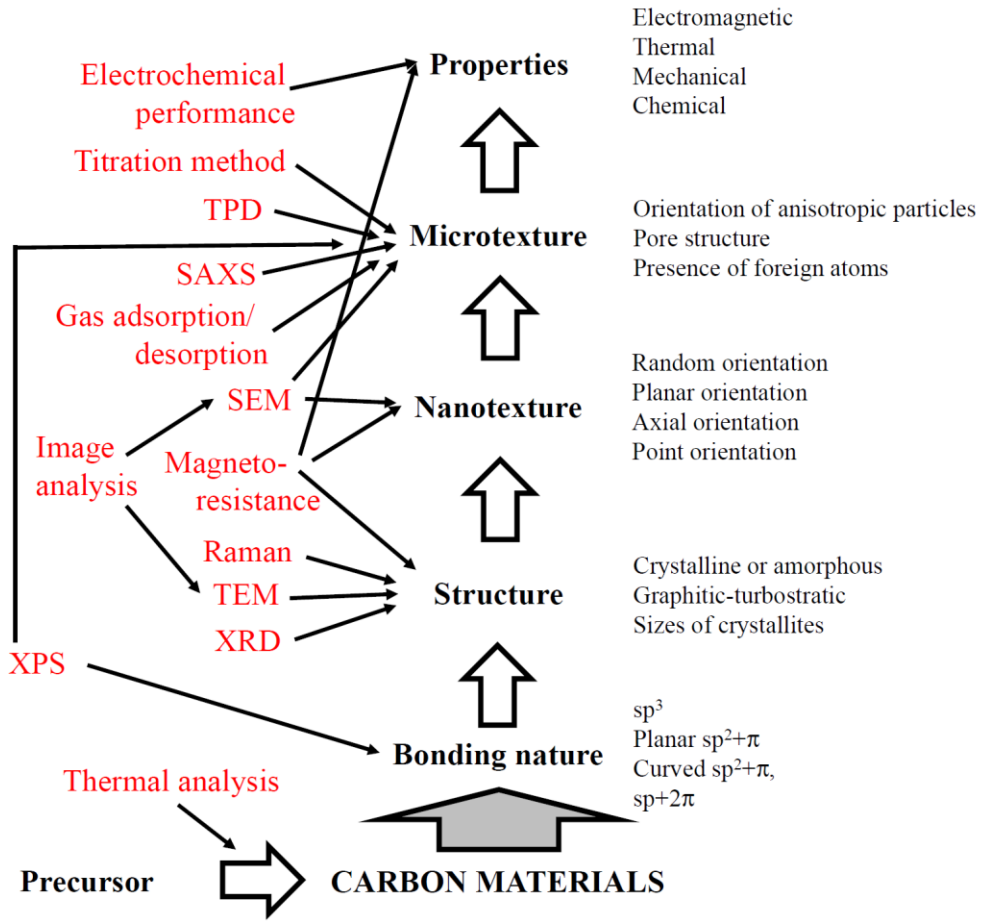


Figure 4. Six steps for complete characterisation of carbon materials (including precursor) and 13 applicable techniques (Inagaki and Kang 2016).

## 1.2.1 Determination of interlayer spacing, degree of graphitisation, crystallite size and crystallite orientation

### 1.2.1.1 Interlayer spacing

The distance, $d_{(002)}$ as shown in Figure 3 above, between graphene layers in a graphitic carbon material is a very important structural parameter and is closely linked to the degree of graphitisation, i.e. how close to perfect crystalline graphite a material is, and more information on this correlation is given in section 1.2.1.2 below. The value of $d_{(002)}$ is calculated from the position of the 002-peak in an XRD profile (see Figure 5) using Bragg's law (Eq. 1 below).

$$2d \cdot \sin\theta = n\lambda \qquad \text{(Eq. 1)}$$

$$d_{(002)} = \frac{\lambda}{2 \cdot \sin\theta} \quad \text{where } \lambda \text{ is the x-ray wavelength} \qquad \text{(Eq. 2)}$$

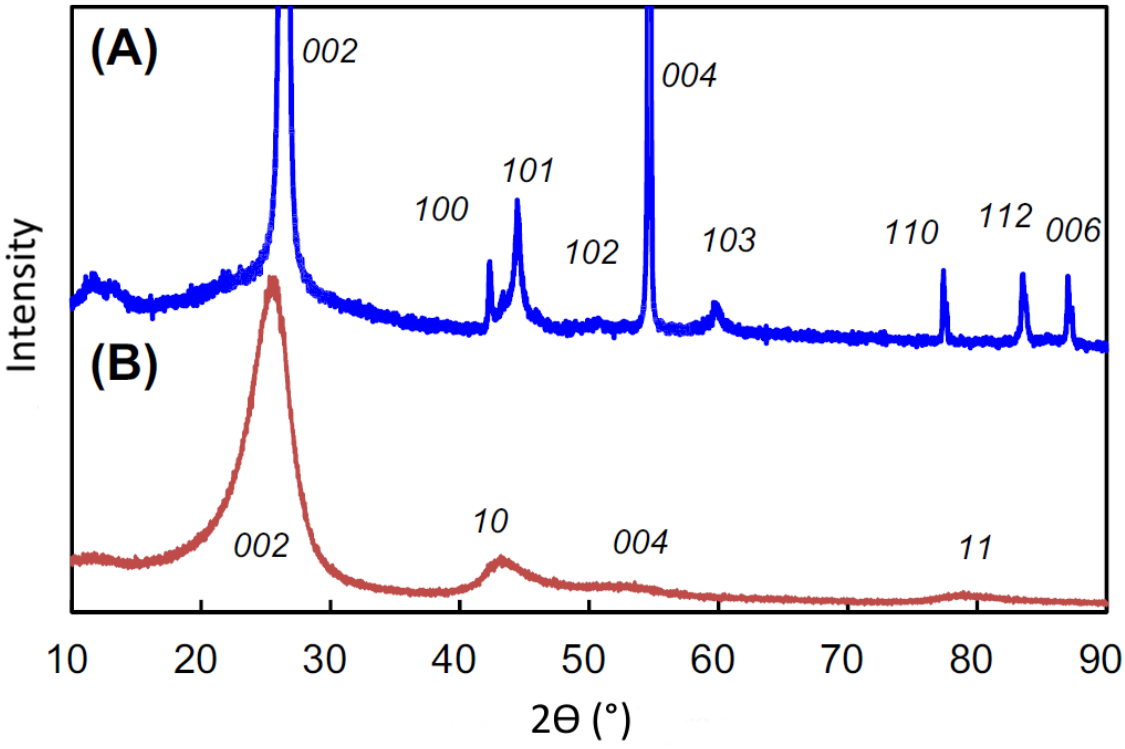


Figure 5. XRD profile for two different graphitic carbon materials, (A) natural graphite and (B) coke heat-treated at 1200 °C. Note that when using the position of the 002-peak together with Bragg's law that the position on the x-axis is 2Θ and that it is Θ that should be used in the Bragg equation (Inagaki and Kang 2016).

### 1.2.1.2 Degree of graphitisation

The best way to calculate "degree of graphitisation" is to determine the probability for adjacent hexagonal layer planes in parallel to having regular graphitic AB stacking, usually denoted $P_1$, as described by Warren (1941), and Houska and Warren (1954). The degree of graphitization ($P_1$) is calculated from the Fourier analysis of XRD profiles of hk lines, see (Houska and Warren 1954) and (Iwashita 2016) for details.

Iwashita and Inagaki (1993) measured $P_1$ and $d_{(002)}$ for various carbon (non-graphitic and graphitic) and the result is shown in Figure 6 below. As seen, there is a strong but not linear relationship between $P_1$ and $d_{(002)}$. For some reason the probability for adjacent hexagonal layer planes in parallel to having regular graphitic AB stacking, $P_1$, is seldom measured and reported within the scientific literature. However, $d_{(002)}$ is far more often measured and reported. In this report the degree of graphitisation reported by the authors were used directly, but in the cases that values on $d_{(002)}$ were given but no values on the degree of graphitisation it was calculated according to the model given by (Maire and Mering 1970):

$$\text{Degree of graphitisation} = g = \frac{0.3440 - d_{(002)}}{0.3440 - 0.3354} \quad \text{with } d_{(002)} \text{ in nm} \qquad \text{(Eq. 3)}$$

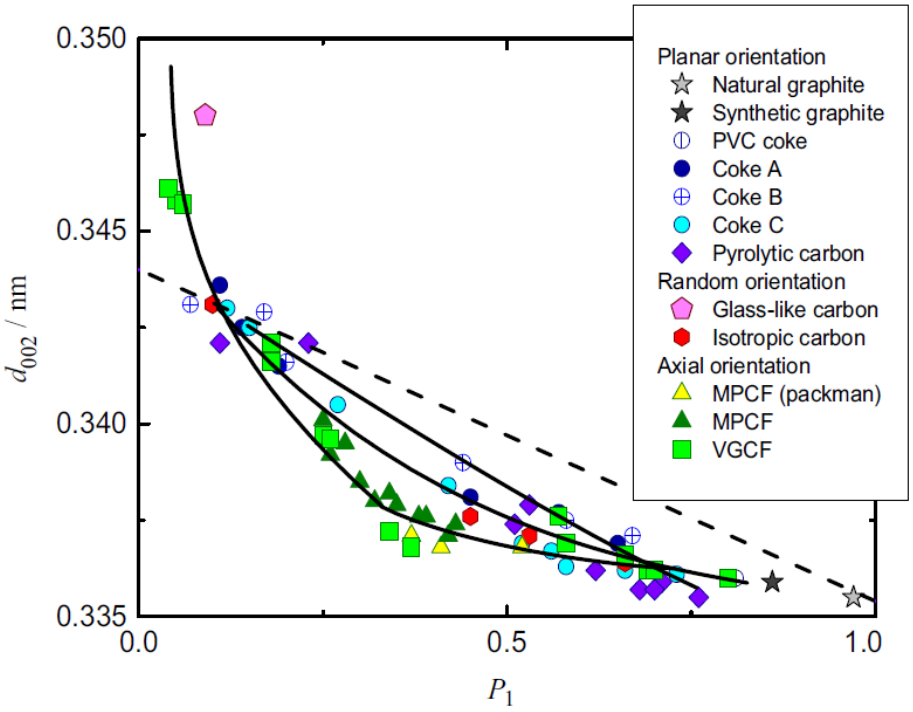


Figure 6. $d_{(002)}$ plotted as function of $P_1$. The strong but non-linear correlation is obvious. Figure copied from (Inagaki and Kang 2016). (MPCF = Mesophase pitch carbon fibre, VGCF = Vapour grown carbon fibre, PVC coke = Coke derived from poly vinyl chloride)

### 1.2.1.3 Determination of crystallite size

The apparent crystallite thickness, $L_c$, is determined using the 002-peak and Scherrer's equation (Eq. 4), whereas to determine the apparent crystallite length/width, $L_a$, the 100- or 110-peak should be used.

$$L = \frac{K\lambda}{\beta \cdot \cos\theta} \qquad \text{(Eq. 4)}$$

Where θ is the scattering angle, λ is the wavelength of the X-rays used, β is the full width at half maximum intensity (FWHM) and K the shape factor. To determine $L_c$ a K-value of 0.9 and to determine $L_a$ a K-value of 1.84 is usually used. It should, however, be noted that the definitions of the crystallite sizes and the meanings of their numerical values are not yet well defined, but crystallite sizes can be used as engineering parameters (Iwashita 2016).

In publications missing values on crystal length/width ($L_a$) and/or crystal height ($L_c$), but having data on $d_{(002)}$, the crystallite dimensions were calculated/estimated using the following empirically derived equations proposed by (Maahs 1968):

$$L_a(nm) = \frac{0.74}{d_{(002)} - 0.3354} \qquad \text{(Eq. 5)}$$

$$L_c(nm) = \frac{3.24}{\sqrt{d_{(002)} - 0.3354}} \quad , with\ d_{(002)}\ having\ the\ unit\ nm \qquad \text{(Eq. 6)}$$

### 1.2.1.4 Determination of crystallite orientation

The degree of misorientation or preferred orientation (in both cases: low value = high orientation) of graphite crystallites to the a-axis (i.e. parallel to the basal plane) can be determined by making an azimuthal scan (X-ray source keep fixed and the sample rotated) at the fixed Bragg position of the 002-reflection and measure/calculate the full width at half maximum (FWHM), commonly denoted Z, see Figure 7 below.

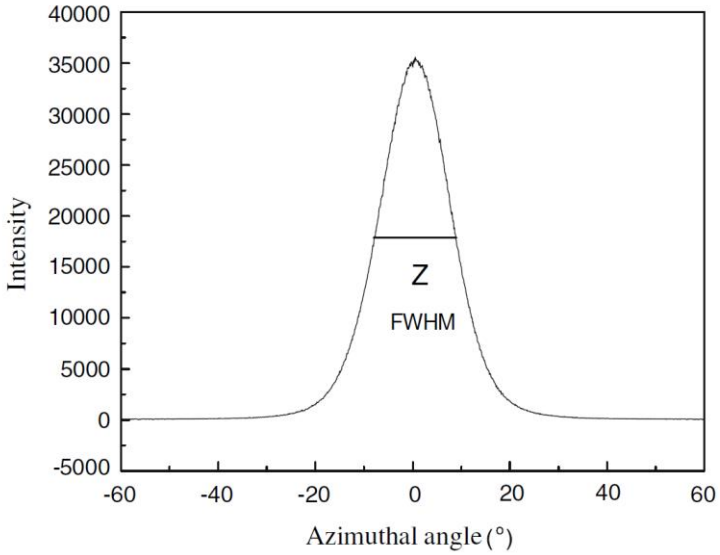


Figure 7. Example of a result of an azimuthal scan at the fixed Bragg position of the 002-reflection and how the full-width at half maximum (FWHM), the same as the degree of misorientation or preferred orientation, usually denoted Z, is calculated/measured.

### 1.2.1.5 Raman spectroscopy

Raman spectroscopy is also useful, valuable, and commonly used to characterise graphitic carbon materials. This report will not go through how Raman spectroscopy is used for that purpose and the interested reader is referred to chapter 7 (Kaburagi, Yoshida et al. 2016) in the book edited by (Inagaki and Kang 2016). In publications with Raman data only values of $d_{(002)}$, $L_c$, and $L_a$ were estimated. $L_a$ was calculated based on the $I_D/I_G$ ratio using the equation developed by Cançado, Takai et al. (2006) (equation 7 below) examining nano graphite's with both XRD and Raman. The equation was also later applied to the graphitisation poly(p-phenylene benzobisoxazole) (PBO)-derived carbon fibres by Vázquez-Santos, Geissler et al. (2011) with fair but far from perfect agreement between the XRD and Raman obtained values on $L_a$. Then, $d_{(002)}$ was calculated from the obtained $L_a$-value using equation 5 above, and finally $L_c$ was calculated from the obtained value of $d_{(002)}$ (using equation 6 above).

$$L_a(nm) = (2.4 \cdot 10^{-10})\lambda_l{}^4 \left(\frac{I_D}{I_G}\right)^{-1} \qquad \text{(Eq. 7)}$$

*where $\lambda_l$ is the excitation wave length of the laser in nm*

Even if Raman spectroscopy is a valuable and commonly used technique to characterise graphitic carbon materials it must, however, be recognised that it has fundamental differences as compared to X-ray powder diffraction (XRD). The interpretation of $L_a$ data as calculated from Raman spectroscopy is different because the technique is not based on a diffraction phenomenon but on propagation of phonons (vibrational spectroscopy). Only a mean size of carbon layers along which vibrations propagate is concerned. This propagation is stopped only by the boundaries of the layers (or by a "physical end", or by defects bordering the layers). When a layer is bent, the coherent domains as detected by XRD are reduced, whereas phonon propagation is not stopped. Consequently, the mean $L_a$ deduced from Raman is larger, and could be much larger than the value calculated from XRD. Moreover, the use of the Raman intensity ratio $I_D/I_G$ to measure/estimate the degree of graphitisation, most likely is different with respect to each carbon material and should be interpreted more cautiously compared to XRD results. Furthermore, Raman measurements only characterizes locally in the area of the laser spot-size (typically 0.5-10 μm diameter) with a penetration depth of ~0.1 to 0.2 μm from the surface and thus does not consider the disorder contribution from the bulk. X-ray measurements which may probe as deep as 500 μm for carbon materials gives a much better bulk measurement.

# 2 Production methods for graphitic carbon materials

## 2.1 Natural graphite

Naturally occurring graphite (referred to as natural graphite) is mined from bedrock that has high content of high-quality graphite (Olson, Virta et al. 2016, Robinson, Hammarstrom et al. 2018, Jara, Betemariam et al. 2019).

## 2.2 Pyrolysis, carbonisation, hydrothermal carbonisation and graphitisation

### 2.2.1 Pyrolysis

Pyrolysis is the thermal decomposition of materials at elevated temperatures in an inert atmosphere, i.e. no oxygen, since presence of oxygen would result in combustion at elevated temperature. It involves a change of chemical composition and is irreversible. In general, pyrolysis of organic substances produces volatile products and leaves a solid residue enriched in carbon, char. The process is used heavily in the chemical industry, for example, to produce ethene (ethylene) and other chemicals from petroleum and coal (sedimentary rock). Pyrolysis of animal and plant tissue such as wood convert it to charcoal. Aspirational

applications of pyrolysis would convert biomass into syngas and biochar, waste plastics back into usable oil, or waste into safely disposable substances.

### 2.2.2 Carbonisation

Extreme pyrolysis, which leaves mostly carbon as the residue, is called carbonisation. Carbonisation typically starts at around 300 °C depending on which material that is carbonised. For wood the transformation to charcoal is practically complete at 400 °C. The charcoal at this temperature still contains appreciable amounts of tar (dark brown or black viscous liquid of hydrocarbons and free carbon), typically 30% by weight trapped in the structure. This soft burned charcoal needs further heating to drive off more of the tar and thus raise the fixed carbon content. This is usually done by heating to 500 °C that raises the fixed carbon content to about 75% which is a normal value for good quality commercial charcoal. If the carbonisation is continued up to 1000 °C the content of tar and volatiles drops to close to zero, but the over-all yield (remaining solids) of the carbonisation process also becomes as low as 25% (Beaumont 1985).

In the production of graphite electrodes for steelmaking a mixture of calcined petroleum coke filler particles mixed with coal tar pitch is carbonised at temperature between 700 and 1200 °C. Sometimes re-impregnation with petroleum tar pitch and re-carbonisation are repeated to fill the pores generated due to impurities in the filler and volatility of the binder is made for a desired number of times. After completion of the re-impregnation and re-carbonisation process the electrode consists almost of pure carbon, but to give it its desired electrical conductivity it is graphitised at elevated temperature to 2500-3000 °C, giving it a structure that is close to true graphite (Tamashausky 2006, Lee, Kang et al. 2015).

### 2.2.3 Hydrothermal carbonisation

Hydrothermal carbonisation (HTC) is a chemical process for the conversion of organic compounds to structured carbons. It can be used to make a wide variety of nanostructured carbons, simple production of brown coal substitute, synthesis gas, liquid petroleum precursors and humus from biomass with release of energy. It also opens the field of potential feedstocks for char production to a range of non-traditional renewable and plentiful wet agricultural residues and municipal wastes (Libra, Ro et al. 2011). Hydrothermal carbonisation is, however, not a very good process for making graphitic carbon materials and therefore not reviewed or described in detail in this report.

### 2.2.4 Graphitisation

Graphitisation is made by heating to a temperature in the range 2500-3000 °C. If this results in highly graphitic carbon with crystalline structure close to that of true graphite depends on which precursor material that is heated. Some precursors are graphitising (so called soft carbon precursors), e.g. petroleum coke, polyvinyl chloride (PVC) and polyimides, whereas other precursors are non-graphitising precursors (so called hard carbon precursors), e.g. polyacrylonitrile (PAN), polyvinylidene chloride (PVDC) and essentially all biomass. Graphitising carbon precursors transforms into highly graphitic and crystalline material when heated to between 2500 and 3000 °C or higher, whereas

non-graphitising carbon precursors cannot be transformed into highly graphitic and crystalline material at any temperature, but into turbostratic non-graphitic carbon that by all means can have very different properties than the precursor itself. See Figure 8 for an illustration of how non-graphitising precursors, i.e. lignin, cellulose and polyacrylonitrile (PAN), are transformed to none crystalline turbostratic carbon, whereas mesophase pitch (derived from for example petroleum coke and coal tar pitch) transforms to highly graphitic and crystalline carbon. Turbostratic carbon materials can have fair electrical and thermal conductivity but will not reach as high values as highly graphitic and crystalline carbon materials derived from graphitising precursors. Note, the use of the term "*graphitisation*" to indicate a process of thermal treatment of carbon materials at T > 2500 K regardless of any resultant crystallinity is incorrect (Graphitization - Chalk 2019), and if a carbon material is heated to above 2500 K without becoming highly graphitic and crystalline the expression *"graphitization heat treatment"* should be used instead .

Graphitising carbon precursors pass through a fluid stage during carbonisation and graphitisation. This fluidity facilitates the molecular mobility of the aromatic molecules, resulting in intermolecular dehydrogenative polymerisation reactions to create aromatic, lamellar (disc-like) molecules. These "associate" to create a new liquid crystal phase, the so-called mesophase that easily can transform to highly crystalline and graphitic carbon. The existence of this fluid phase is a requirement for a carbon precursor to be graphitising (Marsh and Diez 1994).

Graphitisation of polyimides by high-temperature treatment (~3000 °C) has shown to create highly graphitic carbon with very good electrical and thermal in-plane conductivity, and has in commercial applications to a large extent replaced pyrolytic carbon/graphite sheets produced by chemical vapour deposition (Jiangxi Dasen Technology Co. Ltd. 2020, Panasonic Corporation 2020a).

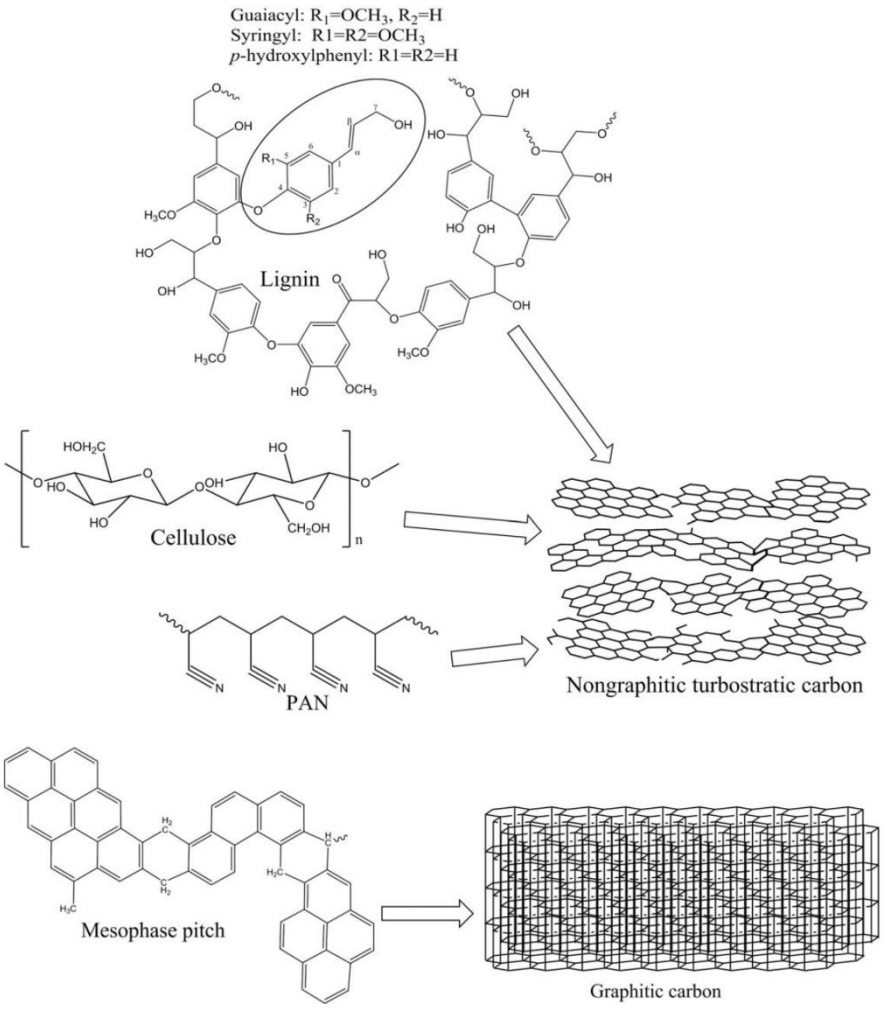


Figure 8. Illustration of non-graphitising precursors, lignin, cellulose and polyacrylonitrile (PAN), as they are transformed to non-crystalline turbostratic carbon, whereas mesophase pitch (derived from graphitising precursors, for example petroleum coke and coal tar pitch) transforms to highly graphitic and crystalline carbon upon heating to above 2500 °C.

### 2.2.5 Effect of heat treatment temperature in carbonisation and graphitisation

There are many studies on how the heat treatment temperature (HTT) affects carbonisation and graphitisation of fossil-based and bio-based raw materials.

Ogale, Lin et al. (2002) made an excellent study on the effect of HTT from no heat treatment (0 °C) up to 2875 °C on mesophase pitch-based carbon fibres. Figure 9 below shows how the interlayer spacing $d_{(002)}$ decreases with increasing HTT, i.e. an increase in degree of graphitisation, as well as increase in crystallite size in both a-plane ($L_a$) and c-plane direction ($L_c$), as well as reduction in misorientation angle, Z. The misorientation angle, Z, show a slight a tendency, but probably not significant to increase up to 600 °C where after it steadily decreases approaching zero degrees close to a HTT of 2875 °C, thus showing a trend very similar to $d_{(002)}$, $L_a$ and $L_c$.

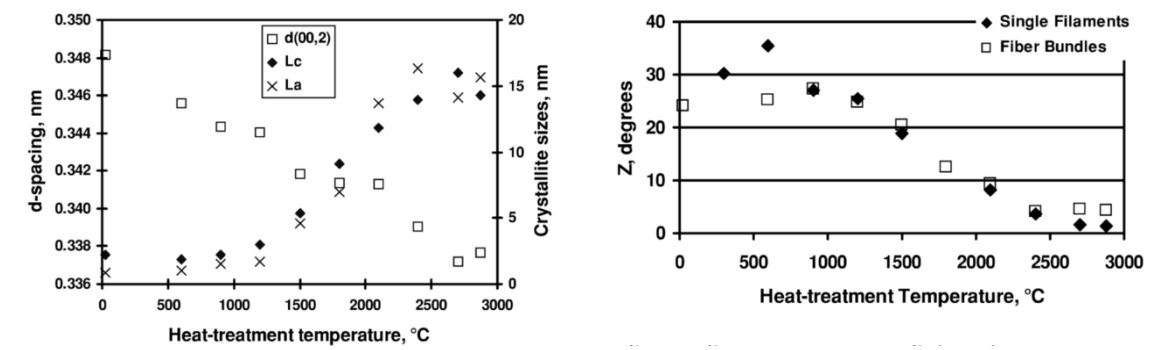


Figure 9. d-spacing ($d_{(002)}$), crystallite size in both a-plane ($L_a$) and c-plane direction ($L_c$), and the misorientation angle, Z, plotted as function of heat-treatment temperature (HTT). Figure copied from (Ogale, Lin et al. 2002).

Also Rhim, Zhang et al. (2010), have made a really good study of the effect of heat-treatment temperature (250 to 2000 °C) on the graphitisation heat treatment of microcrystalline cellulose, including measurements of electrical conductivity as well as the chemical and microstructure evolution. This was studied by Energy dispersive X-ray spectroscopy (EDS), X-ray photoelectron spectroscopy (XPS), Raman spectroscopy, and high-resolution transmission electron microscopy (HR-TEM). This article is a highly recommended read for all interested in carbonisation of cellulose. What they found was in short as follows: In the temperature 250–350 °C region, a decrease in alternating current (AC) conductivity occurs due to the loss of polar oxygen-containing functional groups from cellulose molecules. Going further up in temperature into the 400–500 °C, the AC conductivity starts to increase with heat treatment temperature due to the formation and growth of electrically conducting clusters, composed of crystalline $sp^2$-bonded carbon, surrounded by an amorphous matrix consisting of both $sp^3$- and $sp^2$-bonded carbon. Increasing the temperature even further to the region 550–600 °C, a further increase of AC conductivity with increasing heat treatment temperature is observed. In addition, the AC conductivity demonstrates a non-linear frequency dependency due to electron hopping, interfacial polarization, and onset of a percolation threshold. In next temperature region, 610–1000 °C, a frequency independent conductivity (direct current (DC) conductivity) is observed and continues to increase with increasing temperature due to growth and further percolation of electrically conductive $sp^2$-bonded carbon clusters.

Finally, in the highest temperature region studied, 1200–2000 °C, the DC conductivity reaches a plateau, and do not increase with increasing temperature as the system reaches a fully percolated state at 1200 °C, whilst the amorphous low conducting matrix remains at temperatures above this. It is especially recommended to take a close look at figure 2 in the article, were it can be seen that the increase of percentage of graphitic (C=C) and aliphatic (C-C) as well as bonds able to undergo a $\pi \rightarrow \pi^*$ transition (i.e. the promotion of an electron from a π-bonding orbital to an antibonding π orbital*) with increasing temperature correlates very well with how the electrical conductivity increases with increasing temperature. See below for a visual illustration of how the electrical conductivity increases with increasing heat-treatment temperature. This is a typical example of the behaviour of non-graphitising carbon precursors, i.e. that properties and degree of graphitisation is not influenced above a certain threshold temperature.

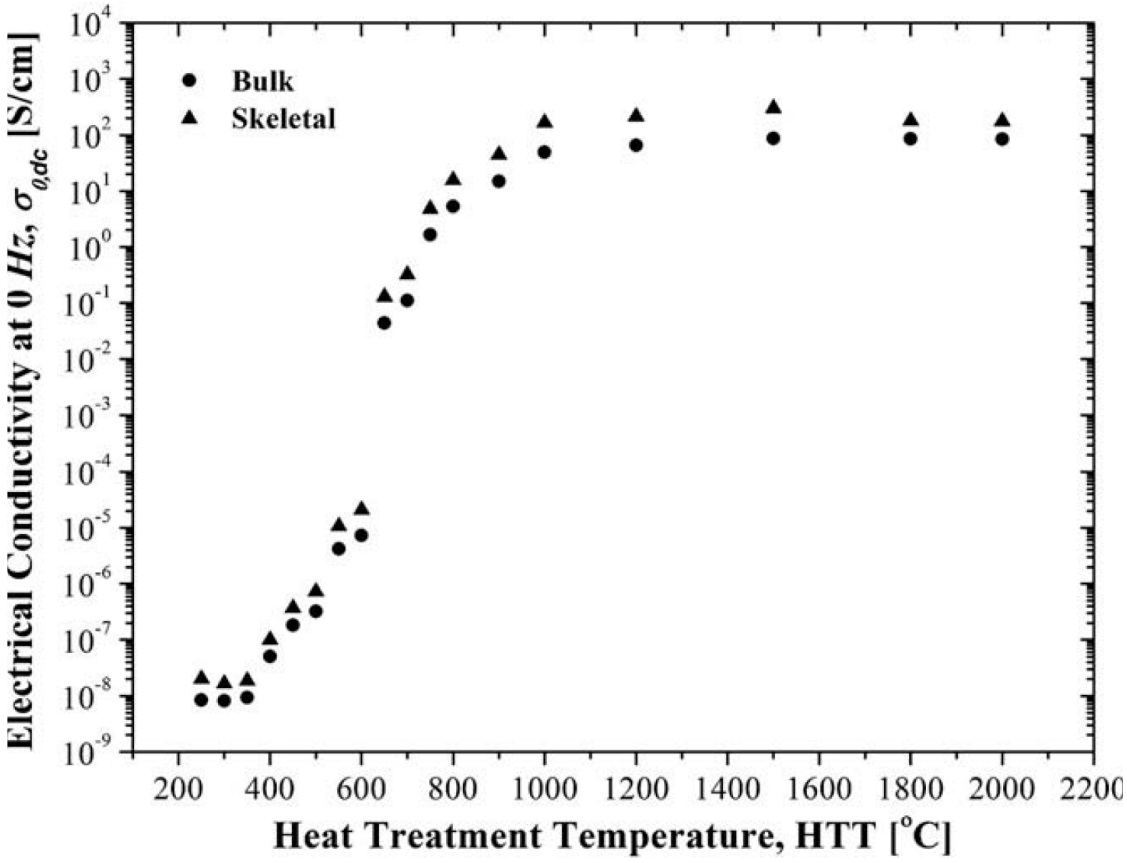


Figure 10. Extrapolated frequency independent electrical conductivity ($\sigma_{0,dc}$) of heat treated microcrystalline cellulose samples as a function of HTT from alternating current (AC) and direct current (DC) conductivity measurements. Measured bulk conductivity, ▲, and calculated skeletal conductivity, ● Figure from (Rhim, Zhang et al. 2010).

## 2.3 Chemical vapour deposition

Chemical vapour deposition is the process used to synthesise pyrolytic carbon (PC) and pyrolytic graphite (PG). By depositing gaseous hydrocarbon compounds on suitable underlying substrates, such as carbon materials, metals and ceramics, at temperatures ranging from approximately 730 to 2230 °C they reform and make a graphitic carbon film/sheet called pyrolytic carbon (Pyrolytic carbon - Chalk 2019). A wide range of microstructures, e.g. isotropic, lamellar, substrate-nucleated and a varied content of remaining hydrogen, can occur in pyrolytic carbons, depending on the deposition conditions, i.e. temperature, type, concentration and flow rate of the source gas, surface area of the underlying substrate, etc. If pyrolytic carbon is heat-annealed at even higher temperatures > 2230 °C or if the chemical vapour deposition of hydrocarbon gases is made at a temperature exceeding 2230 °C, so called pyrolytic graphite (PG) is obtained (sometimes also referred to as annealed pyrolytic graphite (APG) or thermally annealed pyrolytic graphite (TPG)) (Pyrolytic graphite - Chalk 2019). Pyrolytic graphite has a very high degree of preferred crystallographic orientation of the c-axis perpendicular to the surface of the substrate, giving it extremely high electrical and thermal conductivity in the in-plane directions. If the thermal annealing is made under compressive stress, typically at around 3000 °C, so called highly oriented pyrolytic graphite (HPGO) is obtained.

According to IUPAC only material with a misalignment/mosaic spread below one degree should be called highly oriented pyrolytic graphite (Highly oriented pyrolytic graphite - Chalk 2019). Pyrolytic graphite annealed at temperature at or above 3000 °C often have similar in-plane conductivities as highly oriented pyrolytic graphite. Not having to use compressive force during the annealing stage, high temperature annealed pyrolytic graphite tend to have a better performance to cost ratio than highly oriented pyrolytic graphite.

Pyrolytic carbon and graphite sheets have to large extent been replaced by graphitised polyimide films that show similar high in-plane electrical and thermal conductivity but have production advantages (Jiangxi Dasen Technology Co. Ltd. 2020, Panasonic Corporation 2020a).

## 2.4 Kish graphite

Kish graphite is a high-quality flake graphite product that closely resembles natural flake graphite made from steelmaking Kish, which is a large-volume near-molten waste skimmed from the molten iron feed in steelmaking. Kish graphite consists of a mix of graphite (precipitated out of the supersaturated iron), lime-rich slag, and some iron (lime = calcium-containing inorganic minerals composed primarily of oxides and hydroxides). The iron is recycled on site, leaving a mixture of graphite and slag. The best recovery process uses hydraulic classification (which utilizes a flow of water to separate materials by specific gravity - graphite is light and therefore settles nearly last), which gives a fraction containing roughly 70% Kish graphite. Leaching this fraction with hydrochloric acid gives material containing about 95% graphite with a flake size ranging from 2 mm to smaller (Liu and Loper Jr 1991, Yoshida and Hishiyama 1992).

Kish graphite is a good substitute for natural flake graphite in industrial applications (Laverty, Nicks et al. 1994). However, since Kish graphite by definition, i.e. by its production process, is impossible to produce directly from biomass, it is not further addressed or discussed in this report.

## 2.5 Thermal decomposition of carbides

The first commercial artificial graphite in bulk quantities was synthesized by Edward Goodrich Acheson. After synthesizing silicon carbide (SiC), he found that the silicon component evaporates at 4150 °C, leaving behind almost pure graphite. He applied for a patent for this process which he was granted in 1896 (Acheson 1896).

There are also other examples of making graphitic carbon from different carbides, e.g. aluminium carbide (Foster, Long et al. 1958) and magnesium carbide (Osetzky 1974), but it is not a frequently applied synthesis route, and in addition there are no biomass derived carbides and the process is thus not further addressed in this report.

# 3 Current graphite materials and description of two applications

Graphite materials are a good conductors of heat and electricity making them useful in electronic products, such as smart phones and tablet computers, especially for thermal management (i.e. cooling) (Norley 2001), for electromagnetic shielding (Luo and Chung 1996), and as anode material in Li-ion batteries with carbon anodes being completely dominating and graphitic ones having the absolutely major share of these (Syrah Resources Limited 2020). Some research also suggests its potential as counter electrode in solar cells (Rahman, Salleh et al. 2004), and the ability of expanded graphite to make high performance supercapacitors when the expanded graphite is applied as or as part of the electrodes (Xu, Gu et al. 2012, Barzegar, Bello et al. 2016, Masikhwa, Madito et al. 2017).

## 3.1 Natural graphite

Natural graphite has several uses which are summarised in Table 1 below and the review by Jara, Betemariam et al. (2019) provide more in-depth information. For more detailed information on the use as anode material in lithium ion batteries, see section 3.5 “Anode in lithium ion batteries” below.

Table 1. Summary of naturally occurring graphites, advantages, disadvantages and typical uses.

| Graphite type | Vein (lump) graphite | Flake graphite | Amorphous graphite |
|---|---|---|---|
| Description | Purest naturally occurring graphite with carbon-content > 98%. Believed to be naturally occurring pyrolytic graphite. | Flake graphite has a distinctly flaky morphology. Carbon content ranging from 80 to 95%. | A seam mineral, with typically higher impurity and ash content. Carbon content is typically < 85%. |
| Technical uses | None | Anode in lithium ion battery, electrode for steel and aluminium production, brake linings. | None |
| Metallurgical uses | Refractories, crucibles, moulds, castings. | Refractories, crucibles, moulds, castings. | Refractories, crucibles, moulds, castings. |
| Other uses | Pencils, lubricants, paints. | Pencils, lubricants, paints. | Pencils, lubricants, paints. |
| Advantages | Highest crystallinity. Economically significant in terms of C-content. | Lower cost than vein graphite. Low impurity content, high crystallinity, and low porosity. | Lowest cost |
| Disadvantages | Rare and costly. | Inconsistent quality. | Low crystallinity. High in impurities and ash. |
| Morphology | Plate | Plate needle | Granular |

## 3.2 Synthetic graphite materials

Synthetic graphite materials have anisotropic crystals due to the planar structure built on the hexagonal basal plane. As such, the physical properties of synthetic graphitic carbon materials vary depending on the degree of orientation of crystals, as well how well graphitised it is (degree of graphitisation), which depends on the manufacturing method.

### 3.2.1 Anisotropic graphite

The production of anisotropic synthetic graphite always includes use of extrusion or compression moulding processes, which induces alignment of the raw material particles and macromolecules which gives the final graphite material anisotropic properties. The obtained anisotropy ratio depends on the raw materials as well as the specific process conditions and typically varies from 1.7 to 8 (Lee, Kang et al. 2015). The most common and important use of synthetic extruded or compression moulded graphitic carbon is as graphite electrodes used in steel and aluminium manufacturing and processing (Babich and Senk 2013). A much smaller scale application is as graphite electrodes used in electrical discharge machining, commonly used to make injection moulds for plastics and other precision cutting operations needed in mechanical workshops (Pierson 2012). Below follows a description in general terms of a typical process for making graphite electrodes for use in metallurgy (Tamashausky 2006). The reader must keep in mind that many variations in the process and ingredients are possible.

The process of making graphite electrodes begins by mixing calcined petroleum coke (CPC) filler particles with coal tar pitch. This process is performed at elevated temperatures, so the pitch component is soft or liquid, and mixes easily and coats the CPC particles forming a flexible and mouldable dough-like mixture. The mixture always contains more CPC than pitch, and a common ratio is 80% CPC and 20% pitch. The mixture is then extruded (most common), or compression moulded, into roughly the same size as the electrode being manufactured. The obtained object, usually called green electrode blank, is cooled and thus becomes rigid due to that the coal tar pitch freezes. Next stage is carbonisation (baking) of the green electrode blank by slowly heating in an oven to 700-1200 °C. The heating rate must be carefully selected and controlled to prevent excessive degassing, melt flow, or other process that would result in deformations or other disturbance of material structure from occurring. The carbonisation is usually done under reduced pressure or with addition of inert gas to prevent or reduce material loss by oxidation (i.e. combustion). As the carbonisation process proceeds many changes occur to the coal tar pitch fraction. As the pitch thermally matures it passes through the mesophase state (described in section 2.2.4 “Graphitisation” above), polymerises, and cures to a non-melting coal tar pitch-coke. No changes occur to the calcined petroleum coke filler. Upon completion of the carbonisation process the electrode blank consists of calcined petroleum coke particles held together by a non-melting calcined coal tar pitch matrix. During the carbonisation step gases are formed as the pitch changes chemically, resulting in pore formation and density reduction. If a low-porous material is desired, which often is the case, the electrode blank is re-impregnated with pitch, usually of lower viscosity than the one used in the first stage for more efficient pore filling (the reason for that petroleum tar pitch often is used since it has lower viscosity).

When the re-impregnation and re-carbonisation have been finished, it is time to graphitise the electrode blank. The blank is heated to desired temperature typically in the range 2500 and 3000 °C. Due to the very high temperatures it is of vital importance that oxygen is excluded from the furnace. This is often accomplished by covering the electrode blank with some oxygen scavenging material that is called “packing”. Petroleum coke or metallurgical coke is typically used for this. If an Acheson furnace, which operate by the resistive heating principle, is used for the heating, though there are many different furnaces that can be used e.g. magnetic induction furnace, this “packing” must also be somewhat electrically conductive since it will form part of the electrical pathway through the furnace. When an Acheson furnace is started, a low voltage high current electrical field is applied to its content, which heats up due to its own electrical resistance when the electrical current flows through it. When the desired temperature is reached, the heating is stopped and the furnace and its contents cools. When cool enough the now graphitised electrode is removed.

The melt-extrusion of polyacrylonitrile (PAN) and mesophase pitch (most often derived from petroleum coke and coal tar pitch) into continuous carbon or graphite fibres is an extreme example of anisotropic graphitic carbon. These fibres have many different applications especially with in the field of fibre-composites, but the production of carbon fibres and their uses lies outside of the scope of this report.

### 3.2.2 Isotropic graphitic carbon

Isotropic materials are materials having the same properties regardless of direction. Isotropic graphitic carbon is not perfectly isotropic but have a low anisotropy ratio usually ranging from 0.98 to 1.10. The typical manufacturing process is as follows:

- Usually calcined petroleum coke and coal tar pitch are used as raw materials.
- The raw material is pulverised, mixed and sieved to ensure fine particle size.
- A block of the pre-treated raw material is formed.
- The block is isostatically pressed (same pressure in all directions) using a pressure typically in the range 100 to 630MPa. The pressing can be done either cold (ambient temperature) or hot (~1000-2200 °C).
- The pressed block is then baked/carbonised by heating to between 700 and 1200 °C.
- It is then re-impregnated with coal tar pitch and re-carbonised repeatedly until the porosity has become as low as desired.
- The carbonised block is then graphitised using heat-treatment at 2500-3000 °C.

Isotropic graphite materials are easy to machine with precision and their mechanical behaviour rather easy to foresee/simulate, thanks to the isotropic behaviour and high strength. This make it a desirable material in many applications and some especially important are listed below, but there are many more:

- Nuclear graphite used for moderating neutrons in nuclear reactor, where it is important that the anisotropy is low since thermal expansion or neutron bombardment induced expansion otherwise more easily lead to cracking and damages (Haag 2005, Marsden, Haverty et al. 2016).
- Synthesis of single crystals of silicon, germanium, and III—V and II—VI semiconductors by either ribbon or Czochralski crystal-pulling techniques, is a very

common and vital unit operation within the semiconductor industry. This processing requires high-heat resistance since the synthesis of single crystals is made at 1500 °C or higher. Tools that have been manufactured with very high precision These requirements make high density isotropic graphite that material of choice for graphite heaters and crucibles used in this processing, thanks to its heat-resistance, purity, isotropy in electrical resistivity and easy to machine with very high precision.

- Bearings and seals in high-temperature application were the self-lubricating capability, in combination with heat- and wear-resistance make it a top-performer.
- Moulds for casting of metal parts where the heat-resistance, easy of precision machining and low thermal expansion make it a perfect material.
- As sputtering target in the manufacture of hard disks.
- Important use in manufacturing of LCD displays where it used as an electrode for plasma etching and as heater panel.

## 3.3 Pyrolytic carbon and graphite

The production process and definition of pyrolytic carbon (PC) respectively pyrolytic graphite (PG) has been described in section 2.3 “Chemical vapour deposition”. The chemical vapour deposition technique (CVD) for producing pyrolytic carbon (i.e. CVD performed at a temperature below 2230 °C) results in a material with very high anisotropy. This is exemplified by the results of Null, Lozier et al. (1973), who measured thermal conductivity at 300 K of pyrolytic carbon that had been deposited at 2200 °C and got a value of 306 W/(m·K) in the in-plane direction and a value of 2.39 in the out-of-plane direction, giving a anisotropy ratio of 128 in thermal conductivity. The in-plane hexagonally $sp^2$-hybridised covalently bonded carbon atoms accounted for the high in-plane electrical conductivity (due to conjugated $\pi$-electrons) and thermal conductivity and its large in-plane stiffness (due to the stiffness of the covalent bonds and thus good atomic vibration propagation). Through the thickness direction out-of-plane of the pyrolytic carbon, these hexagonal planes are weakly bonded (metallic bonding with a strength similar to van der Waals bonding) resulting in a material with poor through-thickness electrical and thermal conductivity, stiffness, and strength.

As described in section 2.3 “Chemical vapour deposition”, pyrolytic graphite (PG) is produced by heat-annealing pyrolytic carbon at temperatures above 2230 °C, or by performing the CVD process at a temperature above 2230 °C. Highly oriented pyrolytic graphite (HOPG) is manufactured by making the heat-annealing while the pyrolytic carbon specimen is under compressive stress. Null, Lozier et al. (1973) also produced pyrolytic graphite and highly oriented pyrolytic graphite, and the thermal conductivities and corresponding anisotropy ratios are shown in Table 2 below. The anisotropy values are even higher than for the PG and HOPG compared to the PC, clearly showing that the both the thermal- and stress-annealing resulted in the graphite crystals being oriented more in the in-plane, i.e. substrate, direction although some of the effect is due to increased degree of graphitisation and crystal size.

All results on pyrolytic graphite where anisotropy ratios for thermal and electrical conductivity could be calculated (Slack 1962), as well as the results for graphitised polyimide films are included since they have properties very similar to pyrolytic graphite even though not produced by the CVD process (Murakami, Nishiki et al. 1992, Nakamura,

Miyafuji et al. 2017), are included in Table 2. From the table it is seen that the anisotropy ratio is higher for electrical conductivity than for thermal. The anisotropy ratio also become larger the higher the degree of graphitisation. It is a pity that Slack (1962) did not publish any information on how the studied pyrolytic graphites were produced, but the comparably low conductivities leads to the suspicion that the sample were pyrolytic carbons rather than pyrolytic graphites.

In addition it is good to know that the thermal conductivity of pyrolytic carbon and graphite generally increases as the temperature decreases, whereas the electrical conductivity decreases (Buerschaper 1944, Holland, Klein et al. 1966). In the study by Holland, Klein et al. (1966) the thermal conductivity peaked at approximately 150 K with a value of ~2,800 W/(m·K).

Table 2. Degree of graphitisation (based on Mering-Maire's simple model), electrical conductivity in the in-plane ($\sigma_{||}$) and out-of-plane ($\sigma_{\perp}$) and the corresponding anisotropy ratio ($\sigma_{||}/\sigma_{\perp}$), as well as thermal conductivity in the in-plane ($K_{||}$) and out-of-plane ($K_{\perp}$) and the corresponding anisotropy ratio ($K_{||}/K_{\perp}$), collected from the publications reviewed in this report.

| Reference | Sample | DG (%) | $\sigma_{||}$ S/cm | $\sigma_{\perp}$ S/cm | $\sigma_{||}/\sigma_{\perp}$ | $K_{||}$ W/(m·K) | $K_{\perp}$ W/(m·K) | $K_{||}/K_{\perp}$ |
|---|---|---|---|---|---|---|---|---|
| Null, Lozier et al. (1973) | PC, As deposited at 2200 °C | - | - | - | - | 306 | 2.39 | 128 |
| Null, Lozier et al. (1973) | PG, Heat-annealed at 3200 °C | - | - | - | - | 1840 | 6.24 | 295 |
| Null, Lozier et al. (1973) | Stress-annealed at 3000 °C, HOPG | - | - | - | - | 1840 | 8.67 | 212 |
| Slack (1962) | PG-0 | - | 1850 | 1.99 | 930 | 72 | 1.57 | 46 |
| Slack (1962) | PG-19 | - | 4400 | 4.40 | 1000 | 270 | 2.84 | 95 |
| Slack (1962) | PG-20 | - | 4400 | 4.40 | 1000 | 410 | 3.73 | 110 |
| Murakami, Nishiki et al. (1992) | Graphitise PI film 3000 °C, 50 µm | 95 | 15500 | 6 | 2583 | 860 | 5.5 | 156 |
| Murakami, Nishiki et al. (1992) | Graphitise PI film 3000 °C, 25 µm | 98 | 20000 | 5.4 | 3704 | 930 | 5 | 186 |
| Murakami, Nishiki et al. (1992) | Graphitise PI film 3000 °C, 12.5 µm | 100 | 24000 | 5 | 4800 | 1100 | 5 | 220 |
| Nakamura, Miyafuji et al. (2017) | Graphitise PI film 2727 °C, 145 µm | 94 | 2618 | 30.8 | 85 | - | - | - |
| Nakamura, Miyafuji et al. (2017) | Graphitise PI film 2727 °C, 56 µm | 95 | 5882 | 13.2 | 447 | - | - | - |
| Nakamura, Miyafuji et al. (2017) | Graphitise PI film 2727 °C, 29.7 µm | 95 | 7143 | 11.1 | 643 | - | - | - |
| Nakamura, Miyafuji et al. (2017) | Graphitise PI film 2727 °C, 19 µm | 95 | 11236 | 2.4 | 4718 | 1490 | - | - |

The high thermal conductivity makes pyrolytic carbon and graphite ideal to use in heat-spreading and transfer applications, more on this in section 3.6 "Thermal management" below.

Pyrolytic carbon and graphite, however, have other important uses due other properties than only their high thermal conductivity. Some take advantage of the high anisotropy in thermal conductivity, which spread the heat over a large area for efficient heat dissipation

while still being fairly thermally “insulating” in the thickness direction. Applications of this property combination are, e.g. missile nose cones, rocket motors, heat shields, laboratory furnaces and coating of graphite cuvettes (tubes) used in “graphite furnace atomic absorption” furnaces to decrease heat stress, thus increasing cuvette lifetimes. Other applications take advantage of completely other properties, and examples of applications of pyrolytic carbon and graphite are:

- Pebble-bed nuclear reactors uses spherical fuel elements called pebbles. These tennis ball-sized pebbles have a shell of pyrolytic graphite that functions as a neutron moderator. These pebbles contain thousands micro-fuel particles, with a core of the fissile fuel (such as $^{235}U$) coated with a shell of silicon carbide for structural integrity and fission product containment (Lindemer, Long Jr et al. 1978, Hunn, Jellison Jr et al. 2008).
- Fabrication of grid structures used in some high-power vacuum tubes.
- Pyrolytic carbon is used to coat prosthetics in contact with blood to reduce the risk of thrombosis, since blood clots do not easily form on pyrolytic carbon. For example, it finds use in artificial hearts and artificial heart valves (Björk 1972). In addition, pyrolytic carbon is used to coat artificial replacement joints (Cook, Beckenbaugh et al. 1999). These implants have been approved by the U.S. Food and Drug Administration (FDA) for use in the hand for metacarpophalangeal joint (i.e. the finger joint closes to the hand - knuckle) replacements. FDA has also approved the use for proximal interphalangeal joint (the middle of the three finger joints) replacements under the Humanitarian Device Exemption (U.S. Food and Drug Administration 2002).
- For manufacturing monochromators that are use in neutron and X-ray scattering instrumentation (Antonov, Baryshev et al. 1991).
- Highly oriented pyrolytic graphite (HOPG) is used as focusing monochromator in X-ray spectrometers to create highly monochromatized x-ray-radiation, which enables detection of elements present in very low concentration (Kolmogorov and Trounova 2002, Grigorieva and Antonov 2003).

## 3.4 Graphene

Graphene is the basic building block of graphite. This report focuses on graphite materials and the degree of graphitisation is determined by the probability for adjacent hexagonal layer planes, i.e. graphene layers, in parallel to having regular graphitic AB stacking, which cannot be determined for graphene since it in essence is a single-layer 2D-material. This literature review is thus not the right place for a detailed comparison, but since graphene has reached commercial use within heat spreading and thermal management, see section 3.6 “Thermal management” for more details, and the hype around its high electrical conductivity some examples have been included in this report to see how its performance compare with more traditional graphite materials. The reader especially interested in graphene and graphene production is referred to the two reviews by and Choi, Lahiri et al. (2010) and Avouris and Dimitrakopoulos (2012).

## 3.5 Anode in lithium ion batteries

Graphitic carbon is the dominant anode material used in commercial lithium ion batteries (Syrah Resources Limited 2020). However, the current commercial anodes based on graphite materials cannot meet the increasing demand on energy density, operation reliability and system integration arising from the continuous evolution of the field of portable electronic devices, electric vehicles, and electrical energy storage applications. Graphitic anodes exhibit only a moderate intrinsic specific capacity (372 $mAhg^{-1}$), give rise to issues with formation of solid electrolyte interphase, while vital, can create serious issues if not controlled, and if the anode is fully passivated it leads to so called lithium plating and formation of lithium dendrites, which may lead to fires or even exploding batteries (An, Li et al. 2016, Zuo, Zhu et al. 2017). Therefore, modification of graphitic carbon and other carbonaceous anode material has become a research focus in order to develop Li-ion batteries with improved performance and improved safety. The latest progress and research include mild oxidation of graphitic anodes, formation of composites with metals and metal oxides, coating with polymers and other kinds of carbons, nano-structuring as well as inclusion of graphene and carbon nanotubes (Wu, Rahm et al. 2003, Kamali and Fray 2010).

However, despite the progress made with carbon-based anodes they are not yet considered optimal and therefore anodes based on other materials completely without carbon have been and are heavily researched. A wide variety of materials have been tested and researched, e.g. metal alloys, metal oxides, metal sulfides and metal nitrides (Vaughey, Fransson et al. 2003, Timmons and Dahn 2006, Kamali and Fray 2010, Ji, Lin et al. 2011, Kamali and Fray 2011, Liang, Gao et al. 2013, Goriparti, Miele et al. 2014, Roy and Srivastava 2015, Balogun, Qiu et al. 2016, Qi, Shapter et al. 2017, Zuo, Zhu et al. 2017). Despite some success, none of these new anode materials has had commercial success. The biggest issue being massive volume change upon lithium intercalation leading to cracked and damaged anodes (Beaulieu, Eberman et al. 2001), and therefore much focus has been on nano-structured and nano-porous anode materials to try get materials that can tolerate large volume changes without becoming damaged. This research is very well covered by the above references. Despite the dramatic reduction of volume changes achieved by nano-structuring, these anode materials have, according to the knowledge of the authors, not yet been commercialised. One can speculate that this has to do with high manufacturing costs.

## 3.6 Thermal management

Due to the very high thermal conductivity in the in-plane direction of graphitic carbon, for example 1850 W/(m·K) at 27 °C (300 K) for pyrolytic carbon heat-treated at 3250 °C (3523 K) (Holland, Klein et al. 1966), 1900-1950 W/(m·K) for commercial graphitized polyimide film (Jiangxi Dasen Technology Co. Ltd. 2020, Panasonic Corporation 2020a), and 3200 W/(m·K) for macroscopic (10x10 cm) graphene-film produced by reduction of graphene oxide film, thermal annealing (2850 °C) and mechanical pressing (300 MPa) (Wang, Samani et al. 2018), these materials are obviously very interesting to use for heat spreading and thermal management in electronics, as well as in other areas such as cooling of batteries in electrical cars.

These applications are already commercialised (Huawei Technologies Co. Ltd. 2016, Baknor Electronics Industries Inc. 2019, Boyd Corporation 2019, DREYER SYSTEM GmbH 2019, DREYER SYSTEM GmbH 2020, Jiangxi Dasen Technology Co. Ltd. 2020, Panasonic Corporation 2020a).

Pyrolytic carbon and graphite sheets are obviously good heat spreaders, but by placing them perpendicular (as fins) to a hot surface they can also work as efficient heat sink materials. Thermal management using materials with high thermal conductivity, is especially important in mobile devices as smartphones and tablets, as well as flat LED-screens, that simply do not have space for cooling fans, which is the typical way to cool PCs (personal computers). Panasonic is a major producer of pyrolytic graphite sheets from macromolecular films, e.g. polyimide, for thermal management applications (Panasonic Corporation 2020a). The Chinese company Dasen is another producer of pyrolytic graphite sheets from polyimide that are used in for example mobile phones, tablets, LED displays, automotive batteries etc. (Jiangxi Dasen Technology Co. Ltd. 2020). Dasen is also Samsung's strategic partner for thermal management solutions.

The pyrolytic graphite sheets supplied by both Panasonic and Dasen are actually not pyrolytic graphite since it is not obtained by a CVD process but instead by high-temperature graphitisation of polymer films. Both companies have decided to call it pyrolytic graphite sheets since the performance is similar or even better as compared to true pyrolytic graphite. Nakamura, Miyafuji et al. (2017) used uncompressed "pyrolytic graphite" film from Panasonic in their work and also published information on how Panasonic produces their commercial compressed film: *"Commercial PGS is made first by carbonizing a stack of polymer films of a few μm thick at $T \lesssim 1000$ K, then by graphitizing the resultant foamed carbon precursor at $T \approx 3000$ K, and finally by compression (rubbing) which reduces the thickness by 30–50%. Compared to chemical vapor deposition, which is used to synthesize HOPG, this is a convenient mass production method for thin graphite sheets of good crystallinity."*.

The U.S. company Boyd corporation is a company that manufactures heat spreaders that incorporates pyrolytic graphite sheets (Boyd Corporation 2019) and is also a supplier of many different thermal interface materials (Boyd Corporation 2020). The German company DREYER SYSTEM GmbH is another manufacturer of heat spreaders using pyrolytic graphite sheets (DREYER SYSTEM GmbH 2020) and they also manufacture heat sinks incorporating graphite material (DREYER SYSTEM GmbH 2019).

Since pyrolytic carbon and graphite are weak in the out-of-plane direction they are often encapsulated within in structural metallic materials, typically aluminium and copper alloys, as done by for example Boyd Corporation (2019). It is, however, also important to remember that the "new" highly thermally conducting sheets/films produced by graphitising polyimide films do have very good flexibility and mechanical properties (can be bent at sharp angles many times, as many as 30 000 without sacrificing performance according to Panasonic Corporation (2020b)).

Also, graphene-based commercial heat spreaders and systems for thermal management have emerged. The Canadian company Baknor sells heat sinks and spreaders including graphene film with claimed in-plane thermal conductivity of 5600 W/(m·K) as well as an impressive out-of-plane thermal conductivity of 2700 W/(m·K) obtained by adding diamond powder particles and carbon nano-capsules (Baknor Electronics Industries Inc. 2019).

Huawei have also developed and used graphene in Li-ion batteries to limit the temperature rise and enable use of these batteries in hot environments (Huawei Technologies Co. Ltd. 2016). Later Huawei have also developed and applied graphene film in their mobile phone Mate 20, were it is used for quick heat spreading from the battery, the transmitter and receiver circuits and the central processing unit (CPU) to the casing (Fu, Hansson et al. 2019).

It should, however, be noted that it is not only the spreading and dissipation of heat that is essential, but also the heat transfer from the device/circuit to the spreading and dissipating materials, i.e. the interface thermal resistance. This make so called thermal interface materials, which improves heat transfer between materials, very important. Different thermal interface materials including their pros and cons are excellently reviewed in the following publications (Sarvar, Whalley et al. 2006, Due and Robinson 2013, Hansson, Nilsson et al. 2018).

# 4 Comparison of bio- and fossil-based graphitic carbon

Data have been collected from the following publications (Slack 1962, Holland, Klein et al. 1966, Null, Lozier et al. 1973, Murakami, Nishiki et al. 1992, Seehra and Pavlovic 1993, Katzman, Adams et al. 1994, Primo, Atienzar et al. 2012, Ramirez-Rico, Gutierrez-Pardo et al. 2016, Liu, Qu et al. 2017, Nakamura, Miyafuji et al. 2017, Seo, Pineda et al. 2017, Wang, Samani et al. 2018, Jiang, Yao et al. 2019). Results for graphene films are also included to give a comparison with more traditional graphite materials.

Electrical and thermal conductivity are plotted against bulk density, heat treatment temperature, distance between graphene layers ($d_{(002)}$), degree of graphitisation as given in the publication or calculated from $d_{(002)}$ according to Mering-Maire's model (Maire and Mering 1970) and misorientation angle (calculated from x-ray scattering data as FWHM of the 002 line), to try to give as complete picture as possible and thus maximum understanding for how fossil raw material compare to biomass for production of graphite materials.

Seo, Pineda et al. (2017) achieved very high electrical conductivity by using soybean oil in combination with chemical vapour deposition on nickel-foil. Since they used biomass in combination with friendly process conditions (heating to only 800 °C in air at atmospheric pressure – no vacuum pump or inert gases necessary) it is interesting to compare their result to those of highly graphitic fossil-based carbon materials. To do this a value of the electrical conductivity is needed, but in the publication only a sheet resistance of 324 Ω/□ was reported, but no thickness which is needed to calculate conductivity. In the publication it was, however, reported that the film consisted of regions with one, two, three respectively somewhat more than three layered graphene, making it reasonable to assume an average of three layers. This assumption was combined with the graphene layer thickness of 0.47 nm for N-doped chitosan based graphene film as reported by Primo, Atienzar et al. (2012), to calculate and average thickness of 1.41 nm and an electrical conductivity of 21 890 S/cm. These values are considered to be fairly correct but to indicate that these have been calculated based on several assumptions, the data point from Seo, Pineda et al. (2017) is put within parenthesis in the figures/plots below.

## 4.1 Electrical conductivity

Electrical conductivities from the references listed above are plotted as function of the above listed variables in Figure 11 to Figure 17 below.

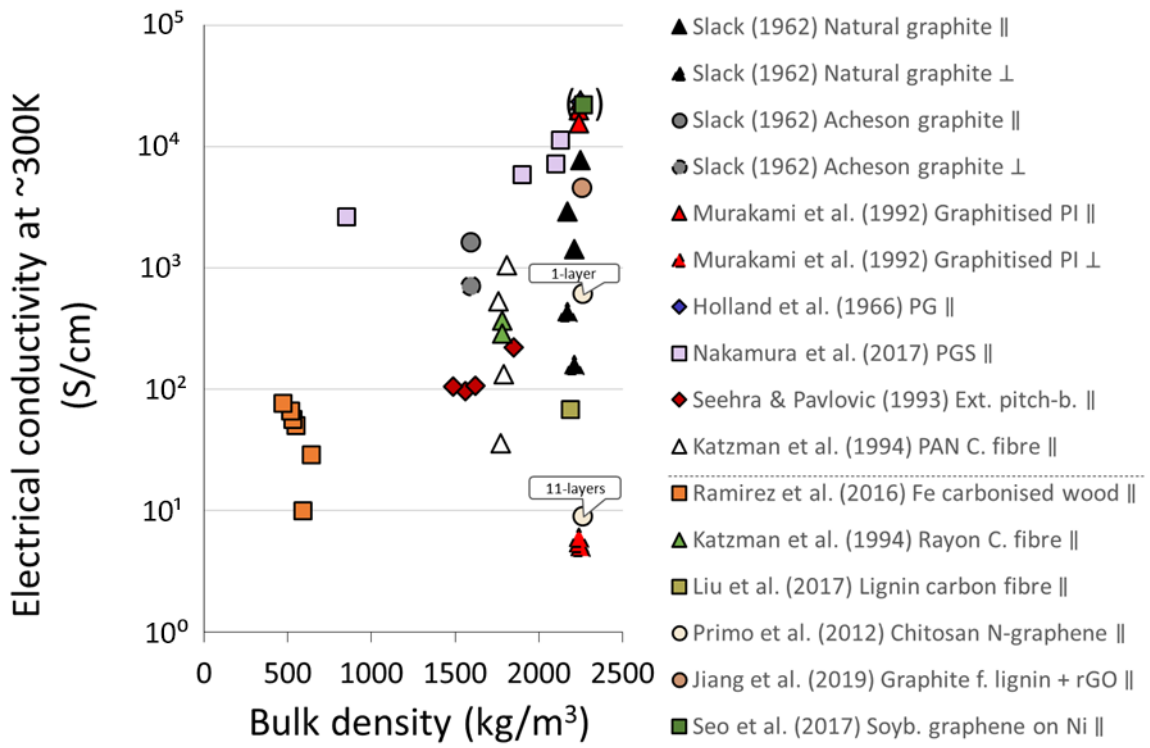


Figure 11. Electrical conductivity at ~300 K plotted as function of bulk density.

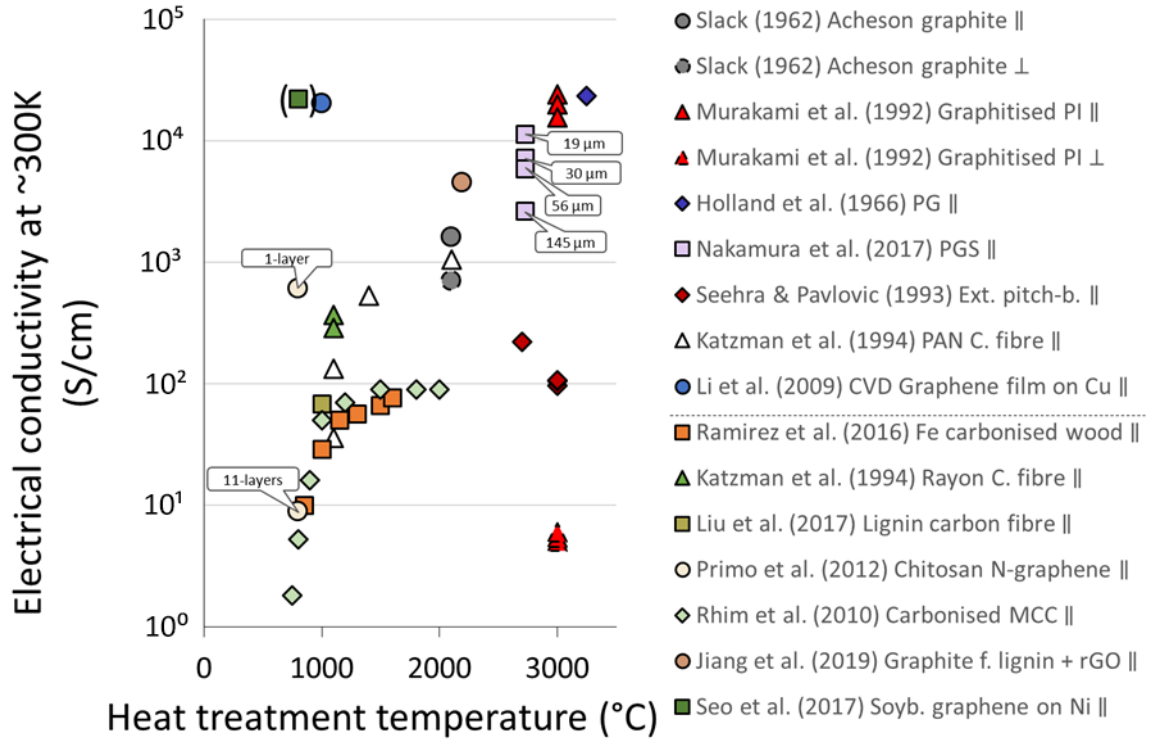


Figure 12. Electrical conductivity at ~300 K plotted as function of heat treatment temperature.

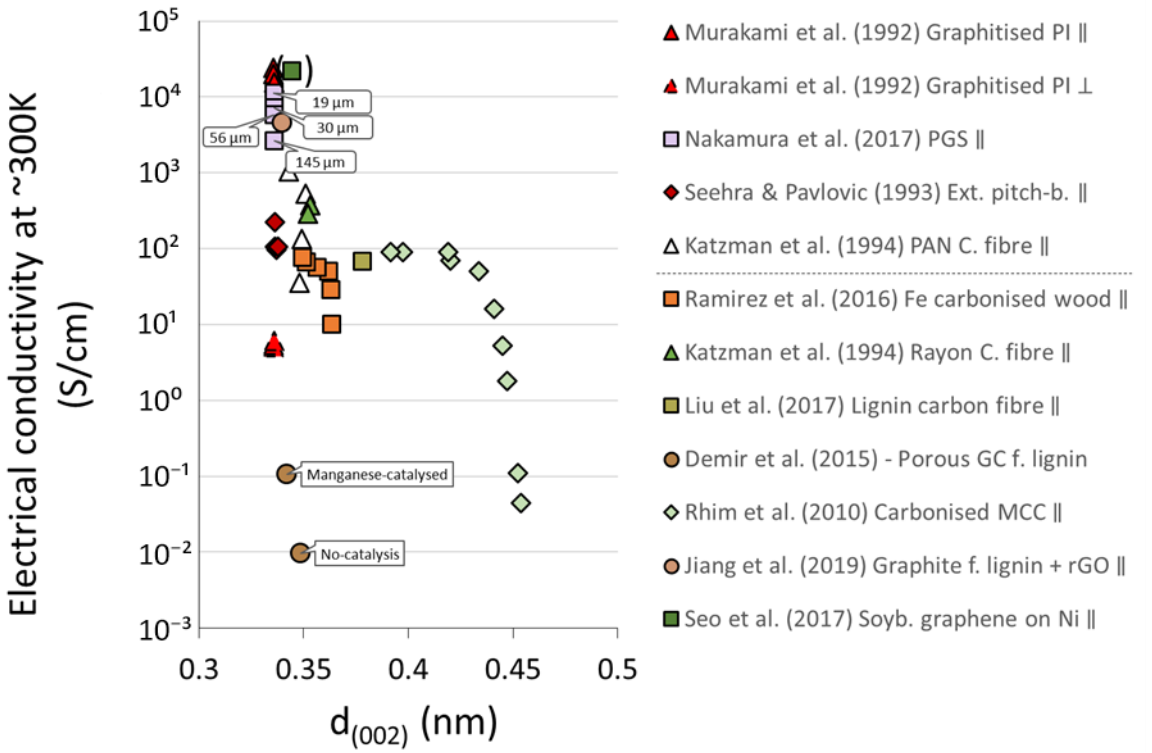


Figure 13. Electrical conductivity at ~300 K plotted as function of $d_{(002)}$ using distances.

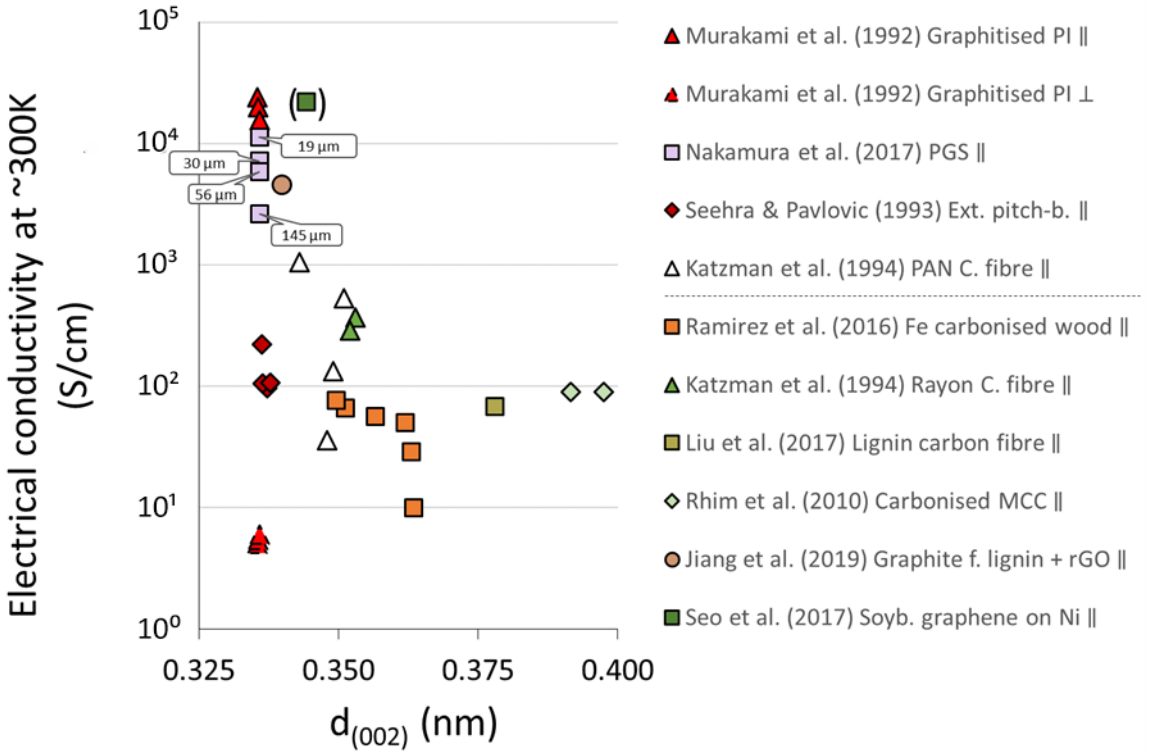


Figure 14. Electrical conductivity at ~300 K plotted as function of $d_{(002)}$, but excluding longer $d_{(002)}$ distances to make it easier to see behaviour and trends at shorter $d_{(002)}$ distances, using distances from the reviewed and above listed publications.

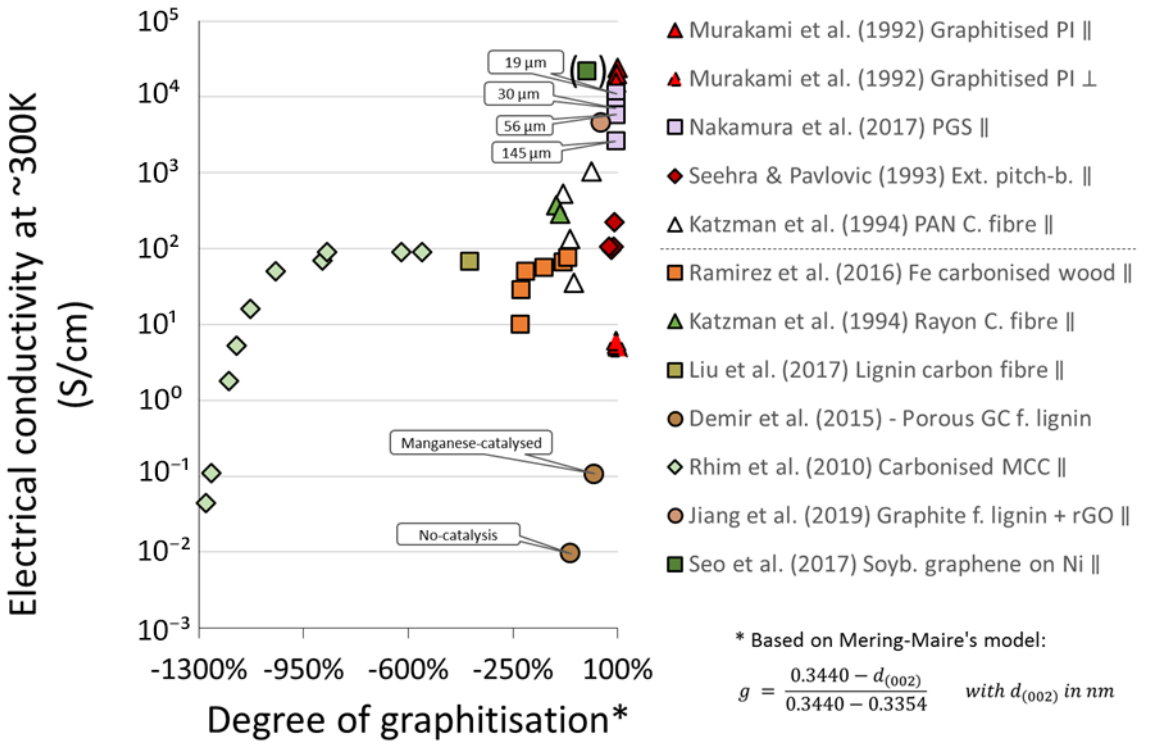


Figure 15. Electrical conductivity at ~300 K plotted as function of degree of graphitisation calculated (according to Mering-Maire's model) using $d_{(002)}$-distances.

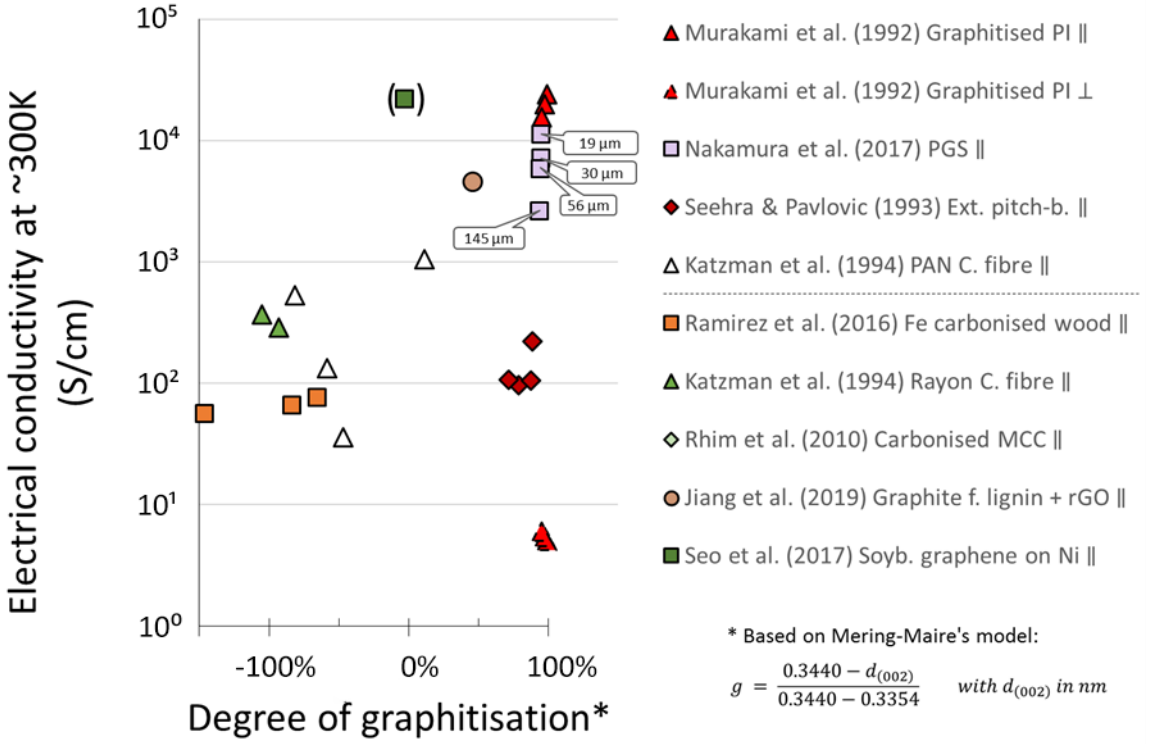


Figure 16. Electrical conductivity at ~300 K plotted as function of degree of graphitisation calculated (according to Mering-Maire's model) using $d_{(002)}$-distances, but with the lowest degrees of graphitisation left out to make it easier to see behaviour and trends at the higher degrees of graphitisation.


Figure 17. Electrical conductivity at ~300 K plotted as function of misorientation angle using values from the reviewed publications.

## 4.2 Thermal conductivity

Thermal conductivities from the references stated above are plotted as function of the above listed variables in Figure 18 to Figure 22 below.

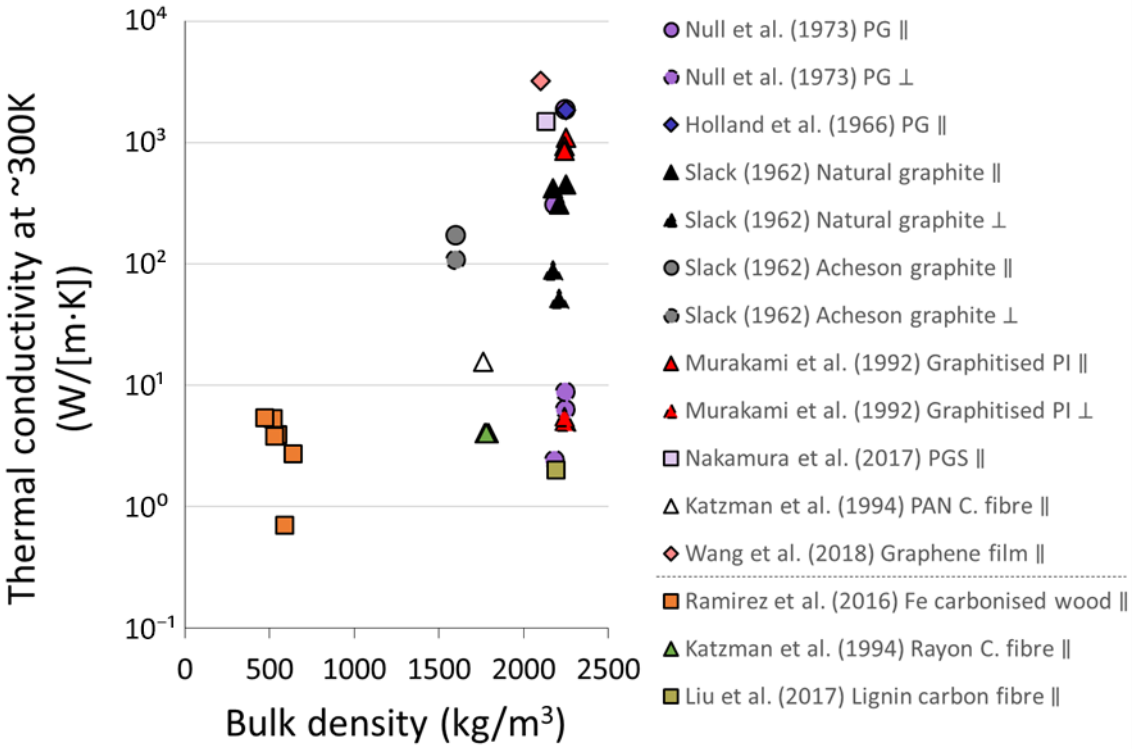


Figure 18. Thermal conductivity at ~300 K plotted as function of bulk density using values from the reviewed and above listed publications.

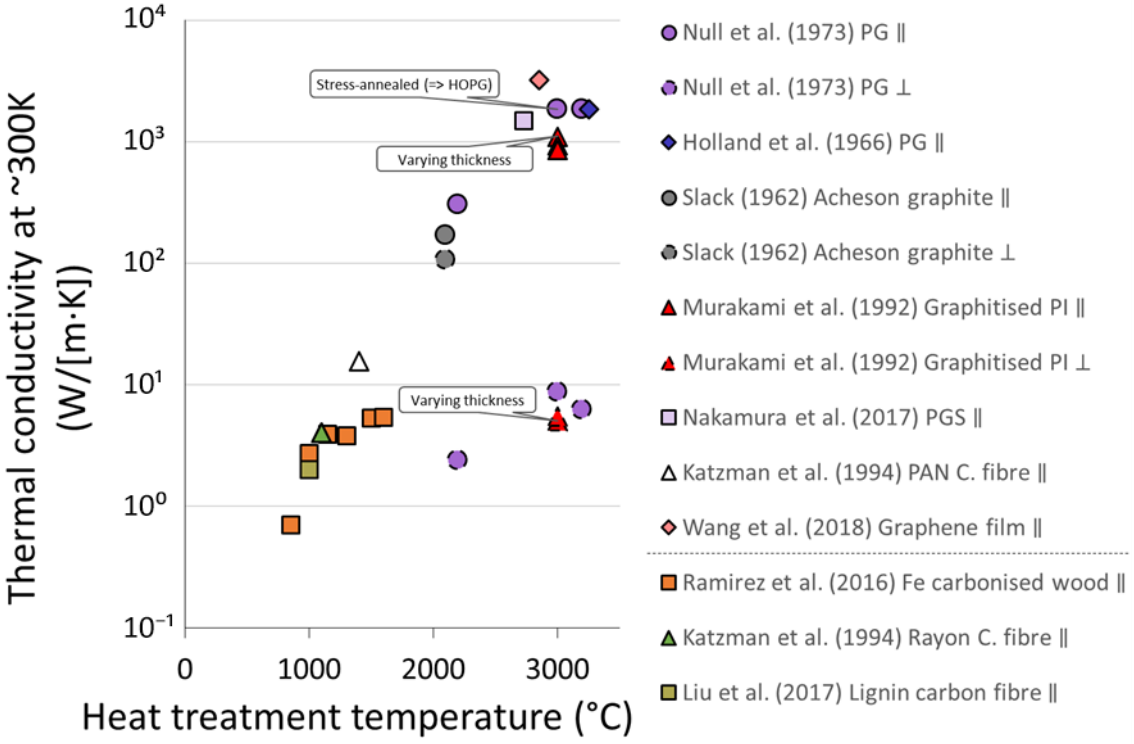


Figure 19. Thermal conductivity at ~300 K plotted as function of heat treatment temperature using values from the reviewed and above listed publications.

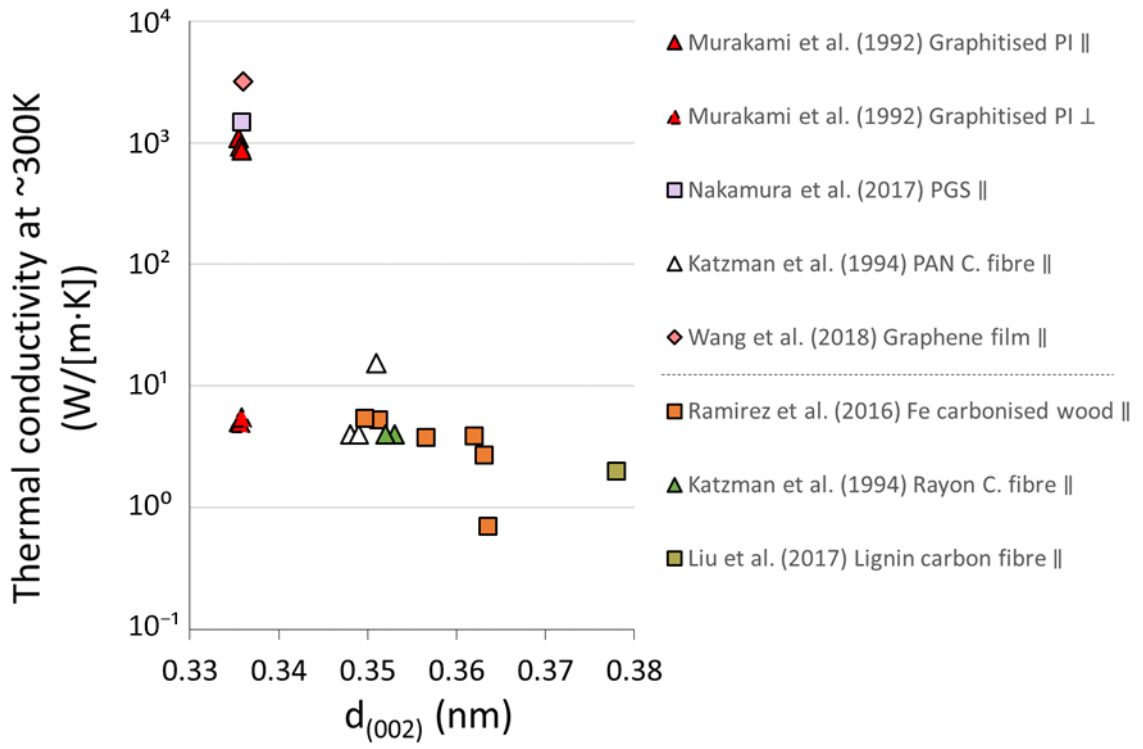


Figure 20. Thermal conductivity at ~300 K plotted as function of $d_{(002)}$ using distances from the reviewed and above listed publications.

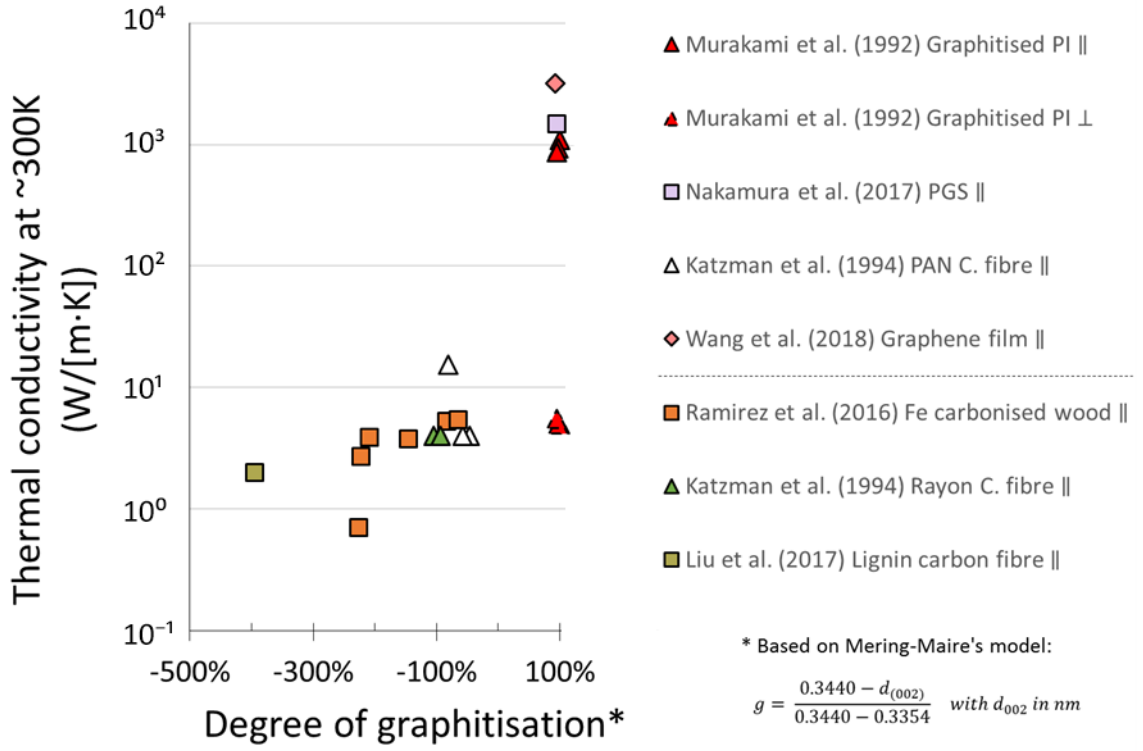


Figure 21. Thermal conductivity at ~300 K plotted as function of degree of graphitisation calculated (according to Mering-Maire's model) using $d_{(002)}$-distances from the reviewed and above listed publications.

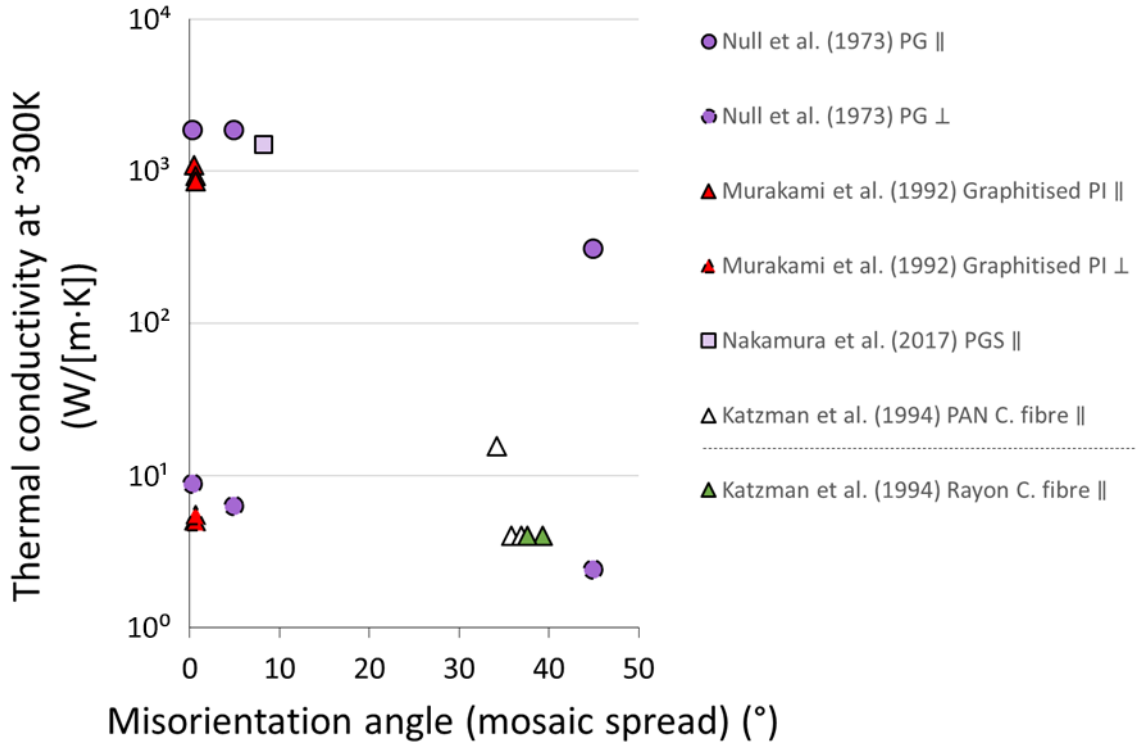


Figure 22. Thermal conductivity at ~300 K plotted as function of misorientation angle using values from the reviewed and above listed publications.

## 4.3 Degree of graphitisation in relation to heat treatment temperature

To further improve the understanding how heat treatment temperature influences the graphitisation of graphitising precursors (so called soft carbon precursors) and non-graphitising precursors (so called hard carbon precursors), the degree of graphitisation was plotted against heat treatment temperature in Figure 23 below. Example of graphitising carbon precursors are petroleum coke, polyvinyl chloride (PVC) and polyimides. Example of non-graphitising are polyacrylonitrile, polyvinylidene chloride (PVDC) and essentially all biomass. As seen in Figure 23 only the known graphitising precursors reach a degree of graphitisation exceeding 70% highlighting the difficulty in manufacturing highly graphitic carbon from biomass. Possible methodologies for circumventing this difficulty will be addressed and discussed in section 6 “Concluding remarks” below.

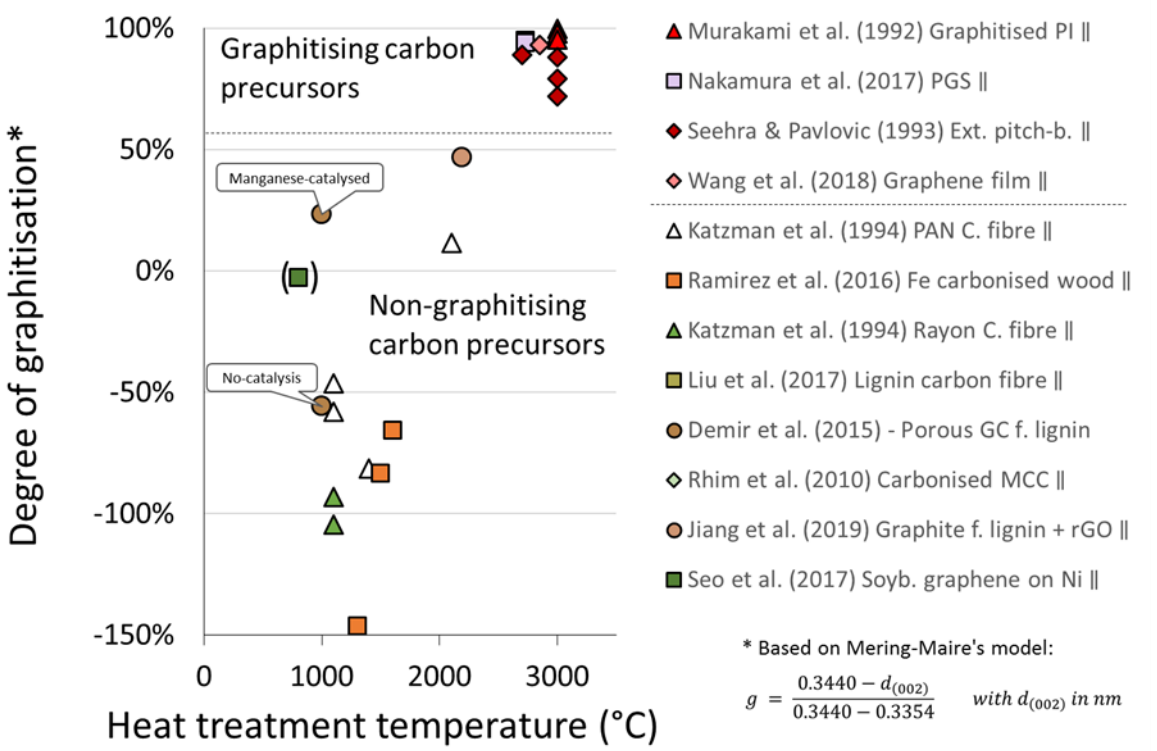


Figure 23. Degree of graphitisation, as calculated (according to Mering-Maire's model) using $d_{(002)}$-distances, plotted as function of heat treatment temperature.

## 4.4 Conclusions regarding electrical and thermal conductivities

The main conclusion that can be drawn from Figure 11 to Figure 22 above, is that it is only graphitic carbon materials that have both a high degree of graphitisation > 70% (which means low $d_{(002)}$) and high bulk density ≥ 1900 kg/m³ that show very high in-plane electrical (> 4000 S/cm) and thermal conductivity (> 800 W/(m·K)). The alignment/misorientation also show some effect for the conductivities, with increasing conductivity in the aligned direction, but the effect is smaller as compared to the effect of degree of graphitisation and bulk density.

To understand the effect of density (coupled to porosity) and degree of graphitisation on the electrical and thermal conductivity, it is important to realise and keep in mind that the electrical conductivity is determined by how easily electrons can move within a material (i.e. how delocalised they are) and that the thermal conductivity is determined by transfer of atomic and molecular vibrations. The graphene layers (ab-layer) within a graphite crystal are $sp^2$-bonded carbon atoms with delocalised $\pi$-electrons and thus contribute to high electrical conductivity within the graphene layer. Graphite and graphitic carbons also show electrical conductivity perpendicular to graphene layers direction (ab-plane), that is in the c-direction, though it is much lower.

This is explained by the fact that there is a small overlap between conduction and the valence bands of neighbouring graphene layers in graphite materials caused by the interaction between B carbon atoms in neighbouring layers, that give some electrical conductivity, although low, between neighbouring graphene layers (McClure 1957, Slonczewski and Weiss 1958, Partoens and Peeters 2006).

In graphite materials the thermal conductivity is primarily determined by coherent vibrations of atoms in the crystal lattice out of their equilibrium positions, so called acoustic phonons, and the transfer of these vibrations through the material (Klemens 2000). In the ab-plane (i.e. the parallel to the graphene layers and the plane with the highest thermal conductivity – which is also the thermal conductivity that mainly has been addressed in this report) the carbon atoms are covalently $sp^2$-bonded, which are strong and stiff bonds that create an efficient propagation of atomic vibrations in the ab-plane. The ab-planes (graphene layers), on the other hand, are held together by metallic bonding with strength and stiffness comparable to Van der Waals bonding i.e. much weaker than covalent boding, thus reducing the efficiency of vibration propagation in the c-direction (Hooker, Ubbelohde et al. 1965, Sun, Stroscio et al. 2009, Wei, Yang et al. 2014). The difference of electron and phonon transport in the ab-plane direction versus c-direction is manifested in the fact that highly graphitic carbon materials have much higher in-plane than out-of-plane conductivities.

The fact that the conductivities are negatively affected by reduced density, i.e. increased porosity, is easy to understand when keeping the above described mechanisms for electrical and heat conduction in mind, since a material with lower density will have more voids, that will stop electron transport and atomic vibrations. To circumvent the voids/pores conduction in the c-direction is required. Since the c-direction conductivities are much lower than the conductivities in the ab-direction, as well as the fact that the need to circumvent the voids increases the effective length which electrons much travel and carbon atoms vibrations must propagate, the conductivities are drastically reduced with decreased density.

Explaining the effect of graphitisation degree is a little more intricate but still relatively easy, by realising that the in-plane crystallite size is closely linked to the interlayer distance ($d_{(002)}$) and thus degree of graphitisation, as shown by e.g. Maahs (1968) (see Figure 1 in the reference). As explained above both the electrical and thermal conductivity is very good in the ab-plane within a crystal, whereas it much less efficient between crystals even if there is a transport of both electrons and atom vibrations. To summarise, in highly graphitic carbon materials with large crystals there are much fewer crystal-crystal boundaries that decrease the conductivity as compared to less graphitic carbon materials with smaller crystals and higher number conductivity limiting crystal-crystal boundaries. Possible strategies to manufacture highly graphitic carbon materials from biomass will, as already mentioned, be discussed in more detail in section 6 “Concluding remarks” below.

# 5 Studies on graphitisation of biomass without conductivity characterization

Due to missing values on electrical and thermal conductivity these publications might be somewhat less interesting, but are still interesting to review in the search for clues that could enable production of highly graphitic and dense carbon materials from biomass, that thus also most likely would show high electrical and thermal conductivity.

## 5.1 No catalyst used

In all three studies reviewed below there were no extra porosity created by carbonisation/graphitisation process since no catalytical substances (that form nanoparticles when heated) were used. This is of course beneficial for electrical and thermal conductivity if a high degree of graphitisation can be achieved.

Rodríguez-Mirasol, Cordero et al. (1996) studied high-temperature treatment (up to 2800 °C) of kraft lignin. They started with kraft lignin with different ash-content that they pre-carbonised at 350 °C followed by further carbonisation at 1100 °C obtaining lignin-based chars with different ash-content. They continued with heat-treating the medium ash-content char (2.9% ash) at four different temperatures: 1400 °C, 2000 °C, 2400 °C and 2800 °C. They found that when the temperature was 2400 °C or higher they observed a significant change in the X-ray diffraction pattern of the heated lignin. The (002) reflection of the 2400 °C and 2800 °C carbon exhibited a shoulder, and two distinct peaks (not seen for 1400 °C and 2000 °C), which was interpreted as existence of one graphitic (highly ordered) and one turbostratic (less ordered) fraction. By deconvoluting the X-ray diffractograms they could calculate the $d_{(002)}$-distance for both fractions and their result is shown in Table 3 below. It is impressive that the graphitic fraction of the lignin char heat-treated at 2800 °C had such a high degree of graphitisation as 91.9%. These results that show that carbon containing at least a fraction of highly graphitic material can be derived from biomass are encouraging.

Table 3. X-ray diffraction obtained values of 2Θ, $d_{(002)}$ (nm) and $L_c$ (nm) as reported by Rodríguez-Mirasol, Cordero et al. (1996), and degree of graphitisation calculated from $d_{(002)}$-distances using Mering-Maire's model

| Sample | 2Θ | $d_{(002)}$ (nm) | $L_c$ (nm) | DG (%) |
|---|---|---|---|---|
| Original medium ash-content char | 23.273 | 0.3820 | - | -441.9 |
| HTT 1400 °C | 23.400 | 0.3799 | 1.13 | -417.4 |
| HTT 2000 °C | 25.731 | 0.3460 | 1.71 | -23.3 |
| HTT 2400 °C, turbostratic fraction | 26.069 | 0.3416 | 10.34 | 27.9 |
| HTT 2400 °C, graphitic fraction | 26.487 | 0.3363 | 24.00 | 89.5 |
| HTT 2800 °C, turbostratic fraction | 26.054 | 0.3418 | 8.16 | 25.6 |
| HTT 2800 °C, graphitic fraction | 26.505 | 0.3361 | 23.32 | 91.9 |

Kim, Nishiyama et al. (2001) studied carbonisation/graphitisation at 2000 °C of cellulose obtained from the following species: *Halocynthia* (tunicate), *Cladophora* (algae), *Acetobacter* (bacteria), and ramie fibre. X-ray diffraction analysis showed that the order of sharpness of the 002 reflection was: *Halocynthia ~ Cladophora* (sharpest) > *Acetobacter* > ramie (least sharp). This order agrees with that of the crystallinity of the starting materials. High-resolution TEM imaging to the contrary seemed to indicate that graphitised ramie fibres had the most graphitic structure. It is not obvious how to exploit this knowledge, but simply knowing that cellulose from different sources show different tendency to be transformed to graphitic carbon could in the future prove to be useful.

Barin, de Fátima Gimenez et al. (2014) investigated carbonisation at 1500 °C of coconut coir dust, with and without hydrothermal carbonisation as a pre-treatment, and found that by including hydrothermal carbonisation as a pre-step the obtained carbon material was significantly more graphitic. It is questionable if the hydrothermal carbonisation as a pre-step to carbonisation/graphitisation is enough to create a highly graphitic and dense material with high electrical and thermal conductivity. Still, their result must be good knowledge for any scientist working with carbonisation and graphitisation of biomass.

## 5.2 Using catalysis

As already described in section 4.3 “Degree of graphitisation in relation to heat treatment temperature” above, it is by no means trivial to manufacture highly graphitic carbon from biomass. One obvious strategy is to use catalysis since it is well known that use of inorganic compounds lower the heat-treatment temperature required and induce better graphitisation (Marsh and Warburton 1970). For example, the results by Demir, Kahveci et al. (2015), clearly shows that catalysis using manganese (II) nitrate results in significantly higher electrical conductivity and degree of graphitisation, see Figure 13 and Figure 23 above. However, despite the use of catalytic metal salts none of the data for biomass derived carbon materials presented in section 4 “Comparison of bio- and fossil-based graphitic carbon” above, reached a degree of graphitisation above 23% (Demir, Kahveci et al. 2015) (not including the result of 47% of graphitisation by Jiang, Yao et al. (2019) since 50% of the raw material used was reduced graphene oxide not derived from biomass).

Kubo, Uraki et al. (2003) worked with nickel (II) acetate catalysed carbonisation of hardwood acetic acid lignin at temperatures up to 1000 °C. At a nickel concentration of 5.0% and a temperature of 1000 °C they obtained a interlayer distance $d_{(002)}$ of 0.3339 nm which corresponds to a degree of graphitisation of 58%, which is higher than in the publications where conductivity values have been measured. Unfortunately, no information (no data or images) on density and porosity were included in their article, but since nickel acetate is known to form nanoparticles at elevated temperatures is reasonable to assume that their samples were porous and of low density.

Johnson and Faber (2011) used nickel nitrate as the catalytic compound and according to the authors: *“Wood-derived carbon produced after 120 h of catalyst exposure and 1600 °C heat treatment showed graphitic ordering comparable to that of the pitch derived graphite reference”*. However, the porous and fibrous structure of the wood remained, and the sample will thus not show high electrical or thermal conductivity.

Wu, Huang et al. (2016), combined cotton fibres with dissolved iron (III) acetylacetonate. After dropwise addition of the iron (III) acetylacetonate solution to the cotton fibres they were let to rest overnight and thereafter dried at 60 °C for 12 hours. The dried product was then pyrolyzed at 650 °C under an argon environment for 3 hours, to obtain a black iron plus graphitic carbon fibrous precursor. Which was thereafter annealed at 350 °C in air atmosphere for 6 hours, oxidising the iron to $\alpha$-$Fe_2O_3$. To gain pure graphitic carbon hollow capsules, the $Fe_2O_3$ was dissolved with 0.1 M hydrochloric acid. The obtained material was analysed using X-ray diffraction, Raman spectroscopy, thermogravimetry, X-ray photoelectron spectroscopy (XPS), SEM, TEM and high-resolution TEM. The analysis revealed that graphitic carbon, with onion-like structure, encapsulating $\alpha$-$Fe_2O_3$ nanoparticles had been formed, as shown by the TEM and high-resolution TEM images in Figure 24 below. Also, the X-ray diffractograms clearly showed the existence of a clear 002-peak. The obtained particles were used to make an anode in a lithium ion battery that had good performance. However, after removing the $\alpha$-$Fe_2O_3$ these hollow graphitic carbon capsules are not suited to make dense objects with high conductivities, since the hollow nature will force the material to be porous and relatively low in density.

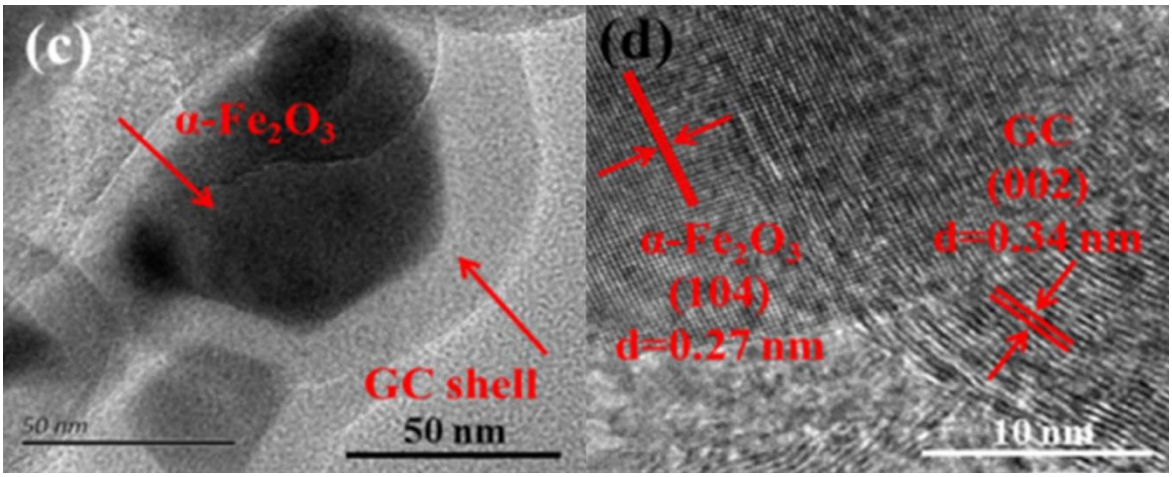


Figure 24. Left: TEM-image showing $\alpha$-$Fe_2O_3$ nanoparticle core surrounded by a shell of graphitic carbon. Right: High-resolution TEM-image showing the 002 fringes that are typical of graphite and spaced approximately 0.34 nm apart, as well as 104 fringes typical of $\alpha$-$Fe_2O_3$ and spaced approximately 0.27 nm apart.

Essentially all catalytic graphitisation use metal salts or metal oxides, which functions by formation of nano-sized metal particles at elevated temperature. Amorphous carbon is dissolved in these metal particles and reprecipitated as graphitic carbon upon cooling, or in the case in which carbon containing gases are formed by a chemical vapour deposition on the surface of the metal particles, the metal will also lead to formation of graphitic carbon (Marsh and Warburton 1970, Sevilla and Fuertes 2010, Hoekstra, Beale et al. 2015, Hoekstra, Beale et al. 2016, Wu, Huang et al. 2016, Zhang, Yan et al. 2018, Li, Yan et al. 2019). When the metal is removed, by for example washing with concentrated acid or by oxidation, voids/pores from the dissolved metal particles remains. This porosity, as described above, will then be an obstacle for reaching high electrical and thermal conductivities. Hence, catalytic graphitisation alone is not the way to achieve high conductivities.

This opinion is further strengthened by the fact that the reviewed publication using catalytic graphitisation, and the resulting carbonaceous materials were porous, where electrical and thermal conductivity was measured (Demir, Kahveci et al. 2015, Ramirez-Rico, Gutierrez-Pardo et al. 2016) showed very mediocre results with an electrical conductivity of 0.106 S/cm (Demir, Kahveci et al.) respectively an electrical conductivity of 76 S/cm and a thermal conductivity of 5.4 W/(m·K) (Ramirez-Rico, Gutierrez-Pardo et al.). The results by Ramirez-Rico, Gutierrez-Pardo et al. (2016) on iron nanoparticle catalysed graphitisation of wood, did indeed show that the crystallinity and crystallite size increased extensively, but the bulk density decreased and the natural porous and fibrous structure of the wood remained, thus limiting the conductivities. Still, highly graphitic but porous structures can be interesting in application where porosity, high surface area, as well as fair electrical conductivity are desired. One example where these properties are desired are electrodes used in supercapacitors, where activated carbon made from coconut shells are the dominating material as of today.

# 6 Concluding remarks

The authors conclude that catalytic graphitisation of biomass cannot easily be used to obtain highly graphitic and dense macroscopic materials, due to the voids formed after removing the catalytic metal particles, but that catalytic graphitisation could be used to make highly graphitic nanoribbons and nanoplatelets (Hoekstra, Beale et al. 2015, Hoekstra, Beale et al. 2016, Zhang, Yan et al. 2018, Li, Yan et al. 2019), with possibly high conductivity. This could be interesting and viable for use in material formulations/composites. One option for removing the porosity in catalytically produced graphitic material from biomass, and maybe obtain high electrical and thermal conductivity, is to compact the material after production by applying high-pressure.

The two most promising ways to obtain macroscopic (> 10x10 cm) highly graphitic and dense carbon material based on this literature review are:

- Chemical vapour deposition on suitable substrate (carbon materials, metals or ceramics) using biomass as carbon source.
- Resistive heating of biomass derived films/objects.

That biomass can be used as carbon source to produce graphene by chemical vapour deposition (CVD) have been shown by both Ruan, Sun et al. (2011) and Seo, Pineda et al. (2017). In both these studies they stopped at single- respectively few-layer graphene, but more traditional thicker pyrolytic carbon sheets that are commonly used in e.g. electronics cooling are commercially manufactured by chemical vapour deposition using fossil raw material, although the trend seems to be moving over to high temperature graphitisation of polymeric films, especially polyimides (Jiangxi Dasen Technology Co. Ltd. 2020, Panasonic Corporation 2020a). Thus, if the CVD process is allowed to proceed for longer times it would hopefully be possible to manufacture highly graphitic and dense carbon films that are several μm thick.

Ruan, Sun et al. (2011) used various carbon sources namely: cookies, chocolate, grass, plastics, roaches, and dog faeces, to produce high-quality single layer graphene indicating that most carbon containing raw materials can be used in their process that uses growth on Cu-foil at 1050 °C under low pressure (10 mTorr obtained by vacuum pumping) with a $H_2$/Ar gas flow. This result indicates that most carbon containing raw materials can be used in their process, which unfortunately have the drawback of using expensive vacuum pumping and purified gases.

The results of Seo, Pineda et al. (2017), though only using a single carbon source, soybean oil, are interesting from another perspective namely that their few-layer graphene growth on Ni-foil was made at a relatively low temperature of 800 °C in ambient air without addition of inert gases. This fact possibly and hopefully makes the process cost-efficient and industrially viable. In their article they used soybean oil as carbon source, which is a mixture of 16% saturated fatty acids, 23% of monounsaturated fatty acids and 58% of polyunsaturated fatty acids, with the following fatty acid composition 7-10% alpha-linolenic acid (C-18:3), 51% linoleic acid (C-18:2), 23%; oleic acid (C-18:1), 4% stearic acid (C-18:0), 4%, and 10% palmitic acid (C-16:0) (Ivanov, Lević et al. 2010). These fatty acids have boiling points from 230 °C (alpha-linolenic acid and linoleic acid) to 361 °C (stearic acid – which decomposes rather than boils).

Within the Digital Cellulose Center there naturally is a desire to use biomass from forests, and most preferable are the most abundant polymers cellulose and lignin. Cellulose have a decomposition temperature range of 315–400 °C and lignin have a wider range of 150-900 °C (Yang, Yan et al. 2007). This is not very different from soybean oil, which might suggest that cellulose or lignin can be successfully used in an ambient air CVD process. However, if the fatty characteristic of the soybean oil is a pre-requisite for success (impossible to say without trying it experimentally or having more data). Then it might be possible to use extractives from the pulping process as raw material, such as tall oil. Normally crude tall oil contains rosins, which contains resin acids (mainly abietic acid and its isomers), fatty acids (mainly palmitic acid, oleic acid and linoleic acid) and fatty alcohols, unsaponifiable sterols (5–10%), some sterols, and other alkyl hydrocarbon derivates. Making its composition not completely but fairly like that of soybean oil. Tall oil can also, if needed, be processed further by fractional distillation to tall oil rosin, with rosin content reduced to 10–35%. By further reduction of the rosin content, so called tall oil fatty acid, can be obtained. Tall oil fatty acid is comparatively cheap, contain only 1-10% rosin, and consists mostly of oleic acid, making it an excellent source of volatile fatty acids. Another option could be condensed tannins that can be hot water extracted from spruce bark (Kemppainen, Siika-aho et al. 2014), which due to their polyphenolic nature with conjugated $sp^2$-hybridised double bonds show some similarity to graphite, and thus may be easy to graphitise?

The interest and hopefully viability of using resistive heating of biomass derived objects is based on two publications. The first one is the publication by Jiang, Yao et al. (2019) in which they managed to produce a 5 μm thick highly graphitic film that had an impressive electrical conductivity of 4480 S/cm. It was prepared by making a film consisting of 50% lignin with low sulphonate content (4 mass% sulphur) and 50% reduced graphene oxide, and resistively heat the film to 2192 °C which turned it highly graphitic. The conductivity thereof was especially impressive 4480 S/cm in the light of that the reported interlayer spacing ($d_{(0002)}$) of 0.34 nm corresponds to a degree of graphitisation of only 47%, according to the model suggested by Maire and Mering (1970).

However, using as much as 50% fossil-derived reduced graphene oxide make the material less attractive. It is hypothesised, that this reduced graphene oxide could be replaced by biomass derived graphene that for example can be manufactured by the above described CVD methods or by using the highly graphitic carbon fraction produced from lignin by Rodríguez-Mirasol, Cordero et al. (1996) using very high-temperature (2800 °C) graphitisation. The latter alternative is dependent on the availability of economically viable ways to separate the turbostratic and graphitic fractions. The graphitic fraction showed an interlayer spacing of 0.3361 nm, and according to Mering-Marie's equation this corresponds to a degree of graphitisation of 91.9%. With this high degree of graphitisation, the graphitic carbon fraction should likely make good nucleating sites for the biomass it is mixed with.

Still, it would be preferable, especially from a cost perspective, if the required loading of graphene or highly graphitic carbon could be reduced. If film formation is an issue with lower content of graphene, RISE have a lot of expertise and knowledge in producing lignin films. For example, mixes of cellulose nanofibrils and lignin show good film forming properties.

The second publication indicating the viability of resistive heating is the one by Luong, Bets et al. (2020), in which the authors found that when different carbon containing amorphous compounds (coal, petroleum coke, biochar, carbon black, discarded food e.g. used ground coffee, rubber tyres and mixed plastic waste) were resistively heated to temperatures around 2800 °C they got turbostratic graphene of high quality within 10-150 mS depending on applied voltage and electrode distance. The restive heating was made at reduced pressure. According to the authors of these articles the reduced pressure was used solely for safety reasons, and they claim that the "*the FJH (flash Joule heating) process works equally well at 1 atm*". Due to the very short time needed the authors decided to refer to the resulting graphene as flash graphene (FG). The fact that they got turbostratic graphene the authors explain as follows: *"The (002) peak of FG occurs at diffraction angle $2\theta = 26.1°$, which corresponds to an interlayer spacing of $I_c = 3.45$ Å. This spacing is larger than that in a typical Bernal (AB-stacked) graphite, 3.37 Å, indicating the expanded and turbostratic structure of FG. The (002) peak was found to be unsymmetric, with a tail at small angles, which further suggests the turbostratic nature of FG. The flash process is fast enough to prevent AB stacking."*. With this explanation in mind it should be possible to make highly graphitic carbon by using a slower heating. The influence of heating rate, and what which would be optimal for obtaining different structured carbon materials need to be determined experimentally.

Luong, Bets et al. (2020) also highlights the energy efficiency of their process requiring only 7.2 kJ/g if a high carbon content material as carbon black is used, which they claim could make flash graphene cheap enough to be used in bulk composites of plastic, metals, plywood, concrete and other building materials. If instead lignin with a carbon content of approximately 60% would be used the energy demand would become approximately 12 kJ/g, which still probably should best cost competitive.

To summarise, the authors of this review consider that further research and development of the resistive heating techniques and CVD-processes using biomass as carbon source, are the two most promising paths to reach cost efficient production of dense and highly graphitic carbon materials with high electrical and thermal conductivity from biomass.

# References


Acheson, E. (1896). "Manufacture of graphite." US568323,

Adamson, G. A. and C. W. Rees (1996). "Towards the total synthesis of cyclo [n] carbons and the generation of cyclo [6] carbon." Journal of the Chemical Society, Perkin Transactions 1(13): 1535-1543.

Akamatu, H., H. Inokuchi, H. Takahashi and Y. Matsunaga (1956). "Studies on the Graphitization. I. Changes of Crystallinity, Diamagnetic Susceptibility and Electrical Conductivity in the Process of Graphitization." Bulletin of the Chemical Society of Japan **29**(5): 574-581.

Amorphous carbon - Chalk, S. J. (2019). "On-line version created by Chalk, S. J. based on the IUPAC. Compendium of Chemical Terminology, 2nd ed. (the "Gold Book"), compiled by McNaught, A. D. and Wilkinson, A. ." Retrieved 2019-10-15, from https://goldbook.iupac.org/terms/view/A00294.

An, S. J., J. Li, C. Daniel, D. Mohanty, S. Nagpure and D. L. Wood III (2016). "The state of understanding of the lithium-ion-battery graphite solid electrolyte interphase (SEI) and its relationship to formation cycling." Carbon **105**: 52-76.

Antonov, A., V. Baryshev, I. Grigoryeva, G. Kulipanov and N. Shchipkov (1991). "Focusing shaped pyrographite monochromators in synchrotron radiation experiments." Nuclear Instruments and Methods in Physics Research Section A: Accelerators, Spectrometers, Detectors and Associated Equipment **308**(1-2): 442-446.

Avouris, P. and C. Dimitrakopoulos (2012). "Graphene: synthesis and applications." Materials today **15**(3): 86-97.

Babich, A. and D. Senk (2013). Chapter 12 - Coal use in iron and steel metallurgy. The Coal Handbook: Towards Cleaner Production: Volume 2: Coal Utilisation. D. Osborne, Elsevier. **2:** 267-311.

Baknor Electronics Industries Inc. (2019). "Baknor Graphene Based Film Heat Sink Solutions." Retrieved 2019-11-05, from http://www.baknorthermal.com/download-files/graphene/Baknor-Graphene-Based-Film-Heat-Sink-Solutions.pdf.

Balogun, M.-S., W. Qiu, Y. Luo, H. Meng, W. Mai, A. Onasanya, T. K. Olaniyi and Y. Tong (2016). "A review of the development of full cell lithium-ion batteries: The impact of nanostructured anode materials." Nano research **9**(10): 2823-2851.

Barin, G. B., I. de Fátima Gimenez, L. P. da Costa, A. G. Souza Filho and L. S. Barreto (2014). "Influence of hydrothermal carbonization on formation of curved graphite structures obtained from a lignocellulosic precursor." Carbon **78**: 609-612.

Barzegar, F., A. Bello, D. Momodu, M. J. Madito, J. Dangbegnon and N. Manyala (2016). "Preparation and characterization of porous carbon from expanded graphite for high energy density supercapacitor in aqueous electrolyte." Journal of Power Sources **309**: 245-253.

Beaulieu, L., K. Eberman, R. Turner, L. Krause and J. Dahn (2001). "Colossal reversible volume changes in lithium alloys." Electrochemical and Solid-State Letters **4**(9): A137-A140.

Beaumont, E. (1985). "Industrial charcoal making." FAO Forestry Paper **63**.

Bhargava, S., H. Bist, S. Sahli, M. Aslam and H. Tripathi (1995). "Diamond polytypes in the chemical vapor deposited diamond films." Applied physics letters **67**(12): 1706-1708.

Björk, V. O. (1972). "The pyrolytic carbon occluder for the Björk-Shiley tilting disc valve prosthesis." Scandinavian journal of thoracic and cardiovascular surgery **6**(2): 109-113.

Blue, M. and G. Danielson (1957). "Electrical Properties of Arc-Evaporated Carbon Films." Journal of Applied Physics **28**(5): 583-586.

Boehm, H.-P., A. Clauss, G. Fischer and U. Hofmann (1962). "Das adsorptionsverhalten sehr dünner kohlenstoff-folien." Zeitschrift für anorganische und allgemeine Chemie **316**(3-4): 119-127.

Boehm, H. P., R. Setton and E. Stumpp (1986). "Nomenclature and terminology of graphite intercalation compounds." Carbon **24**(2): 241-245.

Boyd Corporation. (2019). "Heat Spreading Graphite Technology | k-Core®." Retrieved 2019-11-05, from https://www.boydcorp.com/thermal/conduction-cooling/graphite-technologies.html.
Boyd Corporation. (2020). "Thermal interface materials." Retrieved 2020-02-11, from https://www.boydcorp.com/thermal/conduction-cooling/thermal-interface-materials.html.
Buerschaper, R. A. (1944). "Thermal and electrical conductivity of graphite and carbon at low temperatures." Journal of Applied Physics **15**(5): 452-454.
Bundy, F., H. T. Hall, H. Strong and R. W. Jun (1955). "Man-made diamonds." Nature **176**(4471): 51.
Bundy, F. and J. Kasper (1967). "Hexagonal diamond—a new form of carbon." The Journal of Chemical Physics **46**(9): 3437-3446.
Burgemeister, E. (1978). "Thermal conductivity of natural diamond between 320 and 450 K." Physica B+ C **93**(2): 165-179.
Cançado, L., K. Takai, T. Enoki, M. Endo, Y. Kim, H. Mizusaki, A. Jorio, L. Coelho, R. Magalhaes-Paniago and M. Pimenta (2006). "General equation for the determination of the crystallite size L a of nanographite by Raman spectroscopy." Applied Physics Letters **88**(16): 163106.
Cao, Y., S. Cong, X. Cao, F. Wu, Q. Liu, M. R. Amer and C. Zhou (2017). "Review of Electronics Based on Single-Walled Carbon Nanotubes." Topics in Current Chemistry **375**(5): 75.
Carlomagno, G. M. (2011). Computational methods and experimental measurements XV, WIT press, ISBN-10: 1845645405.
Chaffee Jr, F. H. and B. L. Lutz (1978). "The detection of interstellar diatomic carbon toward Zeta Ophiuchi." The Astrophysical Journal **221**: L91-L93.
Choi, W., I. Lahiri, R. Seelaboyina and Y. S. Kang (2010). "Synthesis of graphene and its applications: a review." Critical Reviews in Solid State and Materials Sciences **35**(1): 52-71.
Comelli, G., J. Stöhr, C. Robinson and W. Jark (1988). "Structural studies of argon-sputtered amorphous carbon films by means of extended x-ray-absorption fine structure." Physical Review B **38**(11): 7511.
Cook, S. D., R. D. Beckenbaugh, J. Redondo, L. S. Popich, J. J. Klawitter and R. L. Linscheid (1999). "Long-term follow-up of pyrolytic carbon metacarpophalangeal implants." JBJS **81**(5): 635-648.
Czarnecki, J. S., M. Blackmore, S. Jolivet, K. Lafdi and P. A. Tsonis (2014). "Bone growth on reticulated vitreous carbon foam scaffolds and implementation of cellular automata modeling as a predictive tool." Carbon **79**: 135-148.
Demir, M., Z. Kahveci, B. Aksoy, N. K. Palapati, A. Subramanian, H. T. Cullinan, H. M. El-Kaderi, C. T. Harris and R. B. Gupta (2015). "Graphitic biocarbon from metal-catalyzed hydrothermal carbonization of lignin." Industrial & Engineering Chemistry Research **54**(43): 10731-10739.
Denisenko, A. and E. Kohn (2005). "Diamond power devices. Concepts and limits." Diamond and related materials **14**(3-7): 491-498.
Diederich, F., Y. Rubin, C. B. Knobler, R. L. Whetten, K. E. Schriver, K. N. Houk and Y. Li (1989). "All-Carbon Molecules: Evidence for the Generation of Cyclo [18] carbon from a Stable Organic Precursor." Science: 1088-1090.
Dorcheh, A. S. and M. Abbasi (2008). "Silica aerogel; synthesis, properties and characterization." Journal of materials processing technology **199**(1-3): 10-26.
DREYER SYSTEM GmbH. (2019). "HighPower-Heat Sinks." http://www.dreyer-system.eu/highpower-heat-sinks.html.
DREYER SYSTEM GmbH. (2020). "SPREADERSHIELD™ Heat Spreaders." https://www.dreyer-system.eu/egraf-heat-spreader.html.
Due, J. and A. J. Robinson (2013). "Reliability of thermal interface materials: A review." Applied Thermal Engineering **50**(1): 455-463.
Fan, Q., C. Chai, Q. Wei, K. Wong, Y. Liu and Y. Yang (2018). "Theoretical investigations of group IV alloys in the Lonsdaleite phase." Journal of materials science **53**(4): 2785-2801.

Federman, S. and W. Huntress Jr (1989). "Diffuse interstellar clouds as a chemical laboratory-The chemistry of diatomic carbon species." The Astrophysical Journal **338**: 140-146.
Foster, L., G. Long and H. Stumpf (1958). "Production of graphite single crystals by the thermal decomposition of aluminum carbide." American Mineralogist: Journal of Earth and Planetary Materials **43**(3-4): 285-296.
Franklin, R. E. (1951). "Crystallite growth in graphitizing and non-graphitizing carbons." Proceedings of the Royal Society of London. Series A. Mathematical and Physical Sciences **209**(1097): 196-218.
Frondel, C. and U. B. Marvin (1967). "Lonsdaleite, a hexagonal polymorph of diamond." Nature **214**(5088): 587.
Fu, Y., J. Hansson, Y. Liu, S. Chen, A. Zehri, M. K. Samani, N. Wang, Y. Ni, Y. Zhang and Z.-B. Zhang (2019). "Graphene related materials for thermal management." 2D Materials **7**(1): 012001.
Fullerenes - Chalk, S. J. (2019). "On-line version created by Chalk, S. J. based on the IUPAC. Compendium of Chemical Terminology, 2nd ed. (the "Gold Book"), compiled by McNaught, A. D. and Wilkinson, A. ." Retrieved 2019-10-15, from https://goldbook.iupac.org/terms/view/F02547.
Gibson, J., M. Holohan and H. Riley (1946). "87. Amorphous carbon." Journal of the Chemical Society (Resumed): 456-461.
Glass-like carbon - Chalk, S. J. (2019). "On-line version created by Chalk, S. J. based on the IUPAC. Compendium of Chemical Terminology, 2nd ed. (the "Gold Book"), compiled by McNaught, A. D. and Wilkinson, A. ." Retrieved 2019-10-15, from http://goldbook.iupac.org/terms/view/G02639.
Gogotsi, Y., A. Nikitin, H. Ye, W. Zhou, J. E. Fischer, B. Yi, H. C. Foley and M. W. Barsoum (2003). "Nanoporous carbide-derived carbon with tunable pore size." Nature materials **2**(9): 591.
González, D., M. Montes-Morán, R. Young and A. Garcia (2002). "Effect of temperature on the graphitization process of a semianthracite." Fuel processing technology **79**(3): 245-250.
Goriparti, S., E. Miele, F. De Angelis, E. Di Fabrizio, R. P. Zaccaria and C. Capiglia (2014). "Review on recent progress of nanostructured anode materials for Li-ion batteries." Journal of power sources **257**: 421-443.
Graphene - Chalk, S. J. (2019). "On-line version created by Chalk, S. J. based on the IUPAC. Compendium of Chemical Terminology, 2nd ed. (the "Gold Book"), compiled by McNaught, A. D. and Wilkinson, A. ." Retrieved 2019-10-15, from https://goldbook.iupac.org/terms/view/G02683.
Graphite - Chalk, S. J. (2019). "On-line version created by Chalk, S. J. based on the IUPAC. Compendium of Chemical Terminology, 2nd ed. (the "Gold Book"), compiled by McNaught, A. D. and Wilkinson, A. ." Retrieved 2019-10-15, from http://goldbook.iupac.org/terms/view/G02684.
Graphitization - Chalk, S. J. (2019). "On-line version created by Chalk, S. J. based on the IUPAC. Compendium of Chemical Terminology, 2nd ed. (the "Gold Book"), compiled by McNaught, A. D. and Wilkinson, A. ." Retrieved 2019-10-15, from https://goldbook.iupac.org/terms/view/G02691.
Grigorieva, I. and A. Antonov (2003). "HOPG as powerful x-ray optics." X-Ray Spectrometry: An International Journal **32**(1): 64-68.
Gupta, R. (2007). "Advanced coal characterization: a review." Energy & Fuels **21**(2): 451-460.
Haag, G. (2005). "Properties of ATR-2E graphite and property changes due to fast neutron irradiation." 0944-2952,
Hall, H. T. (1960). "Diamond synthesis." US2947608A, General Electric Co.
Hansson, J., T. M. Nilsson, L. Ye and J. Liu (2018). "Novel nanostructured thermal interface materials: a review." International Materials Reviews **63**(1): 22-45.

Harris, P. (2004). "Fullerene-related structure of commercial glassy carbons." Philosophical Magazine **84**(29): 3159-3167.
Highly oriented pyrolytic graphite - Chalk, S. J. (2019). "On-line version created by Chalk, S. J. based on the IUPAC. Compendium of Chemical Terminology, 2nd ed. (the "Gold Book"), compiled by McNaught, A. D. and Wilkinson, A. ." Retrieved 2019-10-15, from https://goldbook.iupac.org/terms/view/H02823.
Hoekstra, J., A. M. Beale, F. Soulimani, M. Versluijs-Helder, J. W. Geus and L. W. Jenneskens (2015). "Base metal catalyzed graphitization of cellulose: a combined Raman spectroscopy, temperature-dependent X-ray diffraction and high-resolution transmission electron microscopy study." The Journal of Physical Chemistry C **119**(19): 10653-10661.
Hoekstra, J., A. M. Beale, F. Soulimani, M. Versluijs-Helder, D. Van De Kleut, J. M. Koelewijn, J. W. Geus and L. W. Jenneskens (2016). "The effect of iron catalyzed graphitization on the textural properties of carbonized cellulose: Magnetically separable graphitic carbon bodies for catalysis and remediation." Carbon **107**: 248-260.
Holland, M., C. Klein and W. Straub (1966). "The lorenz number of graphite at very low temperatures." Journal of Physics and Chemistry of Solids **27**(5): 903-906.
Hooker, C., A. R. J. P. Ubbelohde and D. Young (1965). "Anisotropy of thermal conductance in near-ideal graphite." Proceedings of the Royal Society of London. Series A. Mathematical and physical sciences **284**(1396): 17-31.
Houska, C. and B. Warren (1954). "X-ray Study of the Graphitization of Carbon Black." Journal of Applied Physics **25**(12): 1503-1509.
Huawei Technologies Co. Ltd. (2016). "Huawei Achieves Major Breakthrough in Graphene-Assisted High Temperature Li-ion Batteries." Retrieved 2020-02-11, from https://www.huawei.com/en/press-events/news/2016/12/graphene-assisted-li-ion-batteries.
Hunn, J. D., G. E. Jellison Jr and R. A. Lowden (2008). "Increase in pyrolytic carbon optical anisotropy and density during processing of coated particle fuel due to heat treatment." Journal of nuclear materials **374**(3): 445-452.
Inagaki, M. and F. Kang (2014). Materials science and engineering of carbon: fundamentals, Butterworth-Heinemann, ISBN-10: 0128011521.
Inagaki, M. and F. Kang (2016). Materials science and engineering of carbon: characterization, Butterworth-Heinemann, ISBN-10: 0128054689.
Isberg, J., M. Gabrysch, A. Tajani and D. Twitchen (2006). High-field electrical transport in single crystal CVD diamond diodes. Advances in Science and Technology, Trans Tech Publ.
Isberg, J., J. Hammersberg, E. Johansson, T. Wikström, D. J. Twitchen, A. J. Whitehead, S. E. Coe and G. A. Scarsbrook (2002). "High carrier mobility in single-crystal plasma-deposited diamond." Science **297**(5587): 1670-1672.
Itzhaki, L., E. Altus, H. Basch and S. Hoz (2005). "Harder than Diamond: Determining the Cross-Sectional Area and Young's Modulus of Molecular Rods." Angewandte Chemie International Edition **44**(45): 7432-7435.
Ivanov, D. S., J. D. Lević and S. A. Sredanović (2010). "Fatty acid composition of various soybean products." Food and Feed research **37**(2): 65-70.
Iwashita, N. (2016). X-ray Powder Diffraction. Materials science and engineering of carbon: characterization. M. Inagaki and F. Kang, Butterworth-Heinemann**:** 7-25.
Iwashita, N. and M. Inagaki (1993). "Relations between structural parameters obtained by X-ray powder diffraction of various carbon materials." Carbon **31**(7): 1107-1113.
Jara, A. D., A. Betemariam, G. Woldetinsae and J. Y. Kim (2019). "Purification, application and current market trend of natural graphite: A review." International Journal of Mining Science and Technology **29**(5): 671-689.
Ji, L., Z. Lin, M. Alcoutlabi and X. Zhang (2011). "Recent developments in nanostructured anode materials for rechargeable lithium-ion batteries." Energy & Environmental Science **4**(8): 2682-2699.

Jiang, F., Y. Yao, B. Natarajan, C. Yang, T. Gao, H. Xie, Y. Wang, L. Xu, Y. Chen, J. Gilman, L. Cui and L. Hu (2019). "Ultrahigh-temperature conversion of biomass to highly conductive graphitic carbon." Carbon **144**: 241-248.
Jiangxi Dasen Technology Co. Ltd. (2020). "Synthetic graphite sheet." Retrieved 2020-02-11, from http://www.szdasen.com/html/en/products/sitecms/.
Johnson, M. T. and K. T. Faber (2011). "Catalytic graphitization of three-dimensional wood-derived porous scaffolds." Journal of Materials Research **26**(1): 18-25.
Kaburagi, Y., A. Yoshida and Y. Hishiyama (2016). Raman Spectroscopy. Materials science and engineering of carbon: characterization. M. Inagaki and F. Kang, Butterworth-Heinemann**:** 125-152.
Kaiser, K., L. M. Scriven, F. Schulz, P. Gawel, L. Gross and H. L. Anderson (2019). "An sp-hybridized molecular carbon allotrope, cyclo [18] carbon." Science **365**(6459): 1299-1301.
Kamali, A. R. and D. J. Fray (2010). "Review on carbon and silicon based materials as anode materials for lithium ion batteries." J. New Mater. Electrochem. Syst **13**(2): 147-160.
Kamali, A. R. and D. J. Fray (2011). "Tin-based materials as advanced anode materials for lithium ion batteries: a review." Rev. Adv. Mater. Sci **27**(1): 14-24.
Katagiri, N., M. Ishikawa, N. Adachi, M. Fuji and T. Ota (2015). "Preparation and evaluation of Au nanoparticle–silica aerogel nanocomposite." Journal of Asian Ceramic Societies **3**(2): 151-155.
Katzman, H. A., P. Adams, T. Le and C. S. Hemminger (1994). "Characterization of low thermal conductivity PAN-based carbon fibers." Carbon **32**(3): 379-391.
Kemppainen, K., M. Siika-aho, S. Pattathil, S. Giovando and K. Kruus (2014). "Spruce bark as an industrial source of condensed tannins and non-cellulosic sugars." Industrial Crops and Products **52**: 158-168.
Kim, D.-Y., Y. Nishiyama, M. Wada and S. Kuga (2001). "Graphitization of highly crystalline cellulose." Carbon **39**(7): 1051-1056.
Klemens, P. (2000). "Theory of the a-plane thermal conductivity of graphite." Journal of Wide Bandgap Materials **7**(4): 332-339.
Kolmogorov, Y. and V. Trounova (2002). "Analytical potential of EDXRF using toroidal focusing systems of highly oriented pyrolytic graphite (HOPG)." X-Ray Spectrometry: An International Journal **31**(6): 432-436.
Kotrechko, S., A. Mazilov, T. Mazilova, E. Sadanov and I. Mikhailovskij (2012). "Experimental determination of the mechanical strength of monatomic carbon chains." Technical Physics Letters **38**(2): 132-134.
Kotrechko, S., I. Mikhailovskij, T. Mazilova, E. Sadanov, A. Timoshevskii, N. Stetsenko and Y. Matviychuk (2015). "Mechanical properties of carbyne: experiment and simulations." Nanoscale research letters **10**(1): 24.
Kroto, H. (2010). "Carbyne and other myths about carbon." RSC Chemistry World **11**(7).
Kroto, H. W., J. R. Heath, S. C. O'Brien, R. F. Curl and R. E. Smalley (1985). "C60: Buckminsterfullerene." Nature **318**(6042): 162-163.
Kubo, S., Y. Uraki and Y. Sano (2003). "Catalytic graphitization of hardwood acetic acid lignin with nickel acetate." Journal of wood science **49**(2): 188-192.
Kwiecińska, B. and H. Petersen (2004). "Graphite, semi-graphite, natural coke, and natural char classification—ICCP system." International Journal of Coal Geology **57**(2): 99-116.
Lagow, R. J., J. J. Kampa, H.-C. Wei, S. L. Battle, J. W. Genge, D. A. Laude, C. J. Harper, R. Bau, R. C. Stevens and J. F. Haw (1995). "Synthesis of linear acetylenic carbon: the" sp" carbon allotrope." Science **267**(5196): 362-367.
Lalwani, G. and B. Sitharaman (2013). "Multifunctional fullerene-and metallofullerene-based nanobiomaterials." Nano Life **3**(03): 1342003.
Laverty, P., L. Nicks and L. Walters (1994). "Recovery of flake graphite from steelmaking kish."
Lee, C., X. Wei, J. W. Kysar and J. Hone (2008). "Measurement of the elastic properties and intrinsic strength of monolayer graphene." science **321**(5887): 385-388.
Lee, S.-M., D.-S. Kang and J.-S. Roh (2015). "Bulk graphite: materials and manufacturing process." Carbon letters **16**(3): 135-146.

Li, C., E. T. Thostenson and T.-W. Chou (2008). "Sensors and actuators based on carbon nanotubes and their composites: a review." Composites Science and Technology **68**(6): 1227-1249.
Li, J., Q. Yan, X. Zhang, J. Zhang and Z. Cai (2019). "Efficient conversion of lignin waste to high value bio-graphene oxide nanomaterials." Polymers **11**(4): 623.
Li, Z., L. Chen, S. Meng, L. Guo, J. Huang, Y. Liu, W. Wang and X. Chen (2015). "Field and temperature dependence of intrinsic diamagnetism in graphene: Theory and experiment." Physical Review B **91**(9): 094429.
Liang, C., M. Gao, H. Pan, Y. Liu and M. Yan (2013). "Lithium alloys and metal oxides as high-capacity anode materials for lithium-ion batteries." Journal of alloys and compounds **575**: 246-256.
Libra, J. A., K. S. Ro, C. Kammann, A. Funke, N. D. Berge, Y. Neubauer, M.-M. Titirici, C. Fühner, O. Bens and J. Kern (2011). "Hydrothermal carbonization of biomass residuals: a comparative review of the chemistry, processes and applications of wet and dry pyrolysis." Biofuels **2**(1): 71-106.
Lindemer, T. B., E. L. Long Jr and R. L. Beatty (1978). "Pyrolytic carbon-coated nuclear fuel." US4077838A, US Department of Energy.
Liu, J., W. Qu, Y. Xie, B. Zhu, T. Wang, X. Bai and X. Wang (2017). "Thermal conductivity and annealing effect on structure of lignin-based microscale carbon fibers." Carbon **121**: 35-47.
Liu, M., V. I. Artyukhov, H. Lee, F. Xu and B. I. Yakobson (2013). "Carbyne from first principles: chain of C atoms, a nanorod or a nanorope." ACS nano **7**(11): 10075-10082.
Liu, S. and C. R. Loper Jr (1991). "The formation of kish graphite." Carbon **29**(4-5): 547-555.
Luo, X. and D. D. L. Chung (1996). "Electromagnetic interference shielding reaching 130 dB using flexible graphite." Carbon **34**(10): 1293-1294.
Luong, D. X., K. V. Bets, W. A. Algozeeb, M. G. Stanford, C. Kittrell, W. Chen, R. V. Salvatierra, M. Ren, E. A. McHugh and P. A. Advincula (2020). "Gram-scale bottom-up flash graphene synthesis." Nature: 1-5.
Ma, P.-C., N. A. Siddiqui, G. Marom and J.-K. Kim (2010). "Dispersion and functionalization of carbon nanotubes for polymer-based nanocomposites: a review." Composites Part A: Applied Science and Manufacturing **41**(10): 1345-1367.
Maahs, H. G. (1968). "Crystallographic data on selected artificial graphites with comments on the role of the degree of crystal development in oxidation."
Maire, J. and J. Mering (1970). "Graphitization of soft carbons." Chemistry and physics of carbon **6**: 125-190.
Marsden, B., M. Haverty, W. Bodel, G. Hall, A. Jones, P. Mummery and M. Treifi (2016). "Dimensional change, irradiation creep and thermal/mechanical property changes in nuclear graphite." International Materials Reviews **61**(3): 155-182.
Marsh, H. and M. Diez (1994). Mesophase of graphitizable carbons. Liquid Crystalline and Mesomorphic Polymers. V. P. Shibaev and L. Lam, Springer**:** 231-257.
Marsh, H. and A. Warburton (1970). "Catalysis of graphitisation." Journal of Applied Chemistry **20**(4): 133-142.
Masikhwa, T. M., M. J. Madito, A. Bello, J. K. Dangbegnon and N. Manyala (2017). "High performance asymmetric supercapacitor based on molybdenum disulphide/graphene foam and activated carbon from expanded graphite." Journal of colloid and interface science **488**: 155-165.
McClure, J. (1957). "Band structure of graphite and de Haas-van Alphen effect." Physical Review **108**(3): 612.
McLintock, I. and J. Orr (1973). "Evaporated carbon films." Chemistry and physics of carbon **11**(SKA FINNAS I TRYCKT FORMAT PÅ KTHB): 243-312.
Mounier, E., F. Bertin, M. Adamik, Y. Pauleau and P. Barna (1996). "Effect of the substrate temperature on the physical characteristics of amorphous carbon films deposited by dc magnetron sputtering." Diamond and related materials **5**(12): 1509-1515.

Murakami, M., N. Nishiki, K. Nakamura, J. Ehara, H. Okada, T. Kouzaki, K. Watanabe, T. Hoshi and S. Yoshimura (1992). "High-quality and highly oriented graphite block from polycondensation polymer films." Carbon **30**(2): 255-262.
Nakamura, S., D. Miyafuji, T. Fujii, T. Matsui and H. Fukuyama (2017). "Low temperature transport properties of pyrolytic graphite sheet." Cryogenics **86**: 118-122.
Norley, J. (2001). "Technical brief: the role of natural graphite in electronics cooling." Electronics Cooling **7**: 50-51.
Novoselov, K. S., A. K. Geim, S. V. Morozov, D. Jiang, Y. Zhang, S. V. Dubonos, I. V. Grigorieva and A. A. Firsov (2004). "Electric field effect in atomically thin carbon films." Science **306**(5696): 666-669.
Null, M., W. Lozier and A. Moore (1973). "Thermal diffusivity and thermal conductivity of pyrolytic graphite from 300 to 2700 K." Carbon **11**(2): 81-87.
Nur, Y., M. W. Pitcher, S. Seyyidoğlu and L. Toppare (2008). "Facile Synthesis of Poly (hydridocarbyne): A Precursor to Diamond and Diamond-like Ceramics." Journal of Macromolecular Science, Part A **45**(5): 358-363.
O'Malley, B., I. Snook and D. McCulloch (1998). "Reverse Monte Carlo analysis of the structure of glassy carbon using electron-microscopy data." Physical Review B **57**(22): 14148.
Oberlin, A. (1984). "Carbonization and graphitization." Carbon **22**(6): 521-541.
Ogale, A., C. Lin, D. Anderson and K. Kearns (2002). "Orientation and dimensional changes in mesophase pitch-based carbon fibers." Carbon **40**(8): 1309-1319.
Olson, D. W., R. L. Virta, M. Mahdavi, E. S. Sangine and S. M. Fortier (2016). Natural graphite demand and supply—Implications for electric vehicle battery requirements, ISBN-10: 0072-1077.
Osetzky, D. (1974). "Macrocrystalline graphite from magnesium carbide." Carbon **12**(5): 517-523.
Oya, A. and H. Marsh (1982). "Phenomena of catalytic graphitization." Journal of Materials Science **17**(2): 309-322.
Pagni, J. (2010). "Amroy aims to become nano-leader." European Plastics News **5**.
Pan, Z., H. Sun, Y. Zhang and C. Chen (2009). "Harder than diamond: superior indentation strength of wurtzite BN and lonsdaleite." Physical Review Letters **102**(5): 055503.
Panasonic Corporation. (2020a). "Thermal Management Solutions Products Catalog." Retrieved 2020-02-11, from https://industrial.panasonic.com/cdbs/www-data/pdf/AYA0000/AYA0000COL24.pdf.
Panasonic Corporation. (2020b). "PGS Graphite Sheets." Retrieved 2020-02-11, from https://www.panasonic.com/global/corporate/technology-design/technology/pgs.html.
Partoens, B. and F. Peeters (2006). "From graphene to graphite: Electronic structure around the K point." Physical Review B **74**(7): 075404.
Pec, M. K., R. Reyes, E. Sánchez, D. Carballar, A. Delgado, J. Santamaría, M. Arruebo and C. Evora (2010). "Reticulated vitreous carbon: a useful material for cell adhesion and tissue invasion." Eur Cell Mater **20**: 282-294.
Pekala, R. and D. Schaefer (1993). "Structure of organic aerogels. 1. Morphology and scaling." Macromolecules **26**(20): 5487-5493.
Peltonen Ski Oy. (2018). "PELTONEN SKI CATALOG 2019." http://www.peltonenski.fi/download/peltonen-ski-catalog-2019/#.
Pierson, H. O. (2012). Handbook of carbon, graphite, diamonds and fullerenes: processing, properties and applications, William Andrew, ISBN-10: 0815517394.
Presser, V., M. Heon and Y. Gogotsi (2011). "Carbide-Derived Carbons - From Porous Networks to Nanotubes and Graphene." Advanced Functional Materials **21**(5): 810-833.
Primo, A., P. Atienzar, E. Sanchez, J. M. Delgado and H. García (2012). "From biomass wastes to large-area, high-quality, N-doped graphene: catalyst-free carbonization of chitosan coatings on arbitrary substrates." Chemical communications **48**(74): 9254-9256.
Proserpio, D. M., A. A. Golov and A. A. Kabanov. (2019). "SACADA - Samara Carbon Allotrope Database." Retrieved 2019-09-24, from http://sacada.sctms.ru/.

Pyrolytic carbon - Chalk, S. J. (2019). "On-line version created by Chalk, S. J. based on the IUPAC. Compendium of Chemical Terminology, 2nd ed. (the "Gold Book"), compiled by McNaught, A. D. and Wilkinson, A. ." Retrieved 2019-10-15, from https://goldbook.iupac.org/terms/view/P04963.
Pyrolytic graphite - Chalk, S. J. (2019). "On-line version created by Chalk, S. J. based on the IUPAC. Compendium of Chemical Terminology, 2nd ed. (the "Gold Book"), compiled by McNaught, A. D. and Wilkinson, A. ." Retrieved 2019-10-15, from https://goldbook.iupac.org/terms/view/P04964.
Qi, W., J. G. Shapter, Q. Wu, T. Yin, G. Gao and D. Cui (2017). "Nanostructured anode materials for lithium-ion batteries: principle, recent progress and future perspectives." Journal of Materials Chemistry A **5**(37): 19521-19540.
Qiu, L., B. Huang, Z. He, Y. Wang, Z. Tian, J. Z. Liu, K. Wang, J. Song, T. R. Gengenbach and D. Li (2017). "Extremely Low Density and Super-Compressible Graphene Cellular Materials." Advanced Materials **29**(36): 1701553.
Rahman, M. Y. A., M. M. Salleh, I. Talib and M. Yahaya (2004). "Effect of ionic conductivity of a PVC–LiClO4 based solid polymeric electrolyte on the performance of solar cells of ITO/TiO2/PVC–LiClO4/graphite." Journal of power sources **133**(2): 293-297.
Ramirez-Rico, J., A. Gutierrez-Pardo, J. Martinez-Fernandez, V. Popov and T. Orlova (2016). "Thermal conductivity of Fe graphitized wood derived carbon." Materials & Design **99**: 528-534.
Rhim, Y.-R., D. Zhang, D. H. Fairbrother, K. A. Wepasnick, K. J. Livi, R. J. Bodnar and D. C. Nagle (2010). "Changes in electrical and microstructural properties of microcrystalline cellulose as function of carbonization temperature." Carbon **48**(4): 1012-1024.
Robertson, J. (1986). "Amorphous carbon." Advances in Physics **35**(4): 317-374.
Robertson, J. (1991). "Hard amorphous (diamond-like) carbons." Progress in Solid State Chemistry **21**(4): 199-333.
Robertson, J. (2002). "Diamond-like amorphous carbon." Materials science and engineering: R: Reports **37**(4-6): 129-281.
Robinson, G. R. J., J. M. Hammarstrom and D. W. Olson (2018). Graphite. Critical Mineral Resources of the United States: Economic and Environmental Geology and Prospects for Future Supply. K. J. Schulz, J. H. DeYoung, R. R. Seal and D. C. Bradley, Geological Survey.
Rode, A. V., E. G. Gamaly and B. Luther-Davies (2000). "Formation of cluster-assembled carbon nano-foam by high-repetition-rate laser ablation." Applied Physics A **70**(2): 135-144.
Rode, A. V., S. Hyde, E. Gamaly, R. Elliman, D. McKenzie and S. Bulcock (1999). "Structural analysis of a carbon foam formed by high pulse-rate laser ablation." Applied Physics A **69**(1): S755-S758.
Rodríguez-Mirasol, J., T. Cordero and J. Rodríguez (1996). "High-temperature carbons from kraft lignin." Carbon **34**(1): 43-52.
Roy, P. and S. K. Srivastava (2015). "Nanostructured anode materials for lithium ion batteries." Journal of Materials Chemistry A **3**(6): 2454-2484.
Ruan, G., Z. Sun, Z. Peng and J. M. Tour (2011). "Growth of graphene from food, insects, and waste." ACS nano **5**(9): 7601-7607.
Russell, S. A., S. Sharabi, A. Tallaire and D. A. Moran (2012). "Hydrogen-terminated diamond field-effect transistors with cutoff frequency of 53 GHz." IEEE Electron Device Letters **33**(10): 1471-1473.
Sarna, W., J. Kozakiewicz, J. Przybylski and K. Sylwestrzak (2016). "RVC—reticulated vitreous carbon. Structure, precursor polymer materials, process of manufacturing and applications." Materials Engineering **2**: 81-94.
Sarvar, F., D. C. Whalley and P. P. Conway (2006). Thermal interface materials-A review of the state of the art. 2006 1st Electronic Systemintegration Technology Conference, IEEE.
Seehra, M. S. and A. S. Pavlovic (1993). "X-Ray diffraction, thermal expansion, electrical conductivity, and optical microscopy studies of coal-based graphites." Carbon **31**(4): 557-564.

Seo, D. H., S. Pineda, J. Fang, Y. Gozukara, S. Yick, A. Bendavid, S. K. H. Lam, A. T. Murdock, A. B. Murphy and Z. J. Han (2017). "Single-step ambient-air synthesis of graphene from renewable precursors as electrochemical genosensor." Nature communications **8**: 14217.
Sevilla, M. and A. Fuertes (2010). "Graphitic carbon nanostructures from cellulose." Chemical Physics Letters **490**(1-3): 63-68.
Shevlin, P. B. (1972). "Formation of atomic carbon in the decomposition of 5-tetrazolyldiazonium chloride." Journal of the American Chemical Society **94**(4): 1379-1380.
Shi, L., P. Rohringer, K. Suenaga, Y. Niimi, J. Kotakoski, J. C. Meyer, H. Peterlik, M. Wanko, S. Cahangirov and A. Rubio (2016). "Confined linear carbon chains as a route to bulk carbyne." Nature materials **15**(6): 634.
Sinnott, S. B. and R. Andrews (2001). "Carbon nanotubes: synthesis, properties, and applications." Critical Reviews in Solid State and Materials Sciences **26**(3): 145-249.
Slack, G. A. (1962). "Anisotropic thermal conductivity of pyrolytic graphite." Physical Review **127**(3): 694.
Sladkov, A. and Y. P. Kudryavtsev (1969). "Diamond, graphite, carbyne–allotropic forms of carbon." Priroda **5**: 37-44.
Slonczewski, J. and P. Weiss (1958). "Band structure of graphite." Physical review **109**(2): 272.
Smith, P. and P. R. Buseck (1982). "Carbyne forms of carbon: do they exist?", Science **216**(4549): 984-986.
Sun, K., M. A. Stroscio and M. Dutta (2009). "Graphite C-axis thermal conductivity." Superlattices and Microstructures **45**(2): 60-64.
Syrah Resources Limited. (2020). "Graphite and its uses." Retrieved 2020-01-31, from http://www.syrahresources.com.au/graphite-and-its-uses.
Tamashausky, A. V. (2006). "An Introduction to synthetic graphite." Retrieved 2020-02-13, from https://asbury.com/media/1225/syntheticgraphiteparti.pdf.
Terranova, M., R. Polini, V. Sessa, M. Braglia and G. Cocito (1992). "A study of diamond synthesis on glassy carbon by the hot filament chemical vapour deposition technique." Diamond and Related Materials **1**(9): 969-977.
Timmons, A. and J. Dahn (2006). "In situ optical observations of particle motion in alloy negative electrodes for Li-ion batteries." Journal of The Electrochemical Society **153**(6): A1206-A1210.
Törmälä, P. and M. Romppanen (1981). "Preparation of glassy carbon from lignins and lignin condensates." Journal of Materials Science **16**(1): 272-274.
U.S. Food and Drug Administration. (2002). "Ascension PIP®: Summary of Safety and Probable Benefit." Retrieved 2020-02-15, from https://www.accessdata.fda.gov/cdrh_docs/pdf/H010005B.pdf.
Ueda, K., M. Kasu, Y. Yamauchi, T. Makimoto, M. Schwitters, D. Twitchen, G. Scarsbrook and S. Coe (2006). "Diamond FET using high-quality polycrystalline diamond with f T of 45 GHz and f max of 120 GHz." IEEE Electron Device Letters **27**(7): 570-572.
Wallace, P. R. (1947). "The Band Theory of Graphite." Physical Review **71**(9): 622-634.
Walsh, F., L. Arenas, C. P. De León, G. Reade, I. Whyte and B. Mellor (2016). "The continued development of reticulated vitreous carbon as a versatile electrode material: Structure, properties and applications." Electrochimica Acta **215**: 566-591.
Vander Wal, R. L. (1996). "Soot precursor material: Visualization via simultaneous lIF-LII and characterization via tem." Symposium (International) on Combustion **26**(2): 2269-2275.
Wang, N., M. K. Samani, H. Li, L. Dong, Z. Zhang, P. Su, S. Chen, J. Chen, S. Huang and G. Yuan (2018). "Tailoring the Thermal and Mechanical Properties of Graphene Film by Structural Engineering." Small: 1801346.
Warren, B. (1941). "X-ray diffraction in random layer lattices." Physical Review **59**(9): 693.
Vaughey, J., L. Fransson, H. Swinger, K. Edström and M. Thackeray (2003). "Alternative anode materials for lithium-ion batteries: a study of Ag3Sb." Journal of power sources **119**: 64-68.

Vázquez-Santos, M. B., E. Geissler, K. Laszlo, J.-N. Rouzaud, A. Martínez-Alonso and J. M. Tascón (2011). "Comparative XRD, Raman, and TEM study on graphitization of PBO-derived carbon fibers." The Journal of Physical Chemistry C **116**(1): 257-268.
Wei, Z., J. Yang, W. Chen, K. Bi, D. Li and Y. Chen (2014). "Phonon mean free path of graphite along the c-axis." Applied Physics Letters **104**(8): 081903.
Wort, C. J. and R. S. Balmer (2008). "Diamond as an electronic material." Materials today **11**(1-2): 22-28.
Wu, F., R. Huang, D. Mu, B. Wu and Y. Chen (2016). "Controlled synthesis of graphitic carbon-encapsulated $\alpha$-Fe2O3 nanocomposite via low-temperature catalytic graphitization of biomass and its lithium storage property." Electrochimica Acta **187**: 508-516.
Wu, Y.-P., E. Rahm and R. Holze (2003). "Carbon anode materials for lithium ion batteries." Journal of Power Sources **114**(2): 228-236.
Xiao-Ju, G., X. Bo, L. Zhong-Yuan, Y. Dong-Li, H. Ju-Long and G. Li-Cong (2008). "Theoretical hardness of wurtzite-structured semiconductors." Chinese Physics Letters **25**(6): 2158.
Xu, J., X. Gu, J. Cao, W. Wang and Z. Chen (2012). "Nickel oxide/expanded graphite nanocomposite electrodes for supercapacitor application." Journal of Solid State Electrochemistry **16**(8): 2667-2674.
Yang, F., X. Ren, G. E. LeCroy, J. Song, P. Wang, L. Beckerle, C. E. Bunker, Q. Xiong and Y.-P. Sun (2018). "Zero-Dimensional Carbon Allotropes—Carbon Nanoparticles Versus Fullerenes in Functionalization by Electronic Polymers for Different Optical and Redox Properties." ACS Omega **3**(5): 5685-5691.
Yang, H., R. Yan, H. Chen, D. H. Lee and C. Zheng (2007). "Characteristics of hemicellulose, cellulose and lignin pyrolysis." Fuel **86**(12-13): 1781-1788.
Yoshida, A. and Y. Hishiyama (1992). "Electron channeling effect on highly oriented graphites–size evaluation and oriented mapping of crystals." Journal of materials research **7**(6): 1400-1405.
Yuan, Y., Y. Ding, C. Wang, F. Xu, Z. Lin, Y. Qin, Y. Li, M. Yang, X. He and Q. Peng (2016). "Multifunctional stiff carbon foam derived from bread." ACS applied materials & interfaces **8**(26): 16852-16861.
Zhang, X., Q. Yan, J. Li, J. Zhang and Z. Cai (2018). "Effects of physical and chemical states of iron-based catalysts on formation of carbon-encapsulated iron nanoparticles from kraft lignin." Materials **11**(1): 139.
Zuazo, I., B. Hallstedt, B. Lindahl, M. Selleby, M. Soler, A. Etienne, A. Perlade, D. Hasenpouth, V. Massardier-Jourdan and S. Cazottes (2014). "Low-density steels: complex metallurgy for automotive applications." Jom **66**(9): 1747-1758.
Zuo, X., J. Zhu, P. Müller-Buschbaum and Y.-J. Cheng (2017). "Silicon based lithium-ion battery anodes: A chronicle perspective review." Nano Energy **31**: 113-143.
Zyvex Technologies. (2020). "Zyvex Technologies." Retrieved 2020-01-09, from http://www.zyvextech.com/.